

# Sheffield Hallam University

*Noise attenuation by finite barriers.*

PHILLIPS, Steven.

Available from the Sheffield Hallam University Research Archive (SHURA) at:

<http://shura.shu.ac.uk/20226/>

## A Sheffield Hallam University thesis

This thesis is protected by copyright which belongs to the author.

The content must not be changed in any way or sold commercially in any format or medium without the formal permission of the author.

When referring to this work, full bibliographic details including the author, title, awarding institution and date of the thesis must be given.

Please visit <http://shura.shu.ac.uk/20226/> and <http://shura.shu.ac.uk/information.html> for further details about copyright and re-use permissions.

POND STREET  
SHEFFIELD S1 1WB

6882



**Sheffield City Polytechnic  
Eric Mensforth Library**

**REFERENCE ONLY**

This book must not be taken from the Library

PL/26

R5193

ProQuest Number: 10700871

All rights reserved

INFORMATION TO ALL USERS

The quality of this reproduction is dependent upon the quality of the copy submitted.

In the unlikely event that the author did not send a complete manuscript and there are missing pages, these will be noted. Also, if material had to be removed, a note will indicate the deletion.



ProQuest 10700871

Published by ProQuest LLC (2017). Copyright of the Dissertation is held by the Author.

All rights reserved.

This work is protected against unauthorized copying under Title 17, United States Code  
Microform Edition © ProQuest LLC.

ProQuest LLC.  
789 East Eisenhower Parkway  
P.O. Box 1346  
Ann Arbor, MI 48106 – 1346

NOISE ATTENUATION BY FINITE BARRIERS

by

Steven Phillips

BSc (Hons)

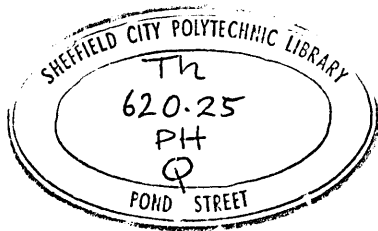
A dissertation submitted to the Council of National Academic Awards for the award of the degree of Master of Philosophy

Collaborating Establishment

Sharland Acoustics Ltd  
Winchester  
Hants

Sheffield City Polytechnic  
Department of Mechanical and Production Engineering

March 1981



7926192-01

## Acknowledgement

I would like to thank Dr G J McNulty, Director of Studies, for this work for his supervision and help. Also Dr J L Wearing of the University of Sheffield for his help. Gratitude is extended to my friends and colleagues in the Department of Mechanical and Production Engineering and in particular to Mr O Bardsley, Head of Department.

## Abstract

The work described in this thesis deals with the noise reduction performance of plane acoustic barriers of finite dimensions. Equations are developed for prediction of sound attenuation based on Fresnel-Kirchhoff diffraction theory. The main feature of this technique is that attenuation can be predicted regardless of the shape and size of the barrier and of the proximity of source and receiver to the barrier. The theory is initially developed for the case of free-field environments and is subsequently extended to reflecting ground conditions. Computer programs were developed to perform the attenuation calculations in given environments. The programs are driven by a set of parameters which uniquely define the source, barrier and environmental configuration. Experimental work was carried out in an anechoic chamber using a series of different source and barrier configurations. The experimental results were tested against the theory by applying the appropriate parameter values to the computer programs.

CONTENTSPage

1. Introduction	1
1.1 Review of Previous Research	1
1.2 Outline of Work Presented in this Thesis	2
2. Noise Reduction by a Plane Finite Screen in the Free Field	5
2.1 Introduction	5
2.2 Insertion Loss by Interposing the Screen	5
2.2.1 The Insertion Loss at any Position Within the Sound Pressure Field	5
2.2.2 Calculation of SPL	6
2.2.3 Calculation of $SPL_B(P)$	7
Application of Babinet's Principle & Fresnel Diffraction Theory	10
A Method of Evaluating the Fresnel-Kirchhoff Integral in the case of a Noise-Reducing Screen	13
The Effect of Barrier Transmission and the Calculation of $SPL_B(P)$	24
2.2.4 Calculation of the Insertion Loss	26
2.3 Summary	27
3. Noise Reduction by a Finite Screen in a Reflecting Ground Environment	31
3.1 Introduction	31
3.2 Calculation of the Insertion Loss	32
3.2.1 Calculation of $SPL_O(P)$	32
3.2.2 Calculation of $SPL_B(P)$	36
U(P) as a Combination of Free-field and Semi-Infinite Diffraction Components	39
The Half-Plane Diffraction Components	50
Final Formulation of U(P), where S is Above Ground Level	60
Formulation of U(P), where S is on the Ground Formulation of $SPL_B(P)$	61
3.2.3 Formulation of IL(P)	63
3.3 Summary	64

<u>CONTENTS</u> (continued)	<u>Page</u>
4. Predicted and Measured Results	67
4.1 Introduction	67
4.2 The Use of the Computer Programs in the Prediction of Barrier Performance	68
4.2.1 Description of the Program for Free-field Predictions	68
4.2.2 Description of the Program for Reflecting Ground Predictions	76
4.3 The Experimental Procedure	79
4.3.1 General Description	79
4.3.2 Free-Field Experiments	81
4.3.3 Experiments With a Reflecting Ground	84
4.4 Tables of Predicted and Measured Results	88
4.4.1 Tables of Insertion Losses in the Free Field	88
4.4.2 Tables of Insertion Losses in the Reflecting Ground Environment	96
4.5 Analysis of Results	105
4.5.1 Free-Field Environment	105
4.5.2 Barrier in the Presence of a Reflecting Ground	107
4.5.3 Summary of Results	109
5. Conclusions and Recommendations for Further Research	111
5.1 Conclusions	111
5.2 Recommendations for Further Research	112
5.2.1 Extension of the Sound Source Properties	112
5.2.2 Extension of the Environment to allow for further reflections	112
5.2.3 In-Situ Representation	113
5.3 Optimization of the Elements forming the sub-division of the barrier's surface	113
Appendix 1. Computer Flow Diagrams	115

<u>LIST OF DIAGRAMS</u> (continued)	<u>Page</u>
Figure 3.12 Bright and shadow zones between S, S <sub>i</sub> and P, P <sub>i</sub>	58
Figure 3.13 Ray paths when S is on the ground	62
Figure 4.1 Computer-printed results for a sample free-space configuration (square barrier)	71
Figure 4.2 Computer-printed results for a sample free-space configuration (rectangular barrier)	72
Figure 4.3 Representation of the missing portion of the 1 m x 1 m barrier by elements in a 25 x 25 element subdivision	74
Figure 4.4 Computer-printed results for a sample free-space configuration (barrier as in fig 4.3)	75
Figure 4.5 The anechoic chamber	80
Figure 4.6 Schematic representation of the apparatus for determination of attenuation by barriers	82
Figure 4.7 Examples of configurations used in the experiments	85
Plate 1 Sound source, barrier and monitoring microphone on the concrete floor of the anechoic chamber	83
Plate 2 The apparatus in the control room external to the anechoic chamber.	83

LIST OF DIAGRAMSPage

Figure 2.1	Diffraction around the edge of the barrier and the co-ordinate system $O_{xyz}$ .	9
Figure 2.2	The 'Complement' of the original barrier and the distances $l$ and $m$ .	11
Figure 2.3	The angles $(n, l)$ and $(n, m)$ .	12
Figure 2.4	Subdivision of the region B into elemental rectangular regions $R_j$ $j = 1, 2, \dots, n$ .	15
Figure 2.5	The rectangular element $R_j$ of the subdivision of the region B	17
Figure 2.6	The angles $(n, L_j)$ and $(n, M_j)$	23
Figure 2.7	The subdivision of an irregularly shaped barrier with a hole in it	29
Figure 3.1	Source above ground level in a reflecting ground environment	33
Figure 3.2	The image of the source with respect to a reflecting ground	35
Figure 3.3	(a) The four different ray paths in a reflecting ground environment	37
	(b) The four ray paths shown independently	38
Figure 3.4	Construction of a semi-infinite region for rays from S to P	42
Figure 3.5	Construction of a semi-infinite region for rays from $S_i$ to P	43
Figure 3.6	Construction of a semi-infinite region for rays from S to $P_i$	44
Figure 3.7	Construction of a semi-infinite region for rays from $S_i$ to $P_i$	45
Figure 3.8	The regions $\{HUB\}$ and $\{\overline{HUB}\}$ .	47
Figure 3.9	The points S', P' and the half plane screen H	51
Figure 3.10	The distances $r, s, r'$ and $s'$ .	53
Figure 3.11	The bright and shadow zones of S' with respect to H	56

## LIST OF SYMBOLS

$a_j$	- mathematical variable
A	- disturbance at 1 m from source in free space
$b_j$	- mathematical variable
B	- region occupied by barrier
$\bar{B}$	- geometrical complement of B
BSA	- computer program parameter
$C(w)$	- value of Fresnel Integral at w
d	- straight line distance from source to receiver
d'	- straight line distance from S' to P'
$\bar{d}$	- straight line distance from image of source to receiver = straight line distance from source to image of receiver
$d_0$	- constant
$d_1$	- constant
$d'_0$	- constant
$d'_1$	- constant
dB	- decibel
dS	- area integration increment over the region S
DSA	- computer program parameter
e	- Napierian constant
E	- constant relating to point of ground reflection
f	- frequency
$f_i$	- frequency (ie $f_1, f_2, \dots, f_{n-1}$ or $f_n$ )
$F_j$	- mathematical variable
$G(v)$	- Fresnel Integral function
H	- half-plane screen
i	- $\sqrt{-1}$
I	- intensity

LIST OF SYMBOLS (continued)

- $I_j$  - Kirchoff-Fresnel integral function
- $I_m$  - imaginary part of a complex number
- $I_n(a,b)$  - Kirchoff-Fresnel integral function
- $I_{ref}$  - reference value of Intensity
- IL - insertion loss
- $j$  - integer variable,  $j = 1, 2, \dots, n$ .
- $k$  - wave number  $k = 2\pi/\lambda$
- $\ell$  - distance from source to variable point on the barrier
- $\ell'$  - distance from  $S'$  to variable point on the barrier
- $L_j$  - distance from  $S$  to  $O_j$
- $m$  - distance from monitoring position to variable point on the barrier
- $m'$  - distance from  $P'$  to variable point on the barrier
- $M_j$  - distance from  $O_j$  to  $P$
- $n$  - integer constant
- $(n,P)$  - angle between  $\ell$  and the perpendicular to the barrier
- $(n,m)$  - angle between  $m$  and the perpendicular to the barrier
- NX - computer program parameter
- NY - computer program parameter
- $O$  - centre of coordinate system  $O_{xyz}$
- $O_j$  - centre point of the rectangular element  $R_j$
- $P$  - monitoring position
- $P'$  - general point used to represent either  $P$  or  $P_i$
- $P_i$  - image of  $P$  in the reflecting ground

LIST OF SYMBOLS (continued)

- Q - variable point of integration on the surface of the barrier
- r - distance from S' to edge of half-plane screen H, such that  $r+s$  is the shortest distance from S' to P' via the edge of the screen.
- r' - distance from S' to the xy-plane, such that  $r' + s'$  is the shortest distance from S' to P'.
- $R_e$  - real part of a complex number
- $R_j$  - an element in the rectangular subdivision of the barrier  $R_1, R_2, \dots, R_n$ .
- $\bar{R}_j$  - geometrical complement of  $R_j$
- $R_1$  - ground reflection coefficient on the source side of the barrier
- $R_2$  - ground reflection coefficient on the receiver side of the barrier
- REP - computer program parameter
- s - distance from P' to edge of half-plane screen H, such that  $r + s$  is the shortest distance from S' to P' via the edge of the screen.
- s' - distance from P' to the xy-plane, such that  $r' + s'$  is the shortest distance from S' to P'
- S - position of sound source
- $S_i$  - image of S
- S(w) - value of Fresnel Integral at w.
- SPL - Sound Pressure Level
- $SPL_0$  - SPL in the absence of any barrier
- $SPL_1$  - SPL at unit distance from the source
- $SPL_B$  - SPL with the barrier in position
- SR - Computer program parameter
- U - complex sound disturbance
- $U_1, U_2, U_3, U_4$  - component sound disturbances in the reflecting ground environment
- $U_0$  - disturbance in the free field.

LIST OF SYMBOLS (continued)

- $U_{01}, U_{02}$  - components of sound disturbance in the absence of a barrier in the reflecting ground environment.
- $U_B$  - disturbance in the presence of the barrier
- $U_{\bar{B}}$  - disturbance in the presence of the infinite screen  $\bar{B}$
- $U_H^S$  - disturbance due to the source at S in the presence of the half-plane screen H
- $v$  - mathematical variable
- $w$  - constant
- $w'$  - constant
- $\bar{w}$  - constant
- $x$  - Cartesian coordinate
- $x_0$  - x-coordinate of S
- $x_1$  - x-coordinate of P
- $x'_0$  - x-coordinate of S'
- $x'_1$  - x-coordinate of P'
- $X_j$  - x-coordinate of  $O_j$
- $y$  - Cartesian coordinate
- $y_0$  - y-coordinate of S
- $y_1$  - y-coordinate of P
- $y'_0$  - y-coordinate of S'
- $y'_1$  - y-coordinate of P'
- $Y_j$  - y-coordinate of  $O_j$
- $z$  - Cartesian coordinate
- $z_0$  - z-coordinate of S
- $z_1$  - z-coordinate of P

LIST OF SYMBOLS (continued)

- $z'_0$  - z-coordinate of  $S'$
- $z'_1$  - z-coordinate of  $P'$
- $\alpha$  - barrier transmission coefficient
- $\xi_j$  - dimension of  $R_j$  in the x-direction
- $\eta_j$  - dimension of  $R_j$  in the y-direction
- $\lambda$  - wavelength

## 1. INTRODUCTION

### 1.1 Review of previous research

Extensive literature is available on the attenuation due to semi-infinite barriers. These are classified as having finite height and infinite length. Particular emphasis is given to outdoor performance of noise attenuation due to barriers such as motorway embankments and fences (see Jonasson [1], Pierce [2] and Scholes et al [3]).

There is a dearth of published work on the noise attenuation due to finite barriers. For example, Kurze [4] reviews the contemporary literature up to 1974 and there was scant reference to finite barriers.

Maekawa [5,6] postulates a method for the prediction of the attenuation due to a finite barrier on reflecting ground by applying the method of calculation of diffraction over the top edge of a semi-infinite screen also to the ends of the finite screen. However his theory limits the location of source and monitoring point and also the barrier is restricted to rectangular shapes. Kurze and Anderson [7] deal with finite barriers in a way which predicts the length of the barrier required in the presence of an infinite line source that gives approximately the same attenuation as an infinitely long barrier.

Considering noise control in enclosed working environments, Moreland and Minto [8] investigated the inclusion of a barrier in one particular process plant based on energy

density equations and estimations of room absorption and source directivity. Royster and Stephenson [9] have published a review of measured noise characteristics in several industrial environments. Other work on the same subject has been mainly concerned with experimental research and prediction of noise effects based on empirical equations and known experimental results.

From the above background work it is shown that rigorous predicted solutions have been confined to straight-edged semi-infinite barriers. Also no theoretical solution has been given for finite barriers except that of Phillips et al [10,11], where the barrier has been subdivided into elements to enable a rigorous solution of any barrier shape to be obtained. The only other work on finite barriers has been restricted to experimental results for definite limited cases. It is therefore the aim of this work to investigate the effect of noise reduction by finite barriers and to provide information where any orientation in the shape of barrier is given. The theoretical background is based on the diffraction theory outlined by Born and Wolf [12] from which an easy to use computer package has been compiled.

## 1.2 Outline of work presented in this thesis

Initially a theoretical approach is made, based on a combination of classical diffraction theory and an elemental subdivision of the barrier's surface, of

predicting the attenuation of sound by a finite barrier in a free space environment. It is assumed that the sound source is a point source of monotonic frequency. This assumption was made for two reasons, firstly because this type of source lends itself most favourably to a clear description of the diffraction technique and secondly because it acts as a basic model upon which the theory for more complex types of source may be developed at a later stage.

It is assumed that the barrier is two-dimensional. The free space environment is initially assumed, again because it serves as a basic theoretical model which can be developed to suit more complex environments at a later stage. The free-field theory is described in Chapter 2.

In the next step, the theory of the free-field environment is extended to that in which a reflecting ground is taken into account. This theory uses the method of images with respect to the ground of the sound source and receiver's position. The theory is covered in Chapter 3.

Experiments in controlled conditions within an anechoic chamber were carried out using configurations of sound source, barrier and receiver's position which corresponded with the theory in Chapters 2 and 3. The results of these experiments are presented in Chapter 4.

The theory of Chapters 2 and 3 was converted into

computer programs which were developed by the author. These programs were written in Fortran V language and developed on the IBM computer belonging to Sheffield City Polytechnic. These programs enabled the calculation of predicted attenuation results based on the theory of Chapters 2 and 3 by inputting parameters which uniquely define a particular configuration. The results obtained by executing these programs are presented in Chapter 4 and are compared with the corresponding experimental results.

Proposals for extending this work to more typical in-situ working environments are given in Chapter 5.

## 2. NOISE REDUCTION BY A PLANE FINITE SCREEN IN THE FREE FIELD

### 2.1 Introduction

In this Chapter, formulae are derived for the prediction of the sound pressure distribution when a sound source and plane screen of finite dimensions are positioned in a free-field environment. It is assumed initially that the sound is transmitted from a single point source S and that it is monotonic. The more general case of a source emitting multiple frequency sound will be discussed in Chapter 5.

The work applies to a planar screen of finite dimensions. Sound transmission by the screen is treated as a constant coefficient in the range 0 to 1, where 0 denotes that sound is transmitted through the screen. This coefficient depends on the material of which the screen is composed. A novel feature of the theory developed here is that there is no restriction on the shape or size of the screen for the formulae to be valid, except that the screen should be finite and two-dimensional. The method is also applicable to barriers with holes. This is demonstrated in more detail in 2.3.

### 2.2 Insertion Loss by Interposing the Screen

#### 2.2.1 The Insertion Loss at Any Position Within the Sound Pressure Field

In order to predict changes in the sound pressure distribution after the barrier is placed in position, it is

necessary to predict the change in Sound Pressure Level (SPL) at any monitoring position P within the field and at each location monitoring the predicted SPL both before and after the barrier is placed in position, the change in sound pressure distribution can be mapped. Thus to formulate a method of predicting the sound pressure distribution, it is sufficient to determine the Insertion Loss  $IL(P)$  at any required position P in the sound field, where  $IL(P)$  is defined by equation (2.1).

$$IL(P) = SPL_O(P) - SPL_B(P), \quad (2.1)$$

where

$SPL_O(P)$  is the SPL at P in the absence of any screen

and

$SPL_B(P)$  is the SPL at P after the screen is placed in position

### 2.2.2 Calculation of $SPL_O$

Since the environment is assumed to be free field and the sound is monotonic transmitted from a point source, S, the sound radiates spherically (see Born and Wolf [12]) and the complex quantity of sound pressure, or disturbance,  $U_O$  at P is given by the Spherical Wave Equation (2.2).

$$U_O(P) = \frac{Ae^{ikd}}{d}, \quad (2.2)$$

where

d is the distance  $\overline{SP}$ ,

k is the wave number of the operating frequency (ie  $k = 2\pi/\lambda$ , where  $\lambda$  is wavelength),

and

A is the amplitude at unit distance from S.

From established properties of wave-theory (eg Born and Wolf [12]), the Intensity I at P is related to the disturbance U by the formula

$$I(P) = |U(P)|^2 \quad (2.3)$$

and it is also known (see Beranek [13]) that the SPL is related to the Intensity by the formula

$$SPL(P) = 10 \log_{10} \frac{I(P)}{I_{ref}} + 0.2 \text{ dB},$$

where  $I_{ref}$  is the reference intensity of  $10^{-12} \text{ W/m}^2$ .

Hence, the SPL is related to the disturbance by the equation

$$SPL(P) = 10 \log_{10} \frac{|U(P)|^2}{I_{ref}} + 0.2 \text{ dB} \quad (2.4)$$

Substituting equation (2.2) into equation (2.4), it follows that

$$SPL_o(P) = 10 \log_{10} \frac{|A|^2}{I_{ref} \cdot d^2} + 0.2 \text{ dB} \quad (2.5)$$

Now suppose that  $SPL_1$  is defined as the SPL at unit distance (ie 1 metre) from S. Then by substituting  $d = 1$  into equation (2.5), it follows that

$$SPL_1 = 10 \log_{10} \frac{|A|^2}{I_{ref}} + 0.2 \text{ dB}. \quad (2.6)$$

If equation (2.6) is now substituted into equation (2.5), then  $SPL_o(P)$  can be defined in terms of  $SPL_1$  and  $d$  as follows

$$SPL_o(P) = SPL_1 - 20 \log_{10} d \text{ dB} \quad (2.7)$$

### 2.2.3 Calculation of $SPL_B(P)$

Determination of the SPL when the barrier is inserted is a more complicated procedure. It is required to derive an

expression for  $SPL_B(P)$  which is generally applicable to any configuration of source, monitoring position and screen satisfying the conditions detailed in Chapter 1. This procedure is important because it forms the basis of the theory developed subsequently in this paper. To the author's knowledge, this technique has not previously been derived in such a widely applicable form by other authors and it is for this reason that a full and detailed explanation is given. A discussion of the advantages of this technique may be found in (2.3).

The technique is based on classical wave diffraction theory which is described in Born and Wolf [12]. A brief summary is necessary of those aspects of the theory which are applicable to the work in this paper. Suppose the plane finite barrier is placed between S and P. Then diffraction will take place around the edge of the barrier, so that the total amplitude of the disturbance at P results from all diffracted rays which pass through P and any direct rays from S to P which are not obstructed by the barrier (see fig 2.1). Let it initially be assumed that the transmission coefficient of the barrier is zero. The more general case of a constant anywhere in the range 0 to 1 will be considered later in this Chapter.

Typical rays incident on the edge of the barrier.

Typical diffracted rays passing through P.

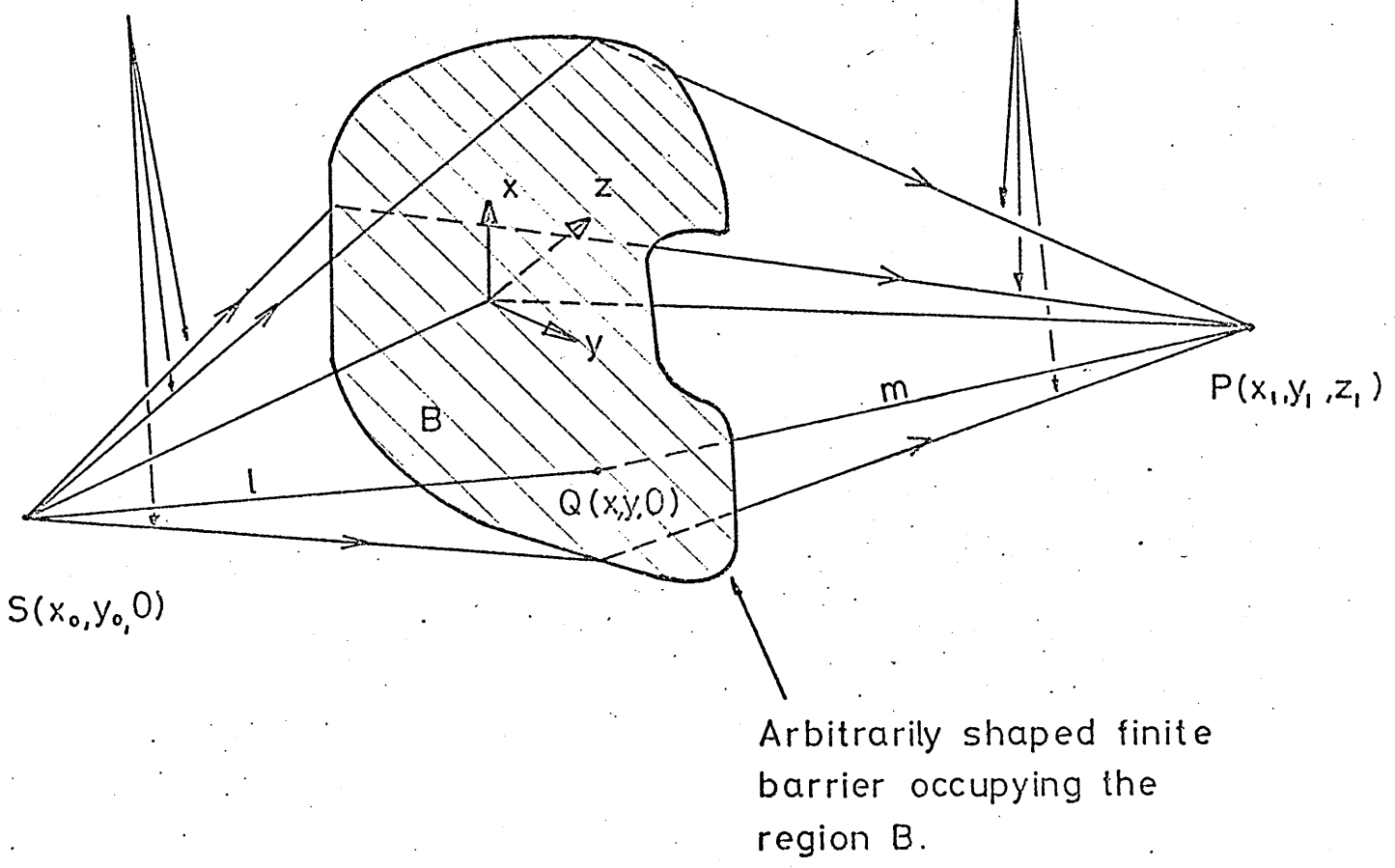


FIG 2.1 DIFFRACTION AROUND THE EDGE OF THE BARRIER AND THE CO-ORDINATE SYSTEM  $Oxyz$ .

Suppose now that a Cartesian co-ordinate system is defined as follows. Let the origin O lie somewhere on B, the region occupied by the barrier, with x- and y- axes defined in the plane of the barrier, and with the z- axis constructed so that the positive z-direction points into the half-space containing P (see fig 2.1). Let S and P have co-ordinates  $(x_0, y_0, z_0)$  and  $(x_1, y_1, z_1)$  in this system.

### Application of Babinet's Principle and Fresnel Diffraction Theory

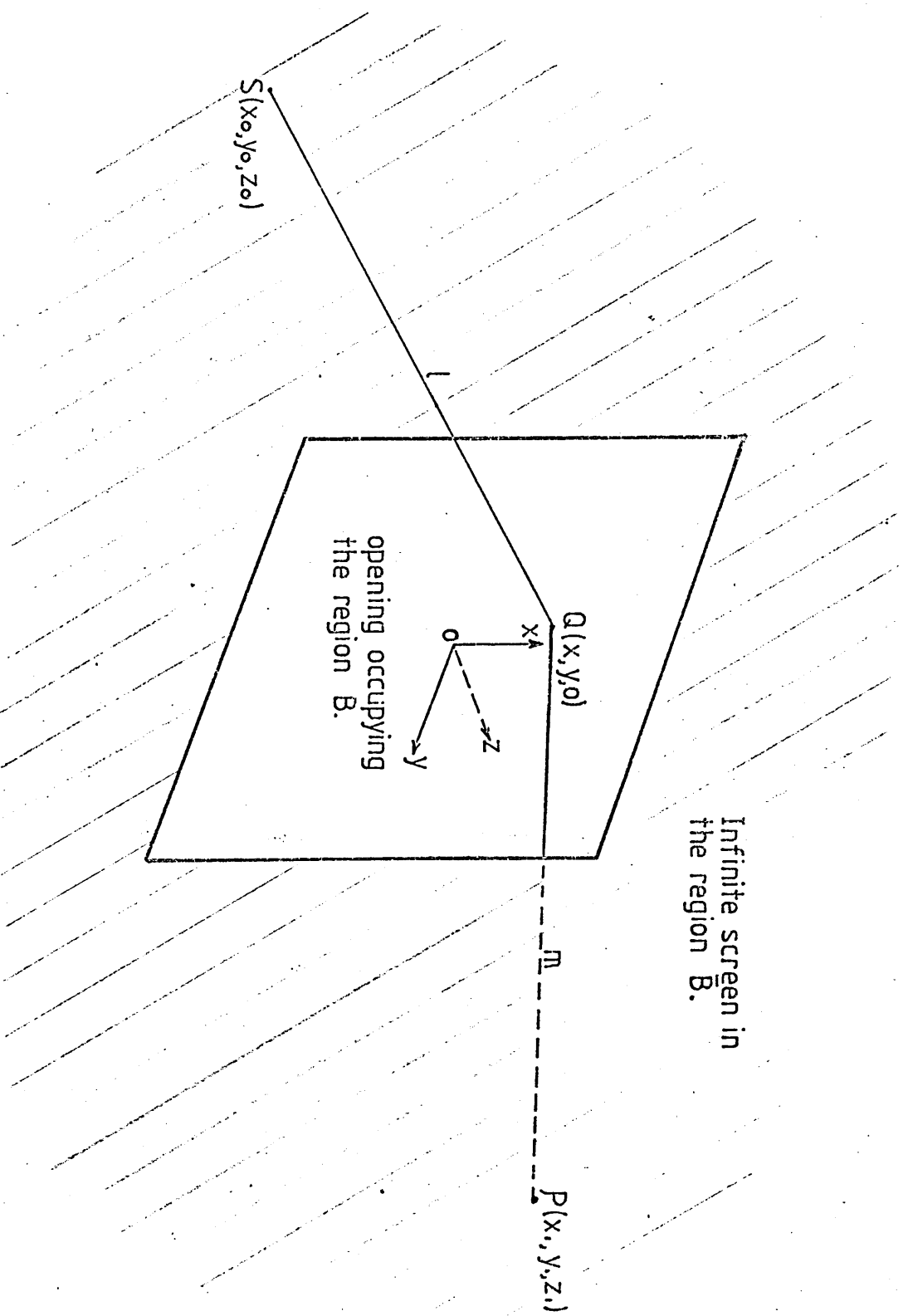
Let  $\bar{B}$  be defined as the infinite region in the xy-plane not occupied by the barrier. Now it will be necessary to consider temporarily a very different barrier configuration. Suppose that the region B is now occupied by the same material as that from which the barrier is made and that the region  $\bar{B}$ , which represents the exact dimensions of the barrier, is now an opening in this complementary plane screen (see fig 2.2). Then the Fresnel-Kirshhoff diffraction integral states that the disturbance  $U_{\bar{B}}(P)$  at P due to the opening B in the infinite screen is given by

$$U_{\bar{B}}(P) = - \frac{Ai}{2\lambda} \iint_B \frac{e^{ik(\ell+m)}}{\ell m} [\cos(n,\ell) - \cos(n,m)] dS \quad (2.8)$$

where

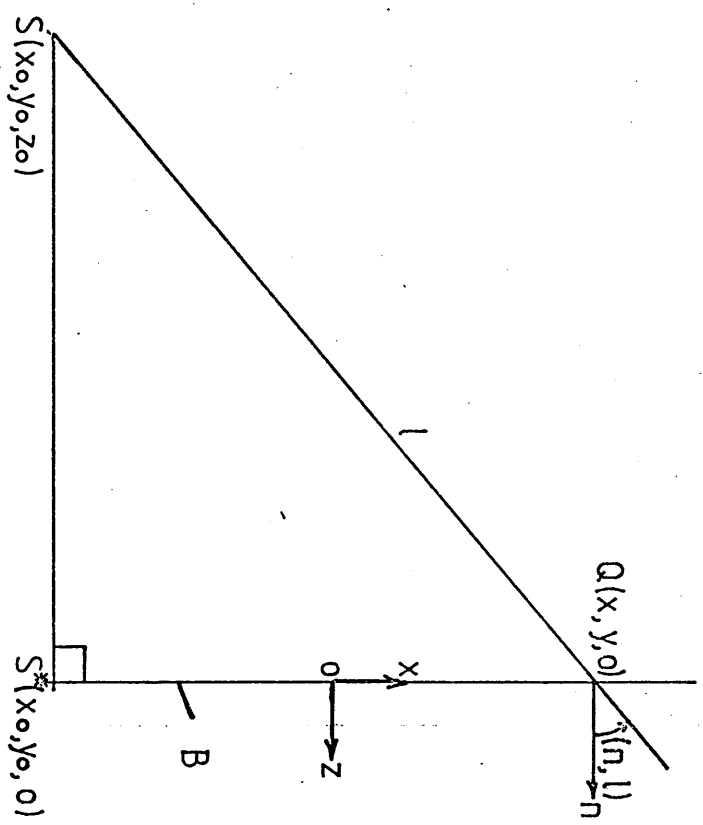
$\ell$  and  $m$  are the variable distances from S and P respectively to the point of integration Q  $(x, y, 0)$  on B (see fig 2.2),

and

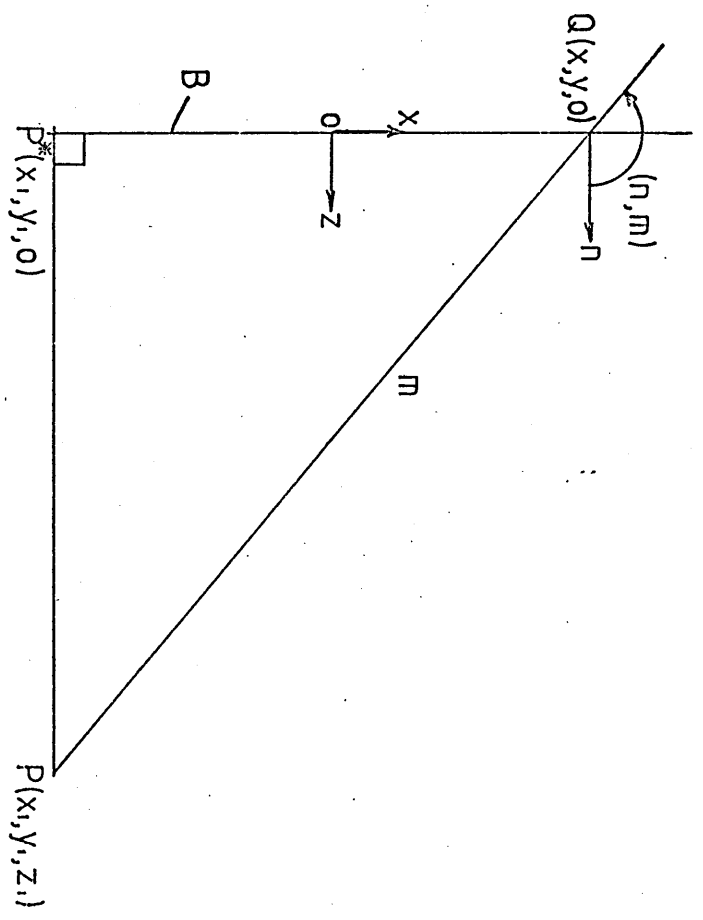


Infinite screen in the region B.

Figure 2.2. The 'Compliment' of the Original Barrier and the Distances  $l$  and  $m$ .



(a) The angle  $(n, l)$



(b) The angle  $(n, m)$

Figure 2.3. The Angles  $(n, l)$  and  $(n, m)$ .

(n,ℓ) and (n,m) are the angles S and P make with the normal to the xy-plane at Q (see fig 2.3).

(see Born and Wolf).

Now reverting to the original configuration of the finite screen as shown in fig 2.1, let  $U_B(P)$  denote the disturbance at P in this case. Then from Babinet's Principle,  $U_B(P)$  may be expressed in terms of  $U_{\bar{B}}(P)$  as follows

$$U_B(P) = U_O(P) - U_{\bar{B}}(P), \quad (2.9)$$

where  $U_O(P)$  was given in equation (2.2). It is immediate from equation (2.4), that  $SPL_B(P)$  may be expressed in terms of  $U_B(P)$  as follows

$$SPL_B(P) = 10 \log_{10} \frac{|U_B(P)|^2}{I_{ref}} + 0.2 \text{ dB} \quad (2.10)$$

In order therefore, to obtain a solution to this equation it is necessary to solve equation (2.9), but since  $U_O(P)$  is already known (equation (2.2)) the problem reduces to a formulation of  $U_{\bar{B}}(P)$ . Thus it remains to solve the double integral in equation (2.8).

#### A Method of Evaluating the Fresnel-Kirchhoff Integral in the Case of a Noise-Reducing Screen

It is important to note that the Fresnel-Kirchhoff Integral cannot be applied immediately in the form given in equation (2.8). There are a number of reasons for this, the first being that the integral is only applicable on regions whose linear dimensions are small in comparison with their distances from the source and monitoring position. In typical cases of barrier design, this condition will not be satisfied, since for example a large barrier is normally required and also it is favourable to place the barrier either close to

the noise source or to the receiver for efficient noise reduction. However, suppose the geometrical region covered by the surface integration in equation (2.8) is subdivided into smaller elemental regions  $R_1, R_2, \dots, R_n$ , say, as shown in fig 2.4. Then, provided that the dimensions of these elements are chosen correctly, the integral will be separately applicable on each of these regions, despite not being generally applicable on the whole region B.

For each  $j = 1, 2, \dots, n$ , let

$$U_{R_j}(P) = \frac{Ai}{2\lambda} \iint_{R_j} \frac{e^{ik(\ell+m)}}{\ell m} [\cos(n,\ell) - \cos(n,m)] dS \quad (2.11)$$

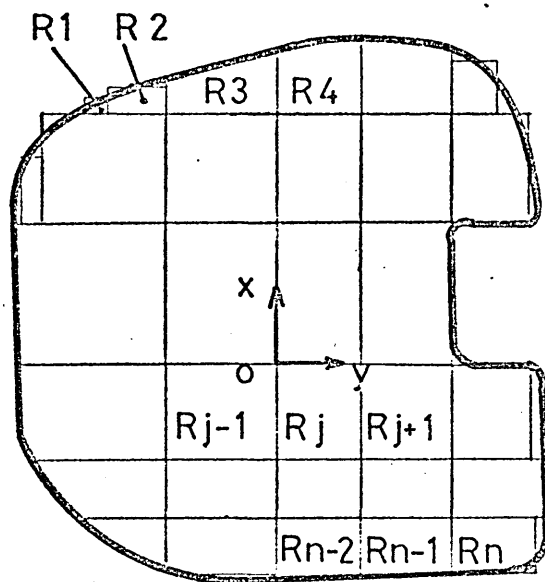
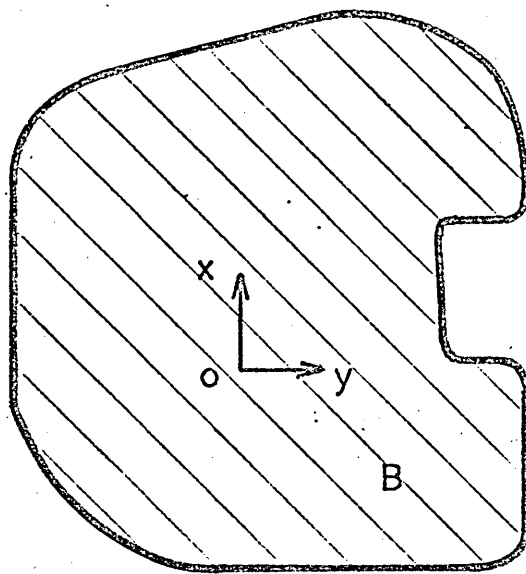


FIG 2.4 SUBDIVISION OF THE REGION B INTO ELEMENTAL RECTANGULAR REGIONS  $R_j, j=1,2, \dots, n$ .

Then it is immediately obvious from equation (2.8) that

$$U_{\bar{B}}(P) = \sum_{j=1}^n U_{\bar{R}_j}(P). \quad (2.12)$$

In this paper, it will be assumed that the elements  $R_j$  are rectangular for reasons which will become apparent later. The dimensions of the elements  $R_j$  must be chosen carefully to best suit the various conditions which make the double integral applicable. A discussion of this appears in 2.3, but at this stage it may be assumed that these elements have already been chosen correctly.

It can be seen that the problem now reduces to that of solving the double integral in equation (2.11) on any valid rectangular element of the form  $R_j$ , since the solution of  $U_{\bar{B}}(P)$  will then follow immediately from equation (2.12).

In order to be able to solve equation (2.11), certain approximations must be made. These may be summarised as follows. First, it is assumed that  $R_j$  is small enough for the variations in the terms ' $\cos(n, \ell) - \cos(n, m)$ ' and ' $1/\ell m$ ' to be negligible over  $R_j$ . Let  $O_j$  be the centre point  $R_j$  with co-ordinates  $(X_j, Y_j, 0)$ . Suppose also that the linear dimensions of  $R_j$  are  $2\xi_j$  in the x-direction and  $2\eta_j$  in the y-direction (see fig 2.5). Let  $L_j$  and  $M_j$  be the distances  $\overline{SO_j}$  and  $\overline{O_jP}$  respectively. Then the above assumption may be expressed by equations (2.13).

On  $R_j$ ,

$$\left. \begin{aligned} \cos(n, \ell) - \cos(n, m) &\cong \cos(n, L_j) - \cos(n, M_j) \\ \text{and } 1/\ell m &\cong 1/L_j M_j \end{aligned} \right\} \quad (2.13)$$

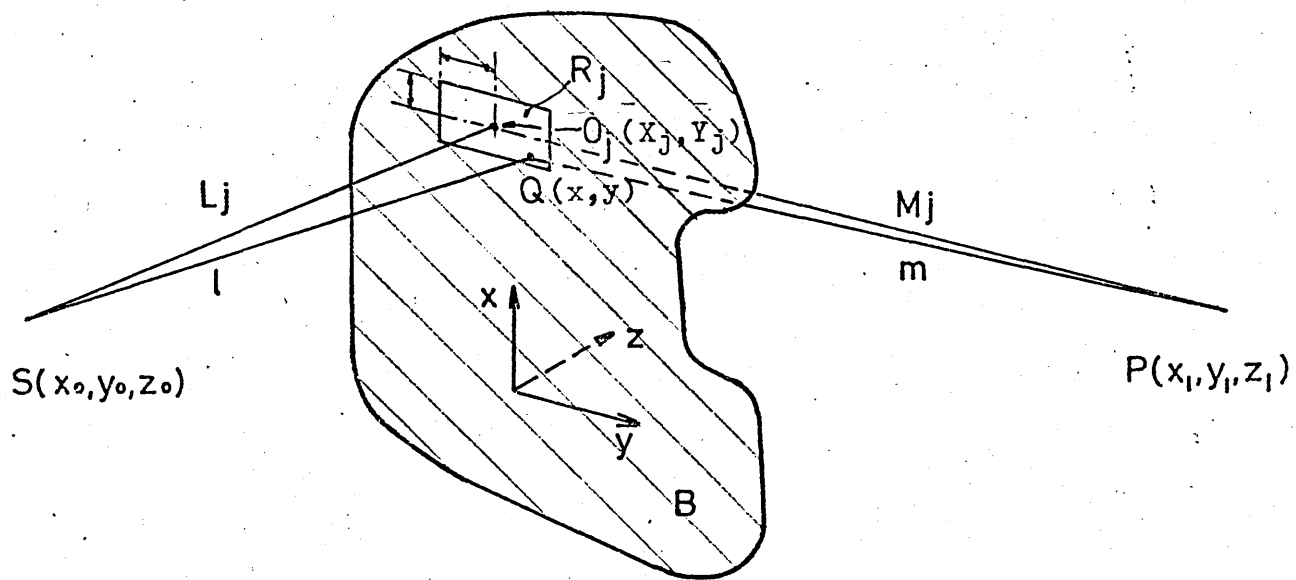


FIG. 2.5 THE RECTANGULAR ELEMENT  $R_j$  OF THE SUBDIVISION OF THE REGION  $B$ .

Hence equation (2.11) may be written

$$U_{\bar{R}_j}(P) = \frac{-2Ai}{\lambda L_j M_j} [\cos(n, L_j) - \cos(n, M_j)] e^{ik(L_j + M_j)} I_j \quad (2.14)$$

where

$$I_j = \frac{e}{4} e^{-ik(L_j + M_j)} \iint_{R_j} e^{ik(\ell + m)} ds \quad (2.15)$$

It may be noted that the justification of making this assumption is one of the criteria in choosing the dimensions of the elements  $R_j$  and is therefore discussed later in the thesis (Chapter 5). It should also be noted that the technique of approximating variables to constants in the Fresnel-Kirchhoff equation has also been used in the theory of Fresnel and Fraunhofer diffraction at a small aperture (see Born and Wolf [12]) and in far-field diffraction by barriers (see McNulty et al [14]).

The second assumption to be made is that the term

$e^{ik(\ell + m)}$  in equation (2.15) is still variable on  $R_j$ .

This is because the variation of  $k(\ell + m)$  [ $= \frac{2\pi}{\lambda} (\ell + m)$ ] will be appreciably large except for very long wavelengths or where  $R_j$  is very small. If either of these exceptions occurs, then the expression  $k(\ell + m)$  can be assumed constant and equal  $k(L_j + M_j)$  on  $R_j$  and equation (2.14) becomes

$$U_{\bar{R}_j}(P) = - \frac{Ai}{2\lambda} \frac{[\cos(n, L_j) - \cos(n, M_j)]}{L_j M_j} e^{ik(L_j + M_j)} 4 \epsilon_j \eta_j \quad (2.16)$$

whence the solution to equation (2.11) is complete.

The remainder of this section considers the more common case, where the term  $e^{ik(\ell+m)}$  is assumed variable on  $R_j$ . It will therefore be necessary to solve equation (2.15).

It can immediately be seen from fig 2.5 that

$$\left. \begin{aligned} \ell^2 &= \overline{SQ}^2 = (x-x_0)^2 + (y-y_0)^2 + z_0^2 \\ m^2 &= \overline{QP}^2 = (x-x_1)^2 + (y-y_1)^2 + z_1^2 \end{aligned} \right\} \quad (2.17)$$

and

$$\left. \begin{aligned} L_j^2 &= \overline{SO_j}^2 = (X_j-x_0)^2 + (Y_j-y_0)^2 + z_0^2 \\ M_j^2 &= \overline{O_jP}^2 = (X_j-x_1)^2 + (Y_j-y_1)^2 + z_1^2 \end{aligned} \right\} \quad (2.18)$$

In making the approximations in equation (2.13) it was assumed that the linear dimensions of  $R_j$  are small in comparison with the distances of  $R_j$  from S and P. This assumption is used again here to expand  $\ell$  and  $m$  as a power series in

$$\frac{x-X_j}{L_j}, \frac{y-Y_j}{L_j}, \frac{x-X_j}{M_j} \text{ and } \frac{y-Y_j}{M_j} \text{ on } R_j$$

giving

$$\ell = L_j \frac{-(x_0 - X_j)(x - X_j) + (y_0 - Y_j)(y - Y_j)}{L_j} + \frac{(x - X_j)^2 + (y - Y_j)^2}{2L_j} + \dots$$

$$m = M_j \frac{-(x_1 - X_j)(x - X_j) + (y_1 - Y_j)(y - Y_j)}{M_j} + \frac{(x - X_j)^2 + (y - Y_j)^2}{2M_j} + \dots$$

It will further be assumed that the size of  $R_j$  is such that the terms  $\frac{(x-X_j)^2}{2L_j}$ ,  $\frac{(y-Y_j)^2}{2L_j}$ ,  $\frac{(x-X_j)^2}{2M_j}$ ,  $\frac{(y-Y_j)^2}{2M_j}$  and those in

higher powers of  $(x-X_j)$  and  $(y-Y_j)$  may be assumed negligible compared with the leading terms  $L_j$  and  $M_j$ . Hence the above equation reduces to

$$\left. \begin{aligned} \ell &= L_j - \frac{(x_0 - X_j)(x - X_j) + (y_0 - Y_j)(y - Y_j)}{L_j} \\ m &= M_j - \frac{(x_1 - X_j)(x - X_j) + (y_1 - Y_j)(y - Y_j)}{M_j} \end{aligned} \right\} \quad (2.19)$$

on  $R_j$ . Again the justification of this assumption is discussed along with the choice of dimensions of  $R_j$  in Chapter 5. It may also be noted here that this technique of expanding the distances  $\ell$  and  $m$  linearly in terms of  $(x-X_j)$  and  $(y-Y_j)$  is also used in the method of Fraunhofer diffraction for a small aperture (see Born and Wolf [12]).

Substituting equation (2.19) into equation (2.15) it follows that

$$I_j = \frac{1}{4} \int_{-\eta_j}^{\eta_j} \int_{-\xi_j}^{\xi_j} e^{i(a_j(x-X_j) + b_j(y-Y_j))} d(x-X_j) d(y-Y_j) \quad (2.20)$$

$$\text{where } a_j = -k \left[ \frac{x_0 - X_j}{L_j} + \frac{x_1 - X_j}{M_j} \right] \quad (2.21)$$

$$\text{and } b_j = -k \left[ \frac{y_0 - Y_j}{L_j} + \frac{y_1 - Y_j}{M_j} \right]$$

The inner integral of equation (2.20) is readily solved giving

$$\frac{1}{2} \int_{-\xi_j}^{\xi_j} e^{i(a_j(x-X_j) + b_j(y-Y_j))} d(x-X_j) =$$

$$\left\{ \begin{array}{l} e^{ib_j(y-Y_j)} \cdot \frac{\sin a_j \xi_j}{a_j} \text{ if } a_j \neq 0 \\ e^{ib_j(y-Y_j)} \cdot \xi_j \text{ if } a_j = 0, \end{array} \right.$$

and since

$$\frac{1}{2} \int_{-\eta_j}^{\eta_j} e^{ib_j(y-Y_j)} \cdot d(y-Y_j) =$$

$$\left\{ \begin{array}{l} \frac{\sin b_j \eta_j}{b_j} \text{ if } b_j \neq 0 \\ \eta_j \text{ if } b_j = 0, \end{array} \right.$$

equation (2.20) becomes

$$I_j = \left\{ \begin{array}{ll} \frac{\sin a_j \xi_j}{a_j} \cdot \frac{\sin b_j \eta_j}{b_j} & \text{if } a_j \neq 0, b_j \neq 0 \\ \frac{\sin a_j \xi_j}{a_j} \cdot \eta_j & \text{if } a_j \neq 0, b_j = 0 \\ \xi_j \cdot \frac{\sin b_j \eta_j}{b_j} & \text{if } a_j = 0, b_j \neq 0 \\ \xi_j \cdot \eta_j & \text{if } a_j = 0, b_j = 0 \end{array} \right. \quad (2.22)$$

It may be noted here that the fourth value  $I_j = \xi_j \cdot \eta_j$ , when substituted into equation (2.14) gives precisely equation (2.16). From this, the condition that the wavelength  $\lambda$  is sufficiently long or the dimensions of  $R_j$  are sufficiently small for the term  $e^{ik(\lambda+m)}$  to be assumed constant on the  $R_j$ 's, may be incorporated into

the above by specifying that  $I_j = \xi_j \cdot \eta_j$  on  $R_j$  independently of the values of  $a_j$  and  $b_j$ . Observation of equations (2.14) and (2.22) shows that it remains only to obtain a working formulation of the term  $[\cos(n, L_j) - \cos(n, M_j)]$  in order to be able to express  $U_{\bar{R}_j}(P)$  in terms of measurable quantities.

This is done as follows. By definition of the angles  $(n, \ell)$ ,  $(n, m)$  subtended at the variable point  $Q(x, y, 0)$  (see fig 2.3), it follows that the angles  $(n, L_j)$  and  $(n, M_j)$  occur in the special case  $Q=O_j$  (see fig 2.6). It can be immediately observed from fig 2.6 that

$$\cos(n, L_j) = \frac{\overline{SS'}}{\overline{SO_j}} = \frac{-z_o}{L_j}$$

and

$$\cos(n, M_j) = -\cos(\pi - (n, M_j)) = \frac{-\overline{PP'}}{\overline{O_j P}} = \frac{-z_1}{M_j}$$

Hence

$$[\cos(n, L_j) - \cos(n, M_j)] = \frac{L_j z_1 - M_j z_o}{L_j^2 M_j^2}. \quad (2.23)$$

Now by substituting equation (2.23) into equation (2.14), and substituting equation (2.14) into equation (2.12), it follows that

$$U_{\bar{B}}(P) = \frac{-2iA}{\lambda} \sum_{j=1}^n F_j, \quad (2.24)$$

where

$$F_j = \frac{L_j z_1 - M_j z_o}{L_j^2 M_j^2} \cdot e^{ik(L_j + M_j)} I_j, \quad (2.25)$$

$I_j$  is given by equation (2.22),  $a_j$  and  $b_j$  are given by equations (1.21) and  $L_j$  and  $M_j$  by equations (2.18).

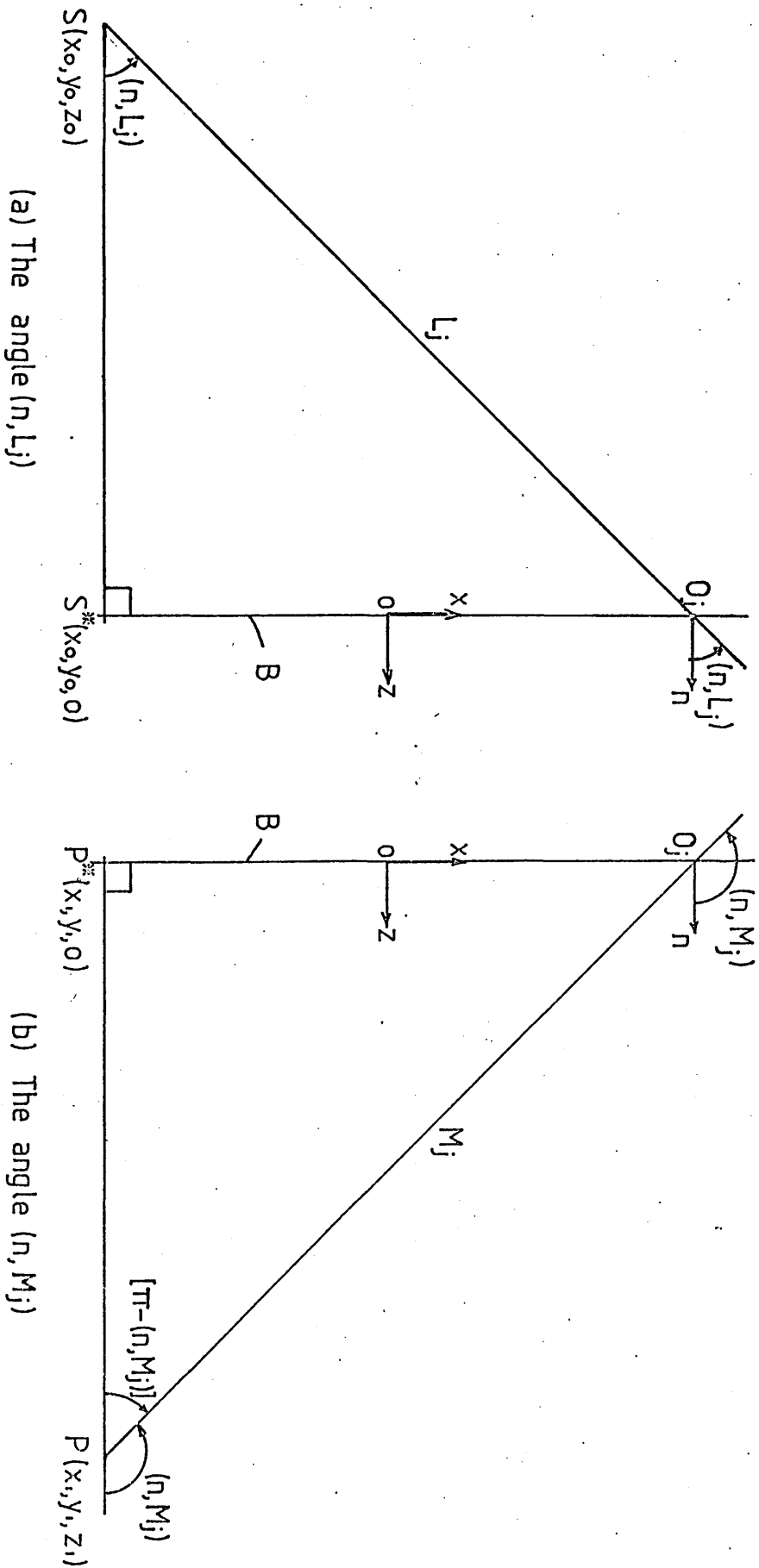


Figure 2.6. The Angles  $(n, L_j)$  and  $(n, M_j)$

This concludes the method of evaluating the Fresnel-Kirchhoff integral (equation (2.8)) for the noise-reducing screens, subject to the conditions concerning the screen described in 2.1.

The Effect of Barrier Transmission and the Calculation of  $SPL_B(P)$

Earlier it was explained that an expression for  $SPL_B(P)$  was required. It is now possible to complete the derivation of this expression in the case of zero barrier transmission. By substituting equations (2.2) and (2.24) into equation (2.9), the disturbance  $U_B(P)$  at P with the non-transmitting barrier in position may be expressed by

$$U_B(P) = \frac{Ae^{ikd}}{d} + \frac{2Ai}{\lambda} \sum_{j=1}^n F_j, \quad (2.26)$$

where  $d$  is the distance  $\overline{SP}$  given by

$$d = \sqrt{[(x_1 - x_0)^2 + (y_1 - y_0)^2 + (z_1 - z_0)^2]} \quad (2.27)$$

It was also stated earlier in this section that transmission of sound by the barrier will be treated as a fractional constant in the range 0 to 1, where zero denotes that the barrier is perfectly non-transmitting. Let this coefficient be denoted by the symbol  $\alpha$ . So far, zero transmission (i.e.  $\alpha = 0$ ) only has been considered. The disturbance  $U_B(P)$  in this case was given by the Babinet equation (2.9) which was

$$U_B(P) = U_0(P) - \frac{U_B(P)}{\alpha} \quad (\alpha = 0) \quad (2.28a)$$

It is necessary here to consider also the effect of non-zero transmission. Suppose in the extreme case that the barrier was perfectly transmitting (i.e.  $\alpha = 1$ ). This is the equivalent situation of there being no barrier present at all. In this case the Babinet equation (2.9) would be

$$U_B(P) = U_O(P), \quad (\alpha = 1) \quad (2.28b)$$

since  $U_O(P)$  represents the free-field disturbance.

To obtain an expression for  $U_B(P)$ , where  $\alpha$  is anywhere between 0 and 1, the expressions in equations (2.28a) and (2.28b) are interpolated linearly in  $\alpha$  to give the general formulation of  $U_B(P)$  as follows

$$U_B(P) = U_O(P) - (1-\alpha) \cdot U_{\bar{B}}(P), \quad (2.29)$$

where  $0 \leq \alpha \leq 1$ .

Hence equation (2.26) becomes, in the general case,

$$U_B(P) = \frac{Ae^{ikd}}{d} + \frac{2A(1-\alpha)}{\lambda} i \sum_{j=1}^n F_j \quad (2.30)$$

The general expression for the required Sound Pressure Level  $SPL_B(P)$  at P with the barrier in position now follows by substituting equations (2.30) and (2.6) into equation (2.10) giving

$$SPL_B(P) = SPL_1 + 20 \log_{10} \frac{1}{d} \left\{ \left[ \cos kd - \frac{2d(1-\alpha)}{\lambda} \sum_{j=1}^n \text{Im}(F_j) \right]^2 + \left[ \sin kd + \frac{2d(1-\alpha)}{\lambda} \sum_{j=1}^n \text{Re}(F_j) \right]^2 \right\}^{1/2} \quad (2.31)$$

(compare with equation (2.7) ).

#### 2.2.4 Calculation Of The Insertion Loss

It was stated in 2.2.1 that the purpose of this section was to devise a method of predicting the Insertion Loss  $IL(P)$  at  $P$ . The expression for  $IL(P)$  now follows by substituting equations (2.31) and (2.7) into equation (2.1), which gives

$$IL(P) = 10 \log_{10} \frac{1}{\left[ \cos kd - \frac{2d(1-\alpha)}{\lambda} \sum_{j=1}^n \text{Im}(F_j) \right]^2 + \left[ \sin kd + \frac{2d(1-\alpha)}{\lambda} \sum_{j=1}^n \text{Re}(F_j) \right]^2}$$

where  $F_j$  is defined by equation (2.25).

It is now possible, by using equation (2.29), to formulate a computer program which can be used to calculate the Insertion Loss  $IL(P)$  at any given monitoring position  $P$ , due to the interposition of the barrier. It may be demonstrated here that the program requires the following parameters of the configuration for input:

the co-ordinates  $(x_0, y_0, z_0)$  and  $(x_1, y_1, z_1)$  of  $S$  and  $P$ ,

the transmission coefficient  $\alpha$  of the barrier,

the wavelength  $\lambda$  of the source,

the Sound Pressure Level  $SPL_1$  at 1m from  $S$  in free space,

the number  $n$  of rectangular elements  $R_j$  forming the subdivision of the finite region  $B$  occupied by the screen, and for each element  $R_j$ ,  $j = 1, 2, \dots, n$ ,

the half  $x$ - and  $y$ - dimensions  $z_j$  and  $\eta_j$  respectively, and the co-ordinates  $X_j, Y_j$  of its centre point.

In a particular configuration of source, screen and monitoring position in the free field, the values of the

above parameters uniquely define that configuration and from those values, both the Sound Pressure Level  $SPL_0(P)$  at P in the absence of the barrier and the Insertion Loss  $IL(P)$  due to the interposition of the barrier, may be calculated numerically. The computer program which performs these calculations has been developed by the author and is described in Chapter 4.

### 2.3 Summary

The aim of this chapter is to derive formulae which can be used to predict the sound pressure field when a sound source and plane screen of finite dimensions are placed in free space. The method used was to consider any monitoring position P in the field and to calculate the Insertion Loss  $IL(P)$  at P due to the interposition of the barrier.

Using equation (2.1) it was thus required to determine both the Sound Pressure Level  $SPL_0(P)$  at P in the absence of any screen and the SPL at P after the screen is placed in position, denoted by  $SPL_B(P)$ . In 2.2.2, an expression for  $SPL_0(P)$  was derived based on the spherical wave equation.

In the derivation of an expression for  $SPL_B(P)$ , several factors had to be considered. The method used involves the novel feature of subdividing the area of the screen into smaller rectangular regions. This was necessary in order to obtain a solution of the diffraction integral over the whole barrier, since the integral is only

applicable to relatively small regions. The diffraction integral itself comes from the classical theory of diffraction and was first given by Fresnel and Kirchhoff. This integral has also been used in the theory of diffraction of sound by barriers, eg [4], [5], [6] and [7], but it has usually only been applied to semi-infinite barriers. In the work where it has been applied to finite barriers, (eg [6]), its use has been rather restricted. One of the important features of the work in this paper is that the use of the integral can be applied in a wider variety of circumstances of finite barriers and especially there is total freedom in the size and shape of the barriers. The barrier may even have holes in it, since any area can be represented as the sum of small rectangular regions to a sufficient degree of accuracy (see fig 2.7). Also an important aspect of this method is that the accuracy of the predicted result in relation to an exact theoretical solution can be monitored. This is demonstrated more fully in the light of actual results of the computer program in Chapter 4.

The formula for  $SPL_B(P)$  is given in equation (2.31). The Insertion Loss  $IL(P)$  then follows immediately as shown in equation (2.32). Finally, values of  $IL(P)$  in particular configurations of source, barrier and monitoring position can be calculated from equation (2.32) by invoking the computer program of Chapter 4. Actual computed results of this type are analysed in Chapter 4.

Another feature of the theory is that the transmission of the barrier may be considered in the form of a coefficient

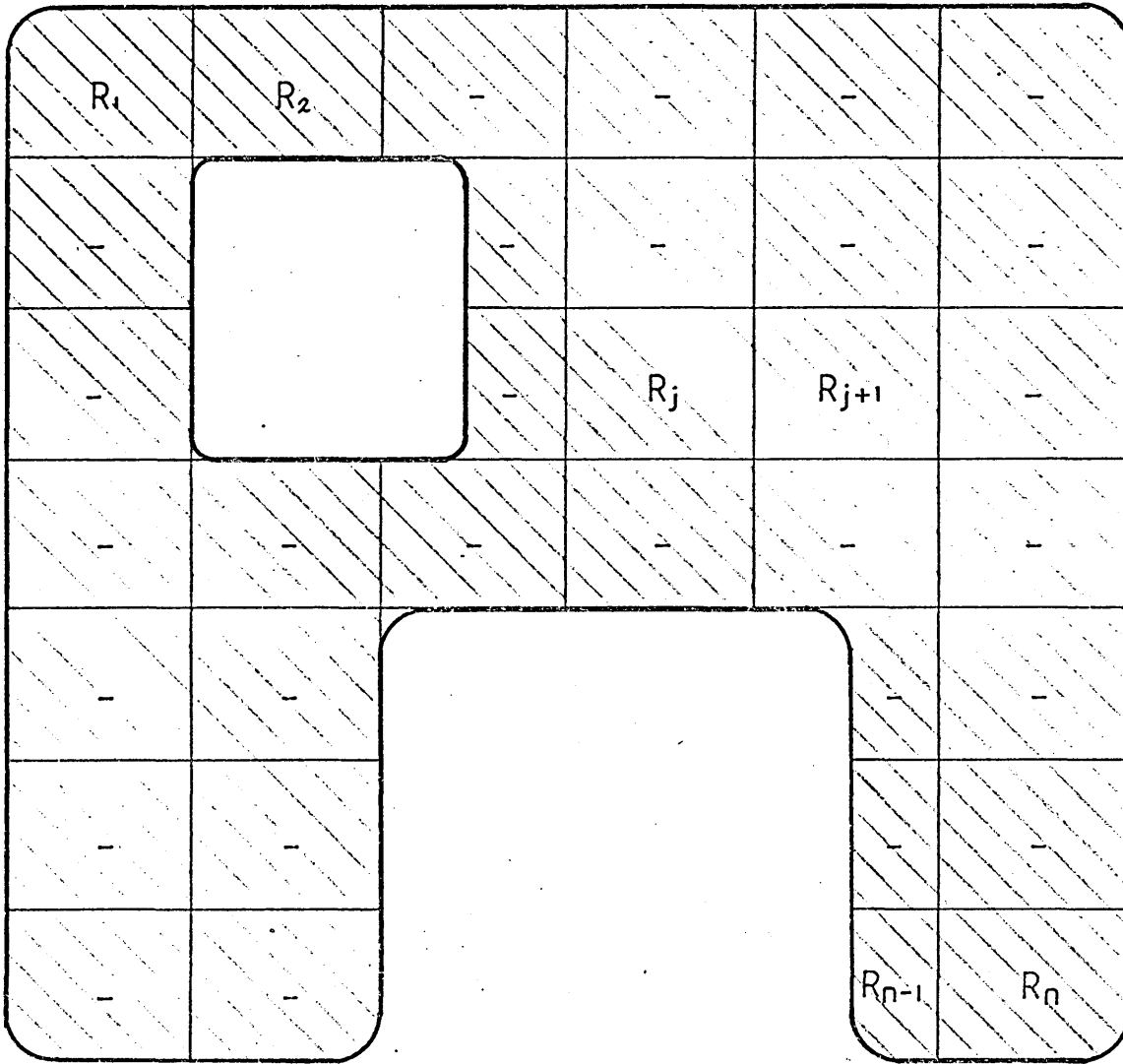


Figure 2.7. The Sub-division of an Irregularly Shaped Barrier with a hole in it.

$\alpha$ , constant over the whole barrier, where  $0 \leq \alpha \leq 1$ . A value of  $\alpha = 0$  represents a non-transmitting barrier and a value of  $\alpha = 1$  represents a completely transmitting barrier. (Hence the extreme case of  $\alpha = 1$  is equivalent to having no barrier at all).

Next, the sound source is assumed to be monotonic emitted from a single point S. A discussion of how the theory may be extended to that of a multiple frequency source appears in Chapter 5.

Finally, it should be noted that this theory is extended in Chapter 3 to apply in the case where there is also a reflecting ground. This next configuration is, of course, much more important, since in most practical environments reflection by the ground must be considered. Thus, although the free field case of this chapter is of little immediate practical use, the theory derived is used directly in conjunction with other techniques (for example, the method of images in Chapter 3), where its importance can be more greatly appreciated.

### 3. NOISE REDUCTION BY A FINITE SCREEN IN A REFLECTING GROUND ENVIRONMENT

#### 3.1 Introduction

In this chapter a screen is fixed in space and an addition to chapter 2 is included where there are ground reflecting surfaces. An extension of the theory outlined in chapter 1 is presented for this additional parameter.

The method of images is employed where the images relative to the ground of the source S and the monitoring position P are used to represent the reflected sound rays. The chapter describes how the SPL at P is determined as a consequence of these reflected rays.

A description is given where the SPL is formulated from constant ground reflection and no barrier. In order to specify a coefficient for ground reflection a range 0 to 1 is adopted where 1 indicates perfect reflection and 0 perfect absorption. The formulation of the equations assumes a value of this coefficient.

The parameters are the same as in chapter 1 and additional parameters are introduced here to account for ground reflection. Similarly the insertion loss  $IL(P)$  is also required.

$$IL(P) = SPL_O(P) - SPL_B(P), \quad (3.1)$$

where

$SPL_O(P)$  is the SPL at P in the absence of any screen and

$SPL_B(P)$  is the SPL at P after the screen is placed in position.

## 3.2 Calculation of the Insertion Loss

### 3.2.1 Calculation of $SPL_0(P)$

There are two cases to consider, first where the source is above the level of the ground and secondly where the source is at ground level.

The first case, where the source is above the ground level, is illustrated in fig 3.1. Suppose that the barrier is to be placed in the xy-plane, with the origin at ground level and that  $R_1$  and  $R_2$  represent the coefficients of ground reflection on respectively the source side and the monitoring position side of the barrier. Suppose the co-ordinates of S and P are  $(x_0, y_0, z_0)$  and  $(x_1, y_1, z_1)$  respectively. In view of the general relationship between  $SPL(P)$  and the disturbance  $U(P)$  at P, it will be sufficient to determine  $U_0(P)$ , from which  $SPL_0(P)$  follows immediately.

The contributions to  $U_0(P)$  come from both direct sound between S and P and sound reflected by the ground before reaching P. In view of theory given by Maekawa [5],  $U_0(P)$  may be expressed by the equation

$$U_0(P) = U_{01}(P) + U_{02}(P), \quad (3.2)$$

where  $U_{01}(P)$  is the disturbance in free space and  $U_{02}(P)$  is the contribution due to ground reflection.

By definition  $U_{01}(P)$  is simply equation (3.2) since it is the disturbance in the free-field. Hence

$$U_{01}(P) = \frac{Ae^{ikd}}{d}, \quad (3.3)$$

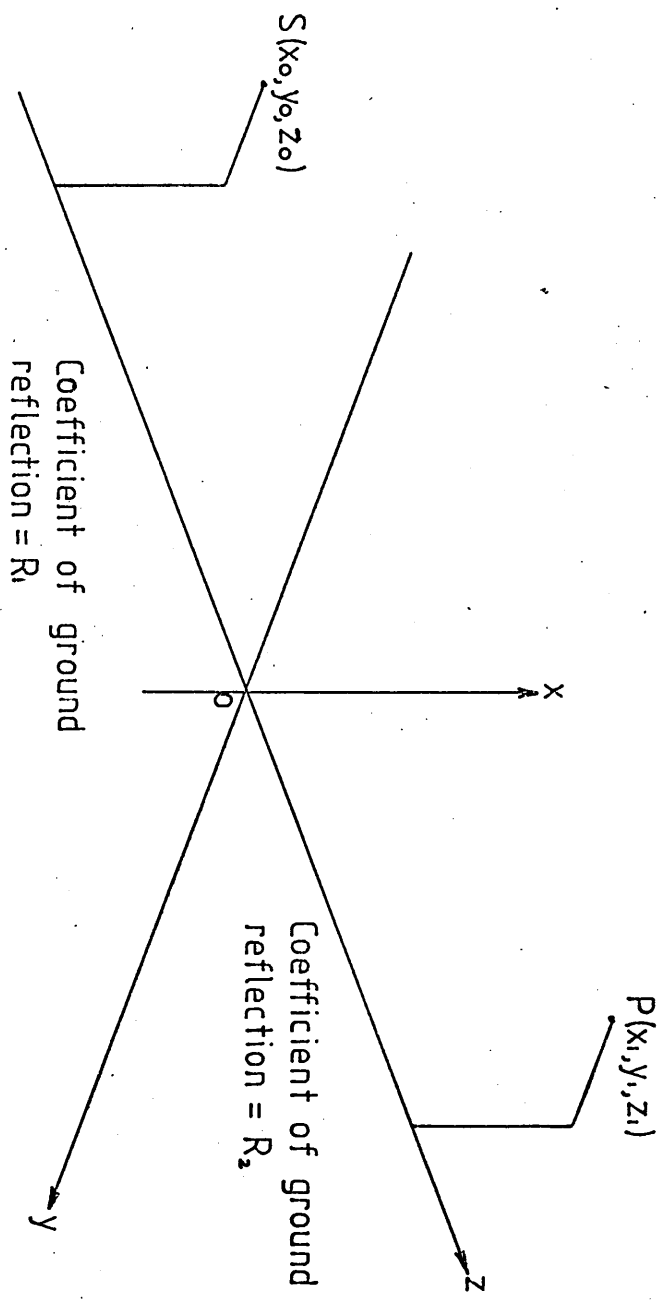


Figure 3.1.

where A, k and are defined in 2.2.2.

In order to establish  $U_{02}(P)$ , the method of considering the image  $S_1$  of S in the ground's surface is employed. This technique has previously been used by Maekawa [5]. By definition  $S_1$  has the co-ordinates  $(-x_0, y_0, z_0)$  (see fig 3.2). The reflected sound at P is considered to be the equivalent of sound of the same wavelength as S emanating from  $S_1$  directly. Hence the reflected sound is equivalent to direct free field sound from  $S_1$ , with the extra condition that a scalar multiplication of the ground reflecting coefficient is required. Thus  $U_{02}(P)$  may be formulated as follows (compare with equation(2.2)).

$$U_{02}(P) = R_E A e^{\frac{ikd}{\bar{d}}} \quad (3.4)$$

where  $R_E$  is the reflection coefficient at the point of ground reflection and  $\bar{d}$  is the distance  $\overline{S_1P}$ , given by

$$\bar{d} = \sqrt{[(x_1 + x_0)^2 + (y_1 - y_0)^2 + (z_1 - z_0)^2]} \quad (3.5)$$

Now  $R_E$  is equal to either  $R_1$  or  $R_2$ , depending on whether the sound ray is reflected on the source side or the monitoring position side of the xy-plane. (For example, in fig 3.2,  $R_E = R_2$ ). Using simple geometry,  $R_E$  may be expressed as follows

$$R_E = \begin{cases} R_1 \\ R_2 \end{cases} \quad \text{if } x_0 z_1 + x_1 z_0 \begin{cases} \leq 0 \\ > 0 \end{cases} \quad (3.6)$$

or the condition may also be written

$$E = \begin{cases} 1 \\ 2 \end{cases} \quad \text{if } x_0 z_1 + x_1 z_0 \begin{cases} \leq 0 \\ > 0 \end{cases} \quad (3.6a)$$

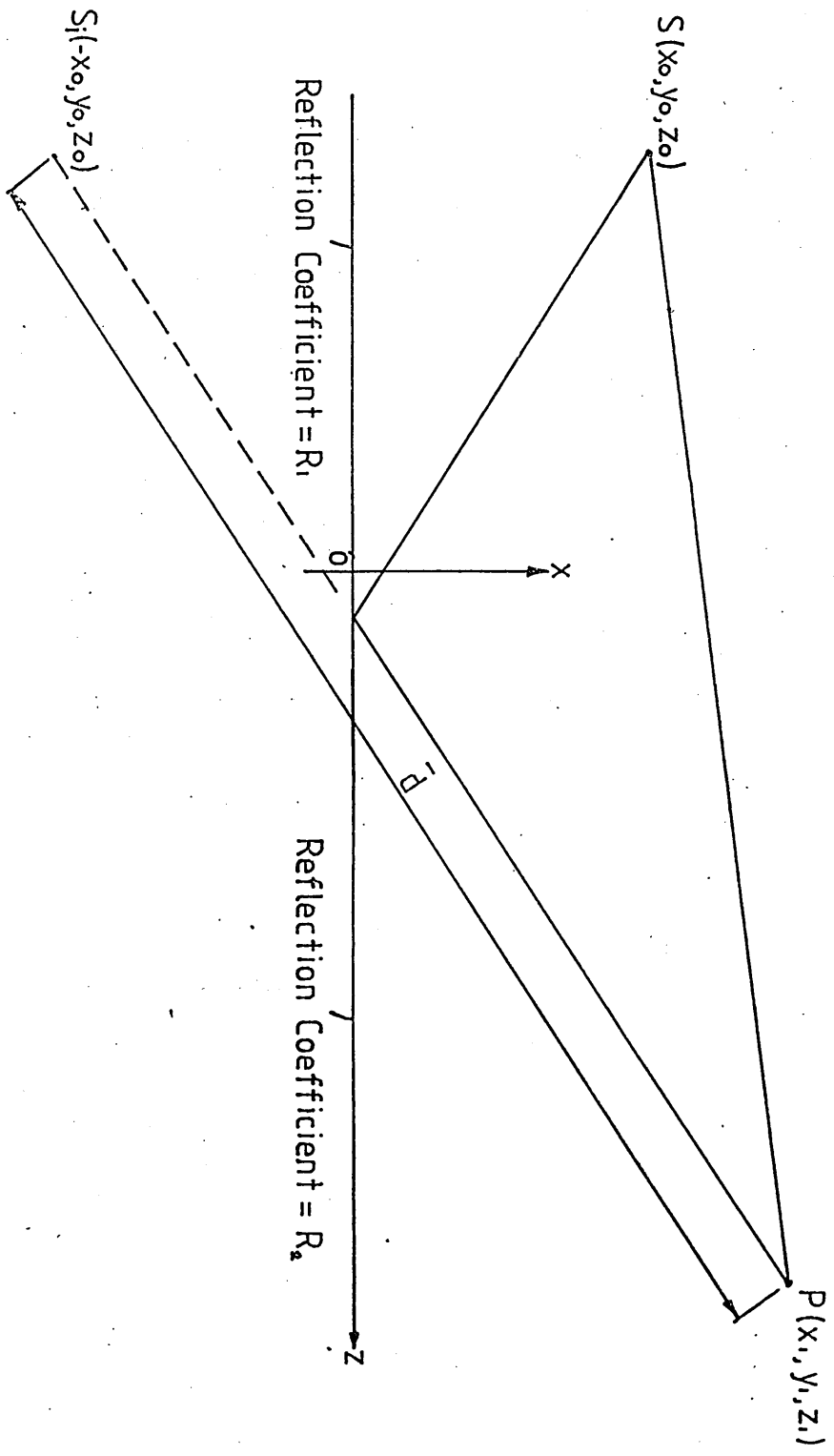


Figure 3.2.

Hence, in view of equations (3.2), (3.3) and (3.4), the disturbance  $U_o(P)$  without the barrier is given by

$$U_o(P) = A \left[ \frac{e^{ikd}}{d} + R_E \frac{e^{ik\bar{d}}}{\bar{d}} \right], \quad (3.7)$$

where  $R_E$  is determined by equation (3.6)

Now, by invoking equation (2.4), the Sound Pressure Level  $SPL_o(P)$  at  $P$  without the barrier may be expressed as follows

$$SPL_o(P) = SPL_1 + 10 \log_{10} \left[ \frac{1}{d^2} + \frac{R_E^2}{\bar{d}^2} + \frac{2R_E}{d\bar{d}} \cos k(\bar{d}-d) \right], \quad (3.8)$$

where  $SPL_1$  is the SPL at unit distance from  $S$  (see 2.2.2).

In the second case, where the source is at ground level,

there is no reflected ray component of  $U_o(P)$  and thus

$U_{o_2}(P)=0$ , and hence from equation (3.2),

$$U_o(P) = U_{o_1}(P), \quad (3.9)$$

and so the situation is identical to that of 2.2.2, where

$$SPL_o(P) = SPL_1 - 20 \log_{10} d. \quad (3.10)$$

### 3.2.2 Calculation of $SPL_P(P)$

As in 3.2.1, the two cases where first the source  $S$  is above ground level and secondly  $S$  is at ground level are considered separately.

When  $S$  is above ground level, there will be four different paths of diffracted rays with and without reflections on both sides of the barrier as illustrated in fig 3.3a. These components are illustrated independently in fig 3.3b. It

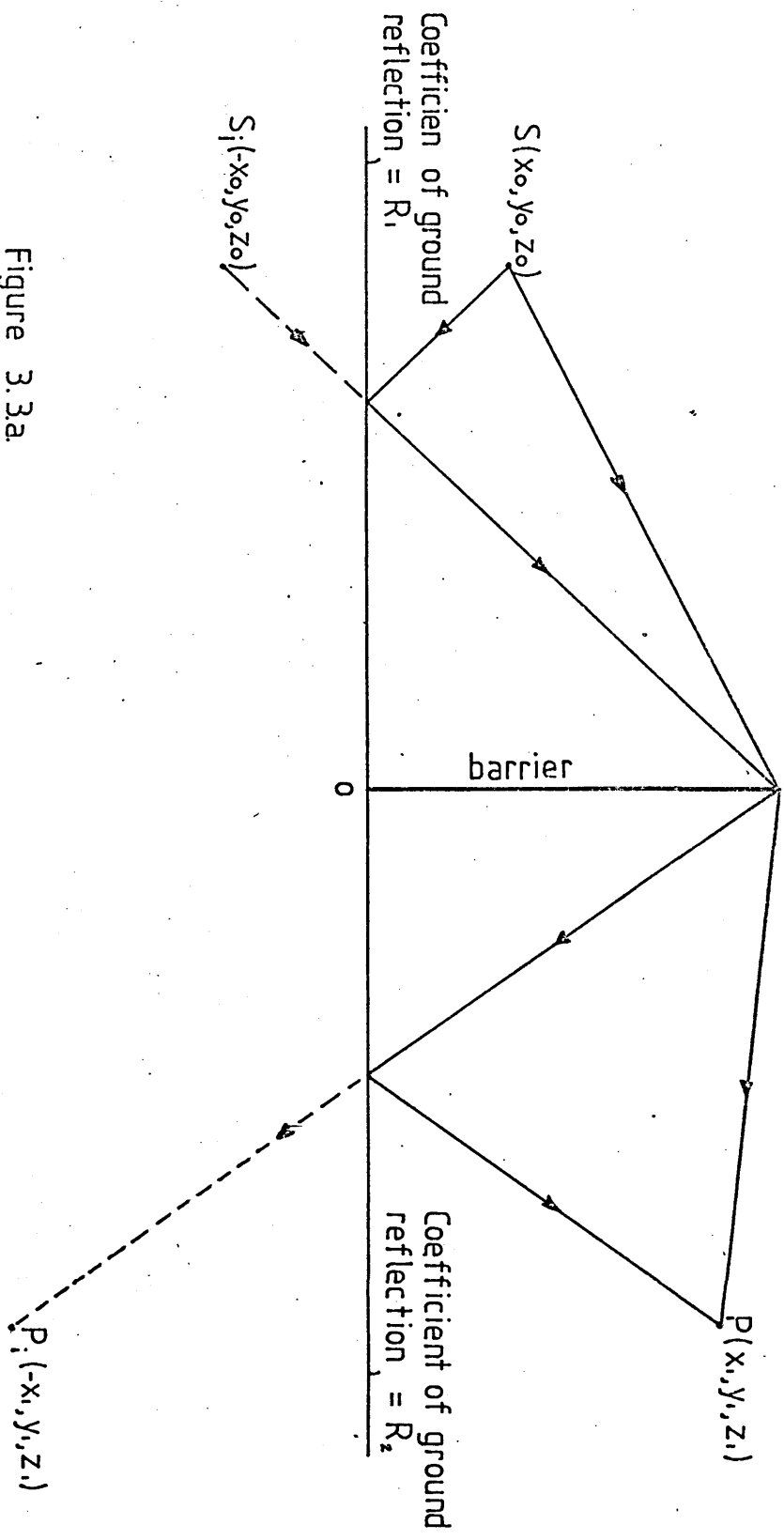
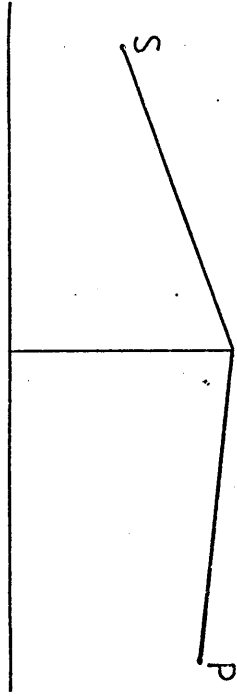
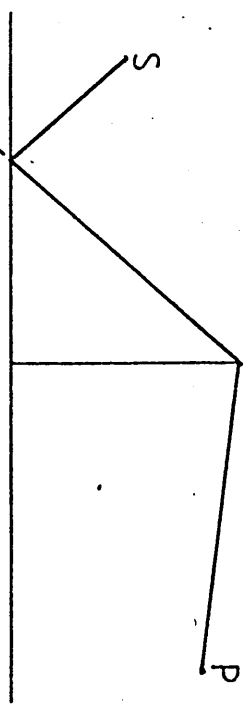


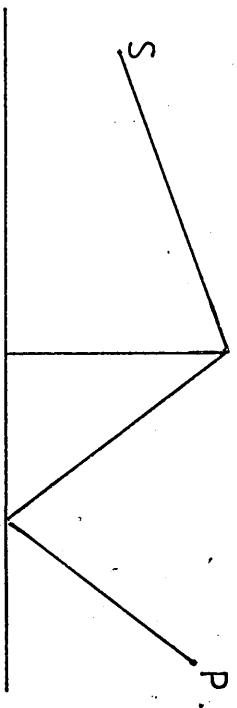
Figure 3.3a



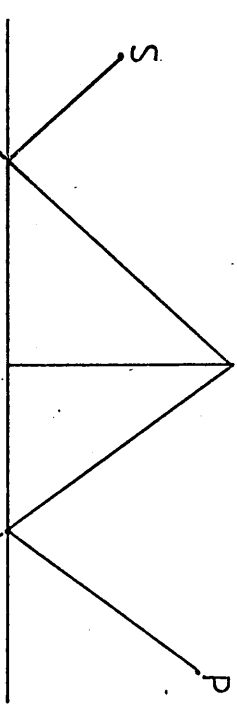
(i)  $P_i$   $S_i$



(ii)  $P_i$   $S_i$



(iii)  $P_i$   $S_i$



(iv)  $P_i$   $S_i$

may be noted that, as in 3.2.1, the image  $S_i$  of  $S$  is considered as the imaginary source of rays reflected by the ground on the source side of the barrier. Also, in a similar way, the image  $P_i$  of  $P$  is also introduced as the imaginary receiving position of rays reflected by the ground on the monitoring side of the barrier. Consider, for example, a ray which is reflected by the ground on both sides of the barrier (fig 3.3b (iv) ). Although the ray actually emanates from  $S$ , is reflected by the ground and diffracted by the barrier before being reflected again by the ground and then reaches  $P$ , it may equivalently be considered, for the purpose of calculation, to have emanated from  $S_i$  before being refracted by the barrier directly to  $P_i$ . The expression for the disturbance  $U(P)$  at  $P$  in this situation is given by Maekawa [5] as

$$U(P) = U_1(P) + R_1 U_2(P) + R_2 U_3(P) + R_1 R_2 U_4(P) \quad (3.11)$$

where  $U_1(P)$  is the disturbance due to the non-reflected component of the sound field,  $U_2(P)$  is the disturbance due to the component of the sound field reflected only on the source side of the barrier,  $U_3(P)$  is the disturbance due to the component of the sound field reflected only on the receiver's side of the barrier, and  $U_4(P)$  is the disturbance due to the component of the sound field reflected on both sides of the barrier.

#### U(P) As a Combination of Free-Field and Semi-Infinite Diffraction Components

It is required now to formulate expressions for  $U_1(P)$ ,  $U_2(P)$ ,  $U_3(P)$  and  $U_4(P)$ . Maekawa [15] has suggested

expressions which are suitable when the barrier is rectangular in shape and has no holes. Also it is apparent that in his method, there are limitations on where S and P may be positioned in relation to the barrier. Finally his method is an approximate one, and there is no facility for checking its accuracy in a given configuration, except by comparison with experimental results. In this work, expressions will be formulated for  $U_1(P)$ ,  $U_2(P)$ ,  $U_3(P)$  and  $U_4(P)$ , for a barrier of arbitrary shape and which may have holes. Also, there is no limitation on where S and P may be positioned relative to the barrier. Further, although some approximations are made, it is possible to make a check on the accuracy of the results in comparison with the exact theoretical solution, and therefore control the accuracy of the technique. The method described in this chapter is based on results gained in Chapter 2 for the free field situation and, to the author's knowledge, has not previously been devised by other authors. As in Chapter 2, the assumption will initially be made that the transmission of the barrier is zero.

The key to this method is the fact that with a barrier on a reflecting ground, diffraction by the barrier can only take place around those parts of the barrier's perimeter which are not in contact with the ground, which enables the following assumptions to be made. Consider firstly the component of disturbance  $U_1(P)$  which represents the non-reflected sound field at P with the barrier in position. This is exactly the same as the total disturbance which

would have been observed at P, if instead of the given configuration of barrier and reflecting ground, there was just the semi-infinite barrier shown in fig 3.4b in free-space. Let B be the region occupied by the original barrier in the xy-plane (see fig 3.4a) and let H be defined as the semi-infinite region in the xy-plane defined by  $\{x < 0, z = 0, \text{ all } y\}$ . Then the above assumption is stating that  $U_1(P)$  is the total disturbance at P due to a barrier occupying the region  $\{B \cup H\}$ .

In a similar way,  $U_2(P)$  may be expressed as the total disturbance at P in the presence of the screen occupying the region  $\{H \cup B\}$  where the source is placed at  $S_i(-x_0, y_0, z_0)$ , the image of S in the reflecting ground (see fig 3.5).

$U_2(P)$  represents the component of the disturbance at P due to that part of the sound field which is reflected by the ground on the source side of the barrier. Similarly  $U_3(P)$  may be expressed as the total disturbance at  $P_i(-x_1, y_1, z_1)$  with the source at S in the presence of the screen  $\{H \cup B\}$ , since  $U_3(P)$  represents the component of the disturbance at P due to that part of the sound field which is reflected by the ground on the monitoring position side of the barrier (see fig 3.6). Finally, in the same way,  $U_4(P)$  may be represented as the total disturbance at  $P_i$  due to the source at  $S_i$  in the presence of the screen  $\{H \cup B\}$  (see fig 3.7).

It will now be necessary to formulate  $U_1(P), U_2(P), U_3(P)$  and  $U_4(P)$  in view of the above assumptions. Let  $\overline{H \cup B}$  represent

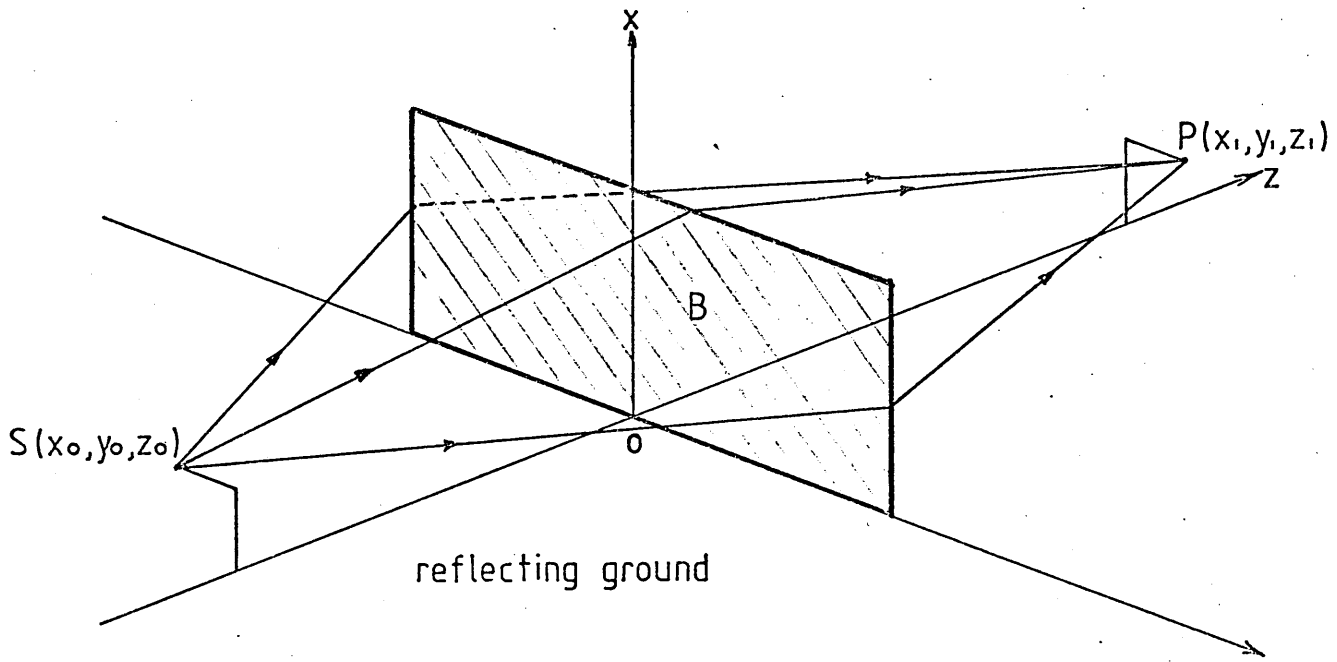


Figure 3.4.a.

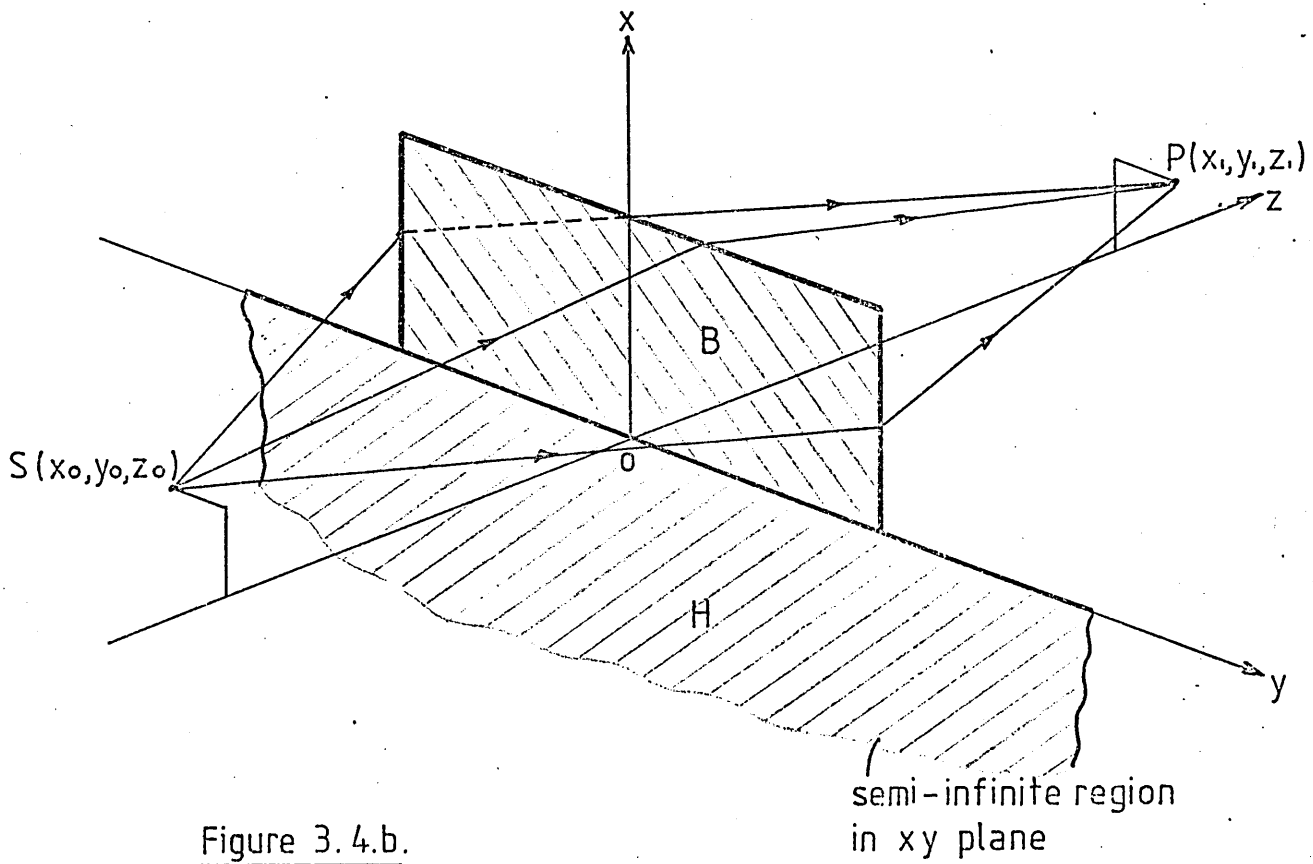


Figure 3.4.b.

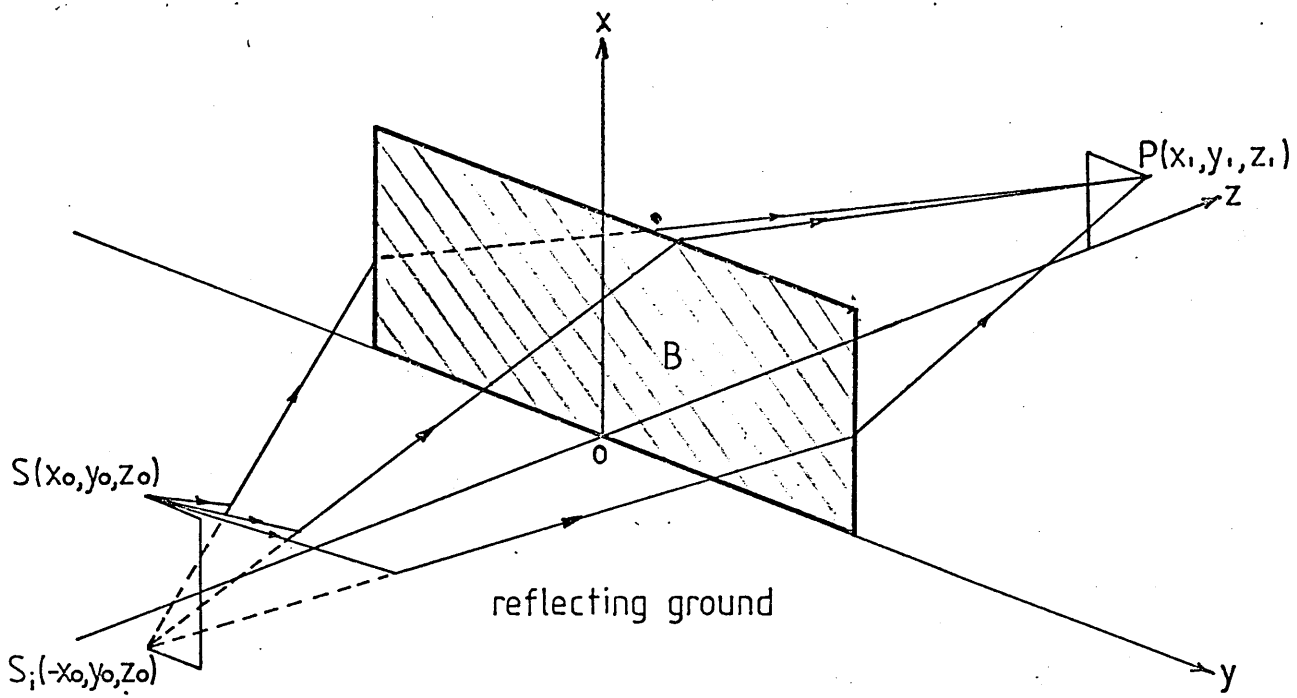


Figure 3.5.a.

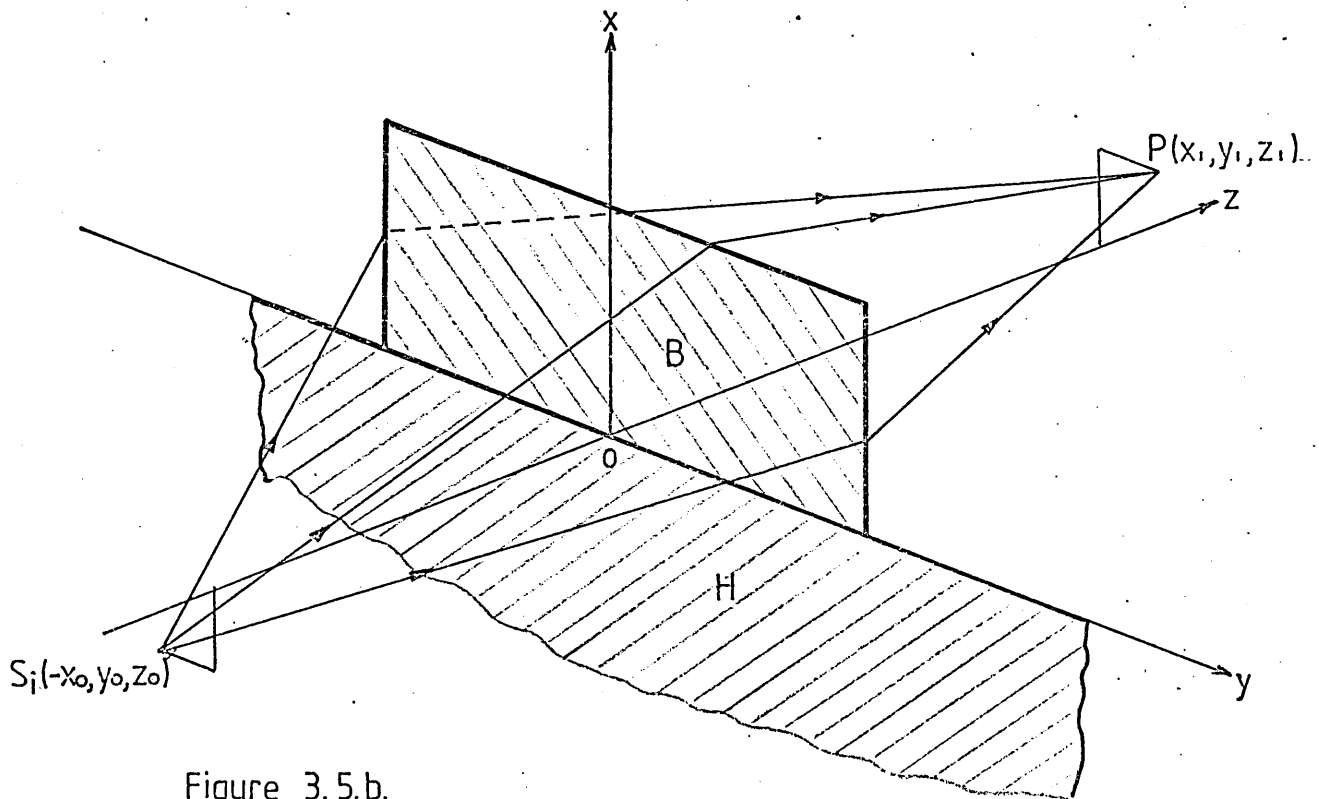


Figure 3.5.b.

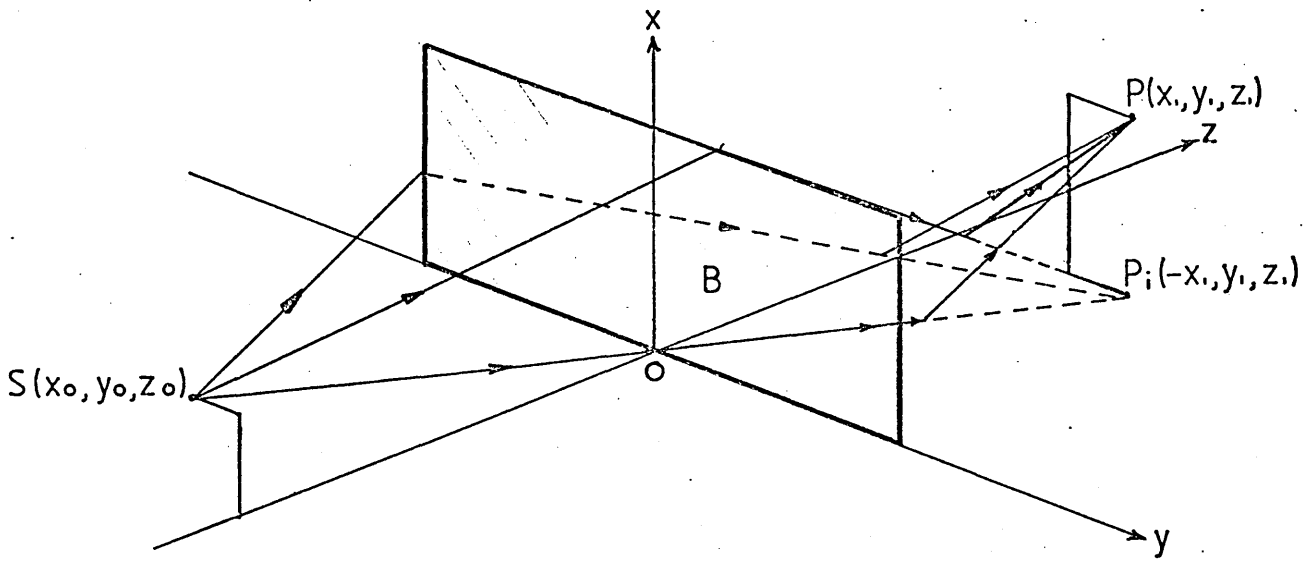


Figure 3.6.a.

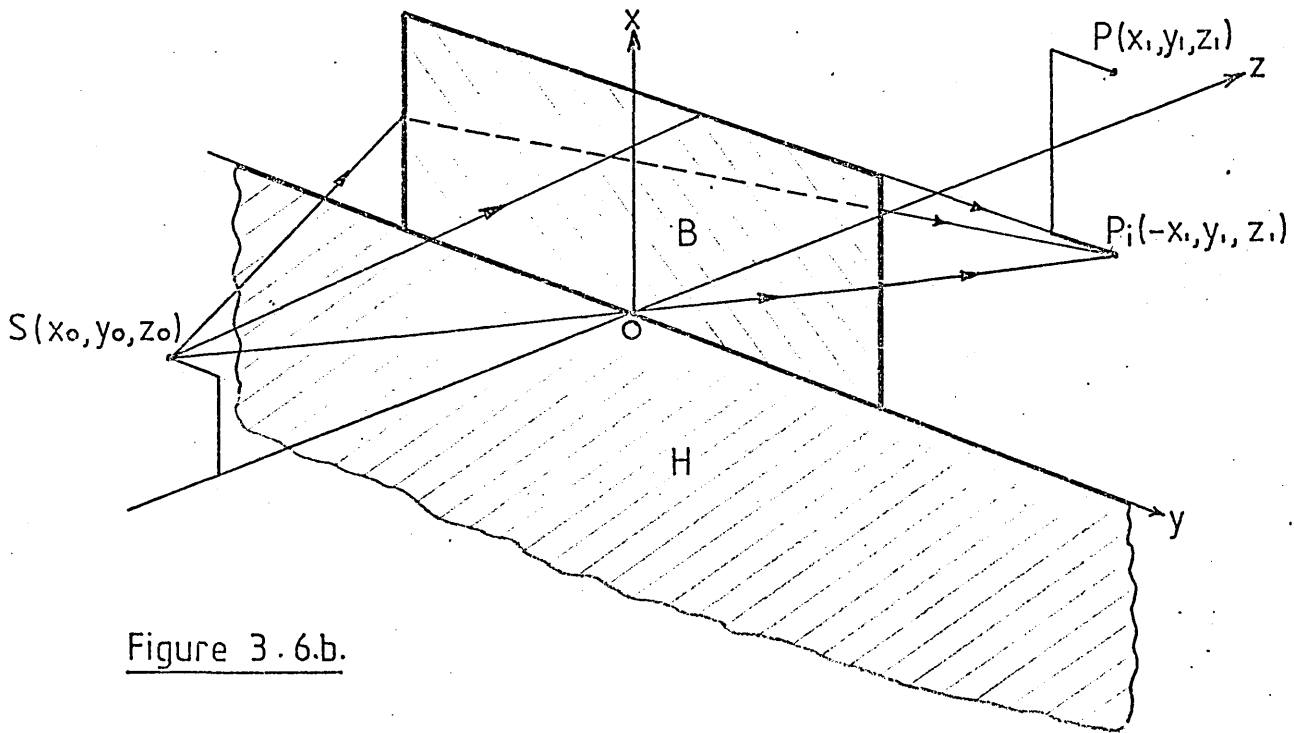


Figure 3.6.b.

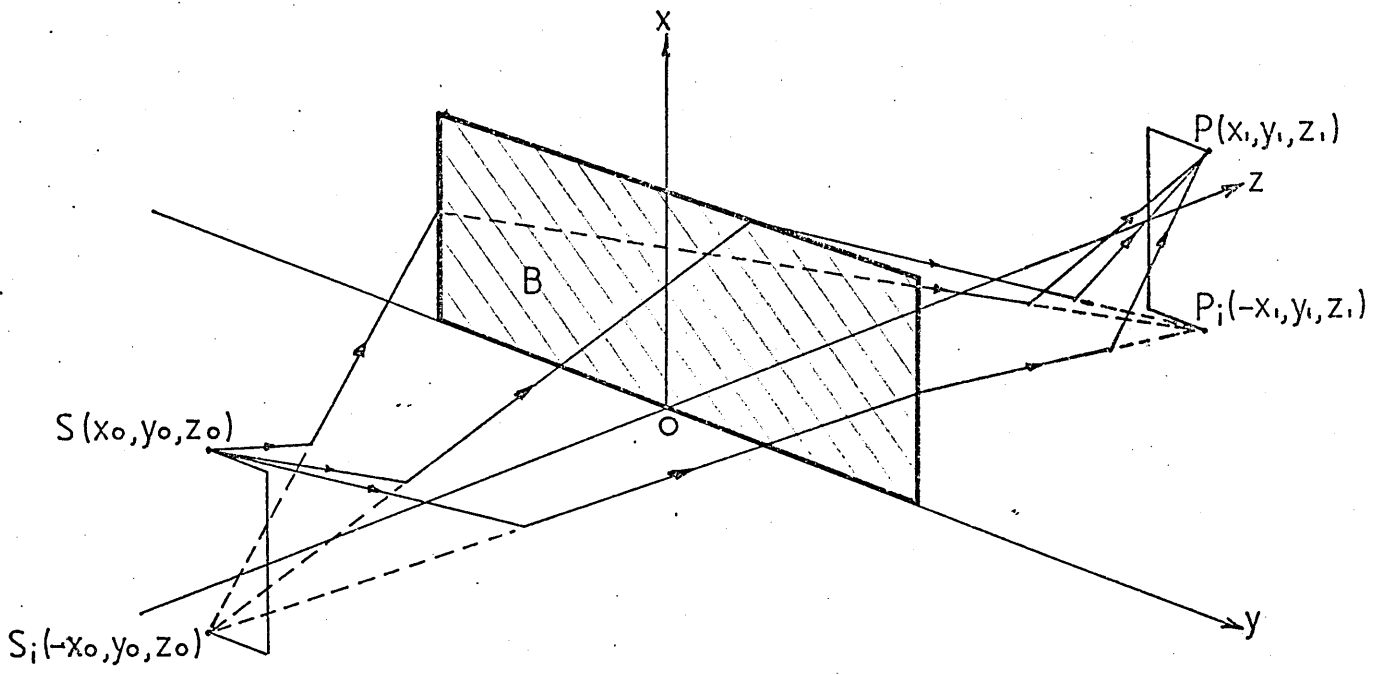


Figure 3.7.a.

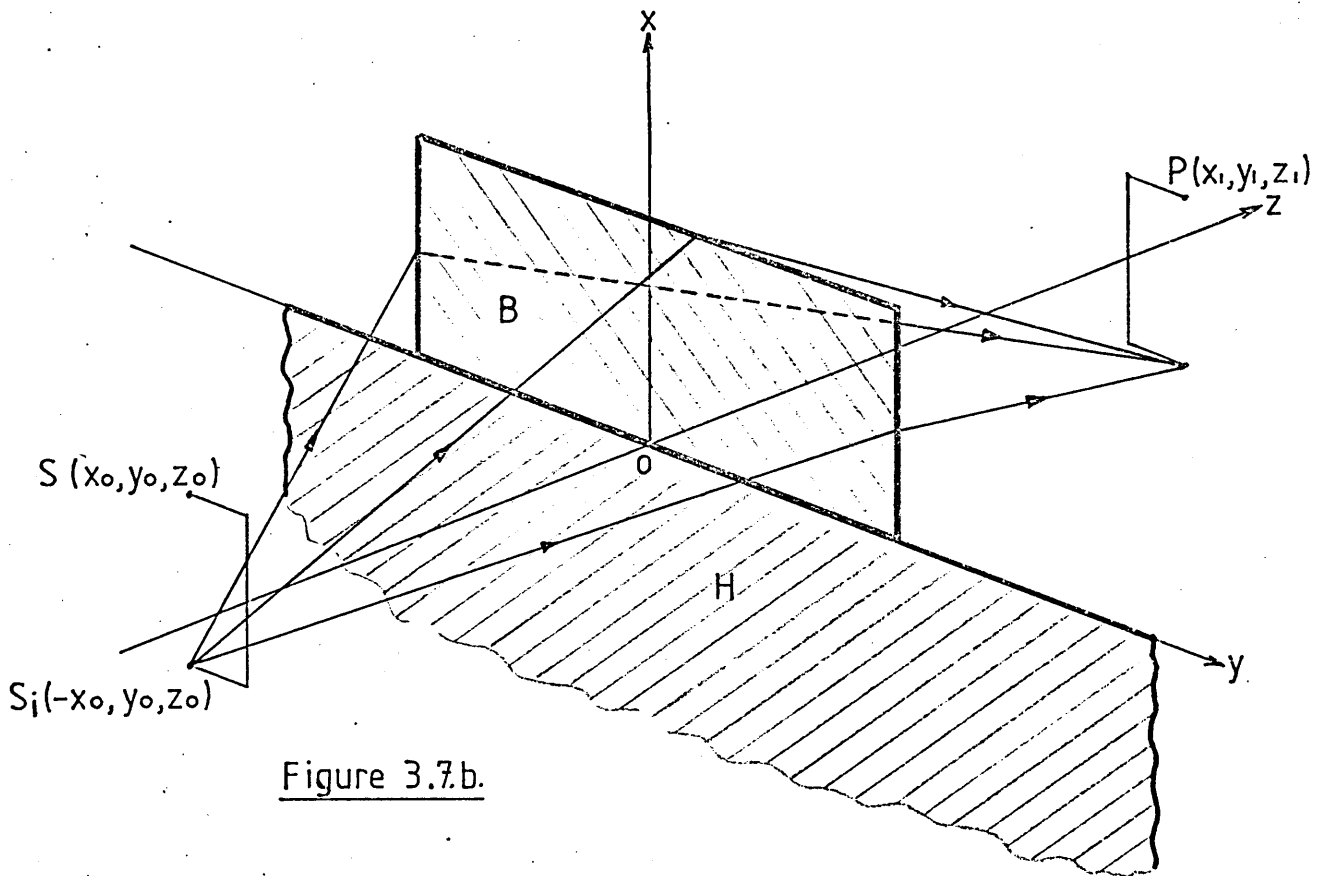


Figure 3.7.b.

that region of the xy-plane which is the complement of the region HUB (see fig 3.8). In other words,  $\overline{\text{HUB}}$  is that part of the xy-plane where  $x \geq 0$  except for the region B. Assume briefly that the xy-plane is now occupied by a screen occupying the region  $\overline{\text{HUB}}$  and that nothing occupies HUB.

Let  $U_1^-(P), U_2^-(P), U_3^-(P)$  and  $U_4^-(P)$  represent the disturbances where the source, monitoring position are at  $(S, P), (S_i, P), (S, P_i)$  and  $(S_i, P_i)$  respectively in this configuration.

Then, by the theory of Fresnel diffraction, (see Born and Wolf [12]).

$$\left. \begin{aligned}
 U_1^-(P) &= -\frac{Ai}{2\lambda} \iint_{\text{HUB}} \frac{e^{ik(\ell+m)}}{\ell m} [\cos(n, \ell) - \cos(n, m)] ds \\
 U_2^-(P) &= -\frac{Ai}{2\lambda} \iint_{\text{HUB}} \frac{e^{ik(\ell'+m)}}{\ell' m} [\cos(n, \ell') - \cos(n, m)] ds \\
 U_3^-(P) &= -\frac{Ai}{2\lambda} \iint_{\text{HUB}} \frac{e^{ik(\ell+m')}}{\ell m'} [\cos(n, \ell) - \cos(n, m')] ds \\
 U_4^-(P) &= -\frac{Ai}{2\lambda} \iint_{\text{HUB}} \frac{e^{ik(\ell'+m')}}{\ell' m'} [\cos(n, \ell') - \cos(n, m')] ds,
 \end{aligned} \right\} (3.12)$$

where  $\ell', m'$  represent the distances from  $S_i$  and  $P_i$  respectively to the variable point of integration on HUB. (cf equation(2.8)).

Also, by Babinet's Principle,

$$\left. \begin{aligned}
 U_1(P) &= U_0^S(P) - U_1^-(P) \\
 U_2(P) &= U_0^S(P) - U_2^-(P) \\
 U_3(P) &= U_0^S(P_i) - U_3^-(P) \\
 \text{and} \\
 U_4(P) &= U_0^S(P_i) - U_4^-(P),
 \end{aligned} \right\} (3.13)$$

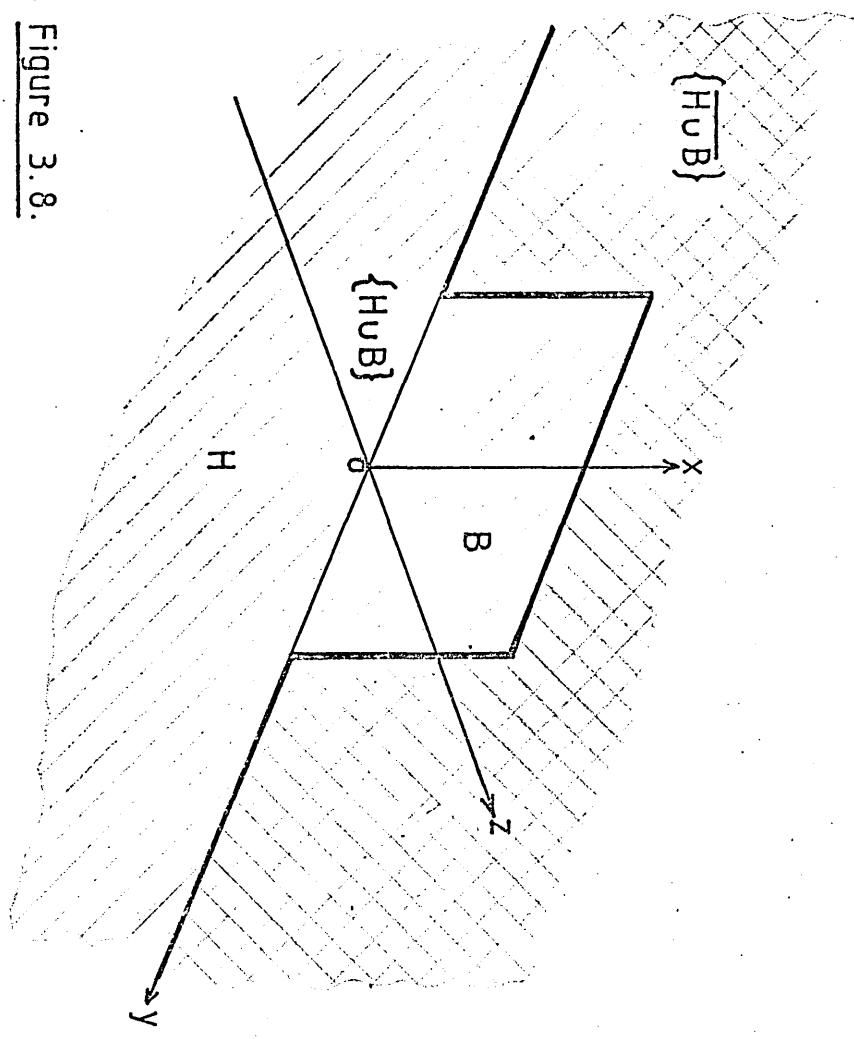


Figure 3.8.

where  $U_0^S(P)$  is the free field disturbance at P in the absence of any screen or ground due to the source at S.  $U_0^{S_i}(P)$ ,  $U_0^S(P_i)$  and  $U_0^{S_i}(P_i)$  are similarly defined except for the obvious difference in positions of the source and monitoring position. Now  $U_0^S(P)$  has already been formulated in equation (2.2). The other terms may be similarly formulated as follows:

$$\left. \begin{aligned}
 U_0^S(P) &= \frac{Ae^{ikd}}{d} \\
 U_0^{S_i}(P) &= \frac{Ae^{ik\bar{d}}}{\bar{d}} \\
 U_0^S(P_i) &= \frac{Ae^{ik\bar{d}}}{\bar{d}} \\
 U_0^{S_i}(P_i) &= \frac{Ae^{ikd}}{d} \quad ,
 \end{aligned} \right\} \quad (3.14)$$

where  $d = \text{distance } \overline{SP} = \text{distance } \overline{SP}$  and  $\bar{d} = \text{distance } \overline{S_iP}$   
 $= \text{distance } \overline{SP_i}$ .

Now, due to standard properties of integration over an area, the double integrals over the region HUB in equations (3.12) may be split into the sums of separate double integrals over the regions H and B as follows:

$$\begin{aligned}
U_1^-(P) &= -\frac{Ai}{2\lambda} \left[ \iint_H + \iint_B \frac{e^{ik(\ell+m)}}{\ell m} [\cos(n, \ell) - \cos(n, m)] ds \right] \\
U_2^-(P) &= -\frac{Ai}{2\lambda} \left[ \iint_H + \iint_B \frac{e^{ik(\ell'+m)}}{\ell' m} [\cos(n, \ell') - \cos(n, m)] ds \right] \\
U_3^-(P) &= -\frac{Ai}{2\lambda} \left[ \iint_H + \iint_B \frac{e^{ik(\ell+m')}}{\ell m'} [\cos(n, \ell) - \cos(n, m')] ds \right] \\
U_4^-(P) &= -\frac{Ai}{2\lambda} \left[ \iint_H + \iint_B \frac{e^{ik(\ell'+m')}}{\ell' m'} [\cos(n, \ell') - \cos(n, m')] ds \right]
\end{aligned}
\tag{3.15}$$

Let  $U_H^s(P)$  denote the disturbance at P due to the source at S in the presence of the half-plane screen which occupies the half-plane H only. Let the terms  $U_H^{s_i}(P)$ ,  $U_H^s(P_i)$ ,  $U_H^{s_i}(P_i)$  be similarly defined. Then by use of the Fresnel diffraction theory and Babinet's principle (see Born and Wolf [12]), it can be shown that the following equations apply

$$\begin{aligned}
U_H^s(P) &= U_O^s(P) + \frac{Ai}{2\lambda} \iint_H \frac{e^{ik(\ell+m)}}{\ell m} [\cos(n, \ell) - \cos(n, m)] ds \\
U_H^{s_i}(P) &= U_O^{s_i}(P) + \frac{Ai}{2\lambda} \iint_H \frac{e^{ik(\ell'+m)}}{\ell' m} [\cos(n, \ell') - \cos(n, m)] ds \\
U_H^s(P_i) &= U_O^s(P_i) + \frac{Ai}{2\lambda} \iint_H \frac{e^{ik(\ell+m')}}{\ell m'} [\cos(n, \ell) - \cos(n, m')] ds \\
U_H^{s_i}(P_i) &= U_O^{s_i}(P_i) + \frac{Ai}{2\lambda} \iint_H \frac{e^{ik(\ell'+m')}}{\ell' m'} [\cos(n, \ell') - \cos(n, m')] ds
\end{aligned}
\tag{3.16}$$

By substituting equations (3.16) and (3.15) into equations (3.13) it follows that

$$\begin{aligned}
 U_1(P) &= U_H^S(P) + \frac{Ai(1-\alpha)}{2\lambda} \iint_B \frac{e^{ik(\ell+m)}}{\ell m} \cdot [\cos(n, \ell) - \cos(n, m)] ds \\
 U_2(P) &= U_H^{Si}(P) + \frac{Ai(1-\alpha)}{2\lambda} \iint_B \frac{e^{ik(\ell'+m)}}{\ell' m'} \cdot [\cos(n, \ell') - \cos(n, m)] ds \\
 U_3(P) &= U_H^S(P_i) + \frac{Ai(1-\alpha)}{2\lambda} \iint_B \frac{e^{ik(\ell+m')}}{\ell m'} \cdot [\cos(n, \ell) - \cos(n, m')] ds \\
 U_4(P) &= U_H^{Si}(P_i) + \frac{Ai(1-\alpha)}{2\lambda} \iint_B \frac{e^{ik(\ell'+m')}}{\ell' m'} \cdot [\cos(n, \ell') - \cos(n, m')] ds,
 \end{aligned}
 \tag{3.17}$$

where the transmission coefficient  $\alpha$  of the finite barrier is taken into account.

The double integrals on the right-hand sides of equations (3.17) can be solved in the same way as in Chapter 2 and can thus be converted directly into a form suitable for solution by computer, when the parameters of a given configuration are known. It thus remains to express the terms  $U_H^S(P)$ ,  $U_H^{Si}(P)$ ,  $U_H^S(P_i)$  and  $U_H^{Si}(P_i)$  in an equally suitable form.

### The Half-Plane Diffraction Components

Let  $S'(x_0', y_0', z_0')$  represent a source of wavelength  $\lambda$ , and let  $P'(x_1', y_1', z_1')$  represent a general receiver's position in a free space environment which also contains the non-transmitting half-plane screen  $H$  (see fig 3.9).

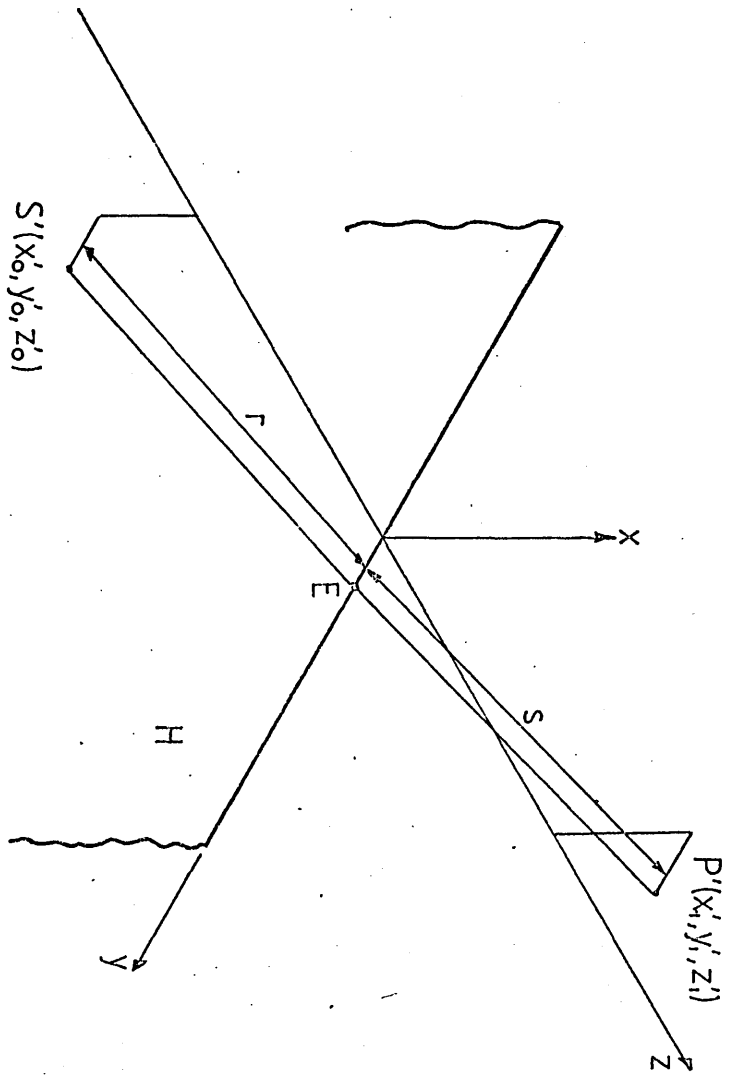


Figure 3.9. The Points  $S'$ ,  $P'$  and the Half Plane Screen  $H$

Then it will be required to determine the complex disturbance  $U_H^{S'}(P')$  at  $P'$  due to the source at  $S'$ . The four terms  $U_H^S(P)$ ,  $U_H^{Si}(P)$ ,  $U_H^S(P_i)$  and  $U_H^{Si}(P_i)$  will then follow immediately by replacing  $S'$  and  $P'$  with the appropriate symbols. The expression for  $U_H^{S'}(P')$  is based on the Sommerfeld wave solution (see Sommerfeld[16]), and has been expressed by Born and Wolf [12] in a form suitable for calculation based on the conventions adopted in this thesis. The Born and Wolf equation has been improved by Maekawa [5] for sound attenuation by a barrier and it is this last form which is used here. The Maekawa expression is as follows

$$U_H^{S'}(P') = -\frac{Aie^{ik(r'+s')}}{2(r'+s')} [ \{C(w') - S(w')\} + i \{1 + C(w') + S(w')\} ], \quad (3.18)$$

where

$$w' = \frac{+2}{\lambda} \sqrt{(r+s) - (r'+s')} , \quad (3.19)$$

and where  $r' + s'$  is the straight line distance from  $s'$  to  $P'$ ,  $r+s$  is the shortest distance from  $s'$  to  $P'$  via the edge of the screen (see fig 3.10) and  $C(w)$  and  $S(w)$  are the Fresnel integrals given by

$$\left. \begin{aligned} C(w) &= \int_0^w \cos\left(\frac{\pi v^2}{2}\right) dv \\ S(w) &= \int_0^w \sin\left(\frac{\pi v^2}{2}\right) dv \end{aligned} \right\} \quad (3.20)$$

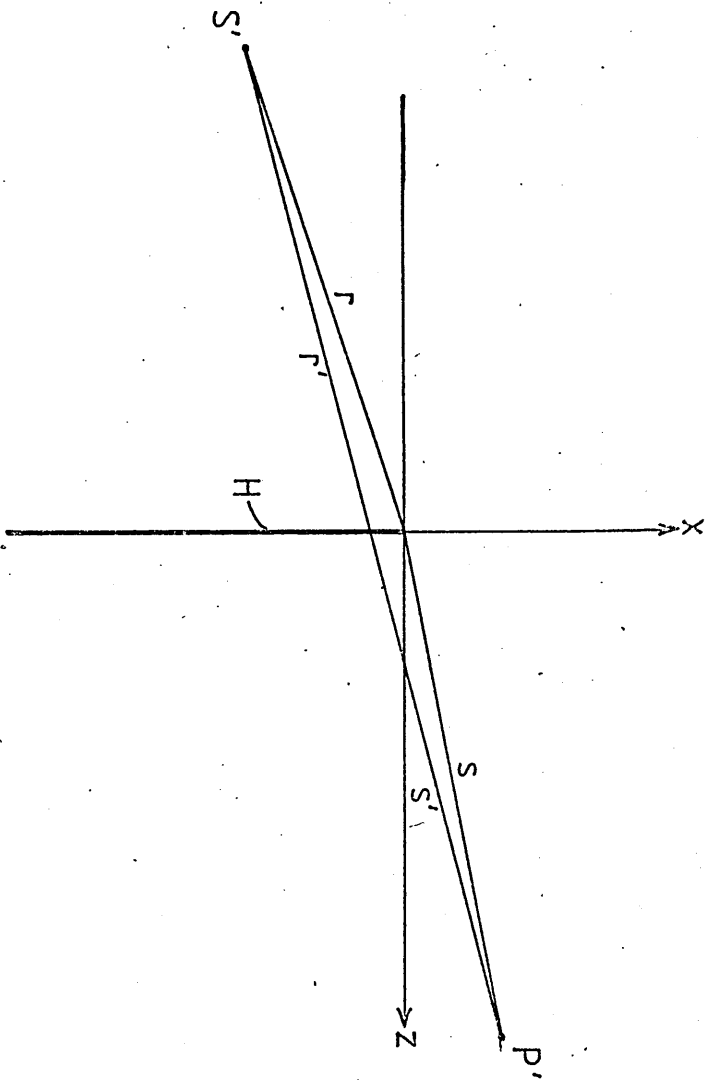


Figure 3.10. The Distances  $r, s, r'$  and  $s'$ .

Now  $r' + s'$  is the distance  $S'P'$ , which may be defined as  $d'$ , say, as follows

$$r' + s' = d' = \sqrt{[(x'_1 - x'_0)^2 + (y'_1 - y'_0)^2 + (z'_1 - z'_0)^2]} \quad (3.21)$$

The distances  $r$  and  $s$  are defined such that  $r + s$  is the shortest distance from  $S'$  to  $P'$  via the edge of the screen.

Let  $E'$  be any point on the edge of the screen with coordinates  $(0, y', 0)$ . Then  $\overline{S'E'} + \overline{E'P'}$  is the distance from  $S'$  to  $P'$  via the edge. Suppose  $E$  is the position such that  $\overline{S'E} = r$  and  $\overline{EP} = s$ , that is  $\overline{S'E} + \overline{EP}$  represents the shortest distance from  $S'$  to  $P'$  via the edge. Then it is required to find the value of  $y'$  which gives the solution  $E' = E$ , or in mathematical terms, it is required to minimise  $\overline{S'E'} + \overline{E'P'}$  with respect to  $y'$ . By using elementary calculus, the solution may be shown to be

$$y'' = \frac{d'_0 y'_0 + d'_1 y'_1}{d'_0 + d'_1} \quad (3.22)$$

where

$$\left. \begin{aligned} d'_0 &= \sqrt{(x'_0)^2 + (z'_0)^2} \\ d'_1 &= \sqrt{(x'_1)^2 + (z'_1)^2} \end{aligned} \right\} \quad (3.23)$$

it follows that

$$\left. \begin{aligned} r &= \overline{S'E} = \frac{d'_0}{d'_0 + d'_1} \left( (d'_0 + d'_1)^2 + (y'_1 - y'_0)^2 \right)^{1/2} \\ s &= \overline{EP} = \frac{d'_1}{d'_0 + d'_1} \left( (d'_0 + d'_1)^2 + (y'_1 - y'_0)^2 \right)^{1/2} \end{aligned} \right\} \quad (3.24)$$

so that

$$r + s = \sqrt{[(d'_0 + d'_1)^2 + (y'_1 - y'_0)^2]} \quad (3.25)$$

In equation (3.19) it can be seen that there are two possible values of  $w'$ , one positive and the other negative. This accounts for the two alternatives where  $P'$  lies in the shadow zone or the bright zone of  $H$  with respect to  $S'$  (see fig 3.11), where the positive value represents the shadow zone. Let  $w'_+$  represent the positive value. Then  $U_H^{S'}(P')$  may be written in terms of  $w'_+$  as follows

$$U_H^{S'}(P') = \left\{ \begin{array}{l} -\frac{Aie^{ikd'}}{2d'} [ \{C(w'_+) - S(w'_+)\} + i \{1 + C(w'_+) + S(w'_+)\} ] \\ \frac{Ae^{ikd'}}{d'} + \frac{Aie^{ikd'}}{2d'} [ \{C(w'_+) - S(w'_+)\} + i \{1 + C(w'_+) + S(w'_+)\} ] \end{array} \right\} \quad (3.26)$$

the first equation applying when  $P'$  is in the shadow zone of  $H$  with respect to  $S'$  and the second equation where  $P'$  is in the bright zone,  $d'$  given by equation (3.21).

Now the four terms  $U_H^S(P)$ ,  $U_H^{S_i}(P)$ ,  $U_H^S(P_i)$  and  $U_H^{S_i}(P_i)$  may be considered.

First, since  $S$  and  $P$  are both above ground level, it is clear that  $P$  is in the bright zone of  $H$  with respect to  $S$ . Also from equation (2.27)  $d$  is the distance  $\overline{SP}$  and in this case

$$r + s = \sqrt{[(d_0 + d_1)^2 + (y_1 - y_0)^2]} \quad (3.27)$$

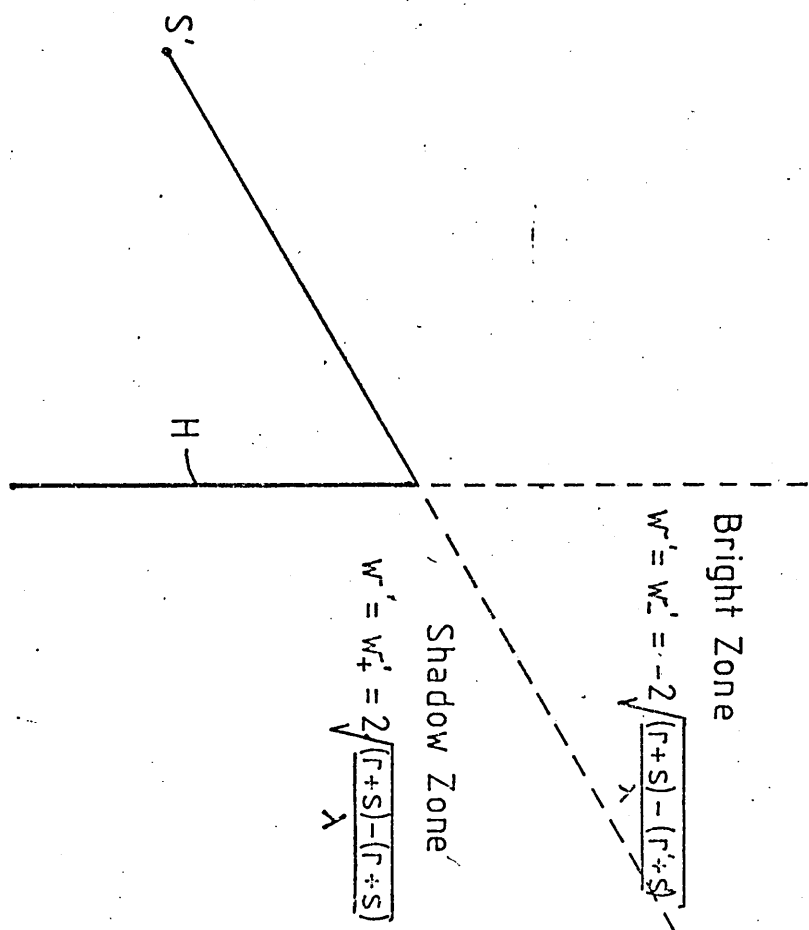


Figure 3.11. The Bright and Shadow Zones of S' with respect to H.

where

$$\left. \begin{aligned} d_0 &= \sqrt{(x_0^2 + x_0^2)} \\ d_1 &= \sqrt{(x_1^2 + z_1^2)} \end{aligned} \right\} \quad (3.28)$$

[compare with equation (3.25) and (3.23)].

Let

$$w = \sqrt{\left(\frac{r+s}{\lambda} - d\right)} \quad (3.29)$$

Then from equation (3.26),

$$U_H^S(P) = \frac{Ae^{ikd}}{d} + \frac{Aie^{ikd}}{2d} \cdot [\{C(w) - S(w)\} + i\{1 + C(w) + S(w)\}] \quad (3.30)$$

Next, since  $S_i$  and  $P_i$  are both below ground level, it follows that  $P_i$  is in the shadow zone of H with respect to  $S_i$ . Also  $d$  is the distance  $\overline{S_i P_i}$  (see note after equation (3.14)). Hence from equation (3.26),

$$U_H^{S_i}(P_i) = \frac{-Aie^{ikd}}{2d} \cdot [\{C(w) - S(w)\} + i\{1 + C(w) + S(w)\}] \quad (3.31)$$

In considering the terms  $U_H^{S_i}(P)$  and  $U_H^S(P_i)$ , it is

necessary to establish whether P is in the bright or shadow zone of H with respect to  $S_i$  and whether  $P_i$  is in the bright or shadow zone of H with respect to S. It is obvious, and can be proved geometrically, that

P is in the  $\left\{ \begin{array}{l} \text{bright} \\ \text{shadow} \end{array} \right\}$  zone of H with respect to  $S_i$

if and only if

$P_i$  is in the  $\left\{ \begin{array}{l} \text{shadow} \\ \text{bright} \end{array} \right\}$  zone of H with respect to S (3.32)

(see fig 3.12).

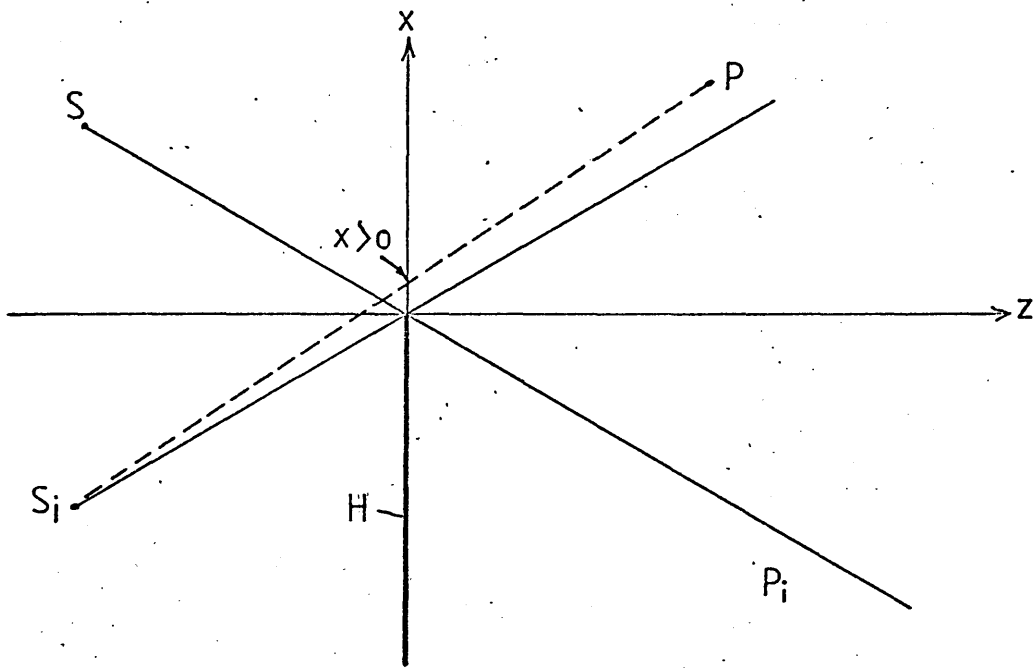


Figure 3.12.a.  $P_i$  in Shadow Zone of H with respect to S  
 $\Leftrightarrow$  P in Bright Zone of H with respect to  $S_i$

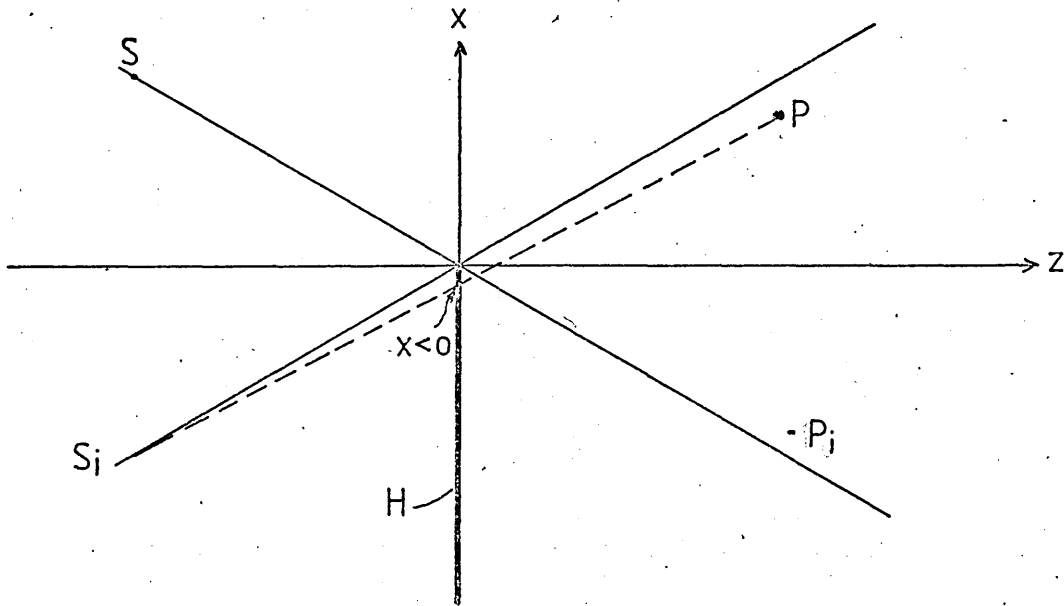


Figure 3.12.b.  $P_i$  in Bright Zone of H with respect to S  
 $\Leftrightarrow$  P is in Shadow Zone of H with respect to  $S_i$

Hence it is sufficient to establish whether P is in the shadow zone or the bright zone of H with respect to  $S_i$ . Again referring to figures 3.12a and 3.12b, it can be seen that if P is in the bright zone with respect to  $S_i$ , then the line  $S_iP$  passes above the edge of the barrier and if P is in the shadow zone, then  $S_iP$  passes below the edge of the barrier. These two alternatives can be formulated by saying that in the former case  $x \geq 0$  on  $S_iP$  when  $z=0$  and in the latter case  $x < 0$  on  $S_iP$  when  $z=0$ .

On the line  $S_iP$ , the following relation holds

$$\frac{x + x_0}{x_1 + x_0} = \frac{z - z_0}{z_1 - z_0} .$$

Hence, when  $z = 0$ ,

$$x = -\frac{(x_0 z_1 + x_1 z_0)}{z_1 - z_0}$$

and so  $x \geq 0$  if and only if  $x_0 z_1 + x_1 z_0 \leq 0$ .

It may therefore be deduced that

P is in the  $\left\{ \begin{array}{l} \text{bright} \\ \text{shadow} \end{array} \right\}$  zone of H with respect to  $S_i$

if  $x_0 z_1 + x_1 z_0 \left\{ \begin{array}{l} \leq 0 \\ > 0 \end{array} \right\}$  . (3.33)

Note that this condition is the same as that in equation (3.6) where it was required to ascertain whether sound reflection by the ground in the absence of a barrier occurred on the source or receiver side of the xy-plane.

It now follows from equation (3.26) that

$$U_H^{S_i}(P) = \begin{cases} \frac{Ae^{ik\bar{d}}}{\bar{d}} + \frac{Aie^{ik\bar{d}}}{2\bar{d}} \cdot [\{C(\bar{w})-S(\bar{w})\} + i\{1+C(\bar{w})+S(\bar{w})\}] \\ \quad \text{if } (x_0 z_1 + x_1 z_0) \leq 0 \\ \\ \frac{-Aie^{ik\bar{d}}}{2\bar{d}} \cdot [\{C(\bar{w})-S(\bar{w})\} + i\{1+C(\bar{w})+S(\bar{w})\}] \\ \quad \text{if } (x_0 z_1 + x_1 z_0) > 0 \end{cases} \quad (3.34)$$

and because of the expression (3.32),

$$U_H^S(P_i) = \begin{cases} \frac{-Aie^{ik\bar{d}}}{2\bar{d}} \cdot [\{C(\bar{w})-S(\bar{w})\} + i\{1+C(\bar{w})+S(\bar{w})\}] \\ \quad \text{if } (x_0 z_1 + x_1 z_0) \leq 0 \\ \\ \frac{Ae^{ik\bar{d}}}{2\bar{d}} + \frac{Aie^{ik\bar{d}}}{2\bar{d}} [\{C(\bar{w})-S(\bar{w})\} + i\{1+C(\bar{w})+S(\bar{w})\}] \\ \quad \text{if } (x_0 z_1 + x_1 z_0) > 0 , \end{cases} \quad (3.35)$$

where

$$\bar{w} = \sqrt{\left(\frac{r+s}{\lambda} - \bar{d}\right)} \quad (3.36)$$

(Compare with equation (3.29), and where  $\bar{d}$  is the distance  $\overline{S_i P}$  which is also the distance  $\overline{SP_i}$  and  $\bar{d}$  is given by equation (3.5). The term  $r+s$  is that given by equation (3.27) since the same terms  $(y_1 - y_0)^2$  and  $d_0$  and  $d_1$  (see equations (3.28)) are equally applicable whether the points  $S$  or  $S_i$  and  $P$  or  $P_i$  are under consideration.

#### Final Formulation of $U(P)$ , Where $S$ is Above Ground Level

Now if the function  $I_n(a,b)$  is defined by

$$I_n(a,b) = \frac{i(-\alpha)}{2\lambda} \iint_B \frac{e^{ik(a+b)}}{ab} \cdot [\cos(n,a) - \cos(n,b)] dS, \quad (3.37)$$

and the function  $G(v)$  is defined by

$$G(v) = \{C(v)-S(v)\} + i \{ | +C(v)+S(v) \} , \quad (3.38)$$

then from equations (3.30), (3.31), (3.34), (3.35), (3.17) and (3.11), the disturbance  $U(P)$  in the presence of the finite barrier on the reflecting ground satisfies the following equation

$$\begin{aligned} \frac{U(P)}{A} = & I_n(\ell, m) + R_1 I_n(\ell', m) + R_2(\ell, m') + R_1 R_2 I_n(\ell', m') \\ & + \frac{e^{ikd}}{\bar{d}} + \frac{ie^{ikd}}{2\bar{d}} \cdot (1 - R_1 R_2) G(w) + (-1)^E (R_2 - R_1) \frac{ie^{ik\bar{d}}}{2\bar{d}} \cdot G(\bar{w}) + R_1 \frac{E e^{ik\bar{d}}}{\bar{d}} , \end{aligned} \quad (3.39)$$

where  $E$  is given by equation (3.6a)

Note that this is the expression for  $U(P)$  where  $S$  is above ground level.

#### Formulation of $U(P)$ , Where $S$ is on the Ground

The situation where the source is at ground level is illustrated in fig (3.13). In this case ground reflection will only occur on the receiver's side of the barrier and consequently there are only two components of the disturbance  $U(P)$ . Therefore  $U(P)$  is given by

$$U(P) = U_1(P) + R_2 U_3(P) \quad (3.40)$$

(see Maekawa) [5])

where  $R_2$  is the coefficient of ground reflection on the receiver's side of the barrier. [Compare with equation (3.11)]. It can be shown that  $U_1(P)$  and  $U_3(P)$  are the same as defined at the beginning of this section and

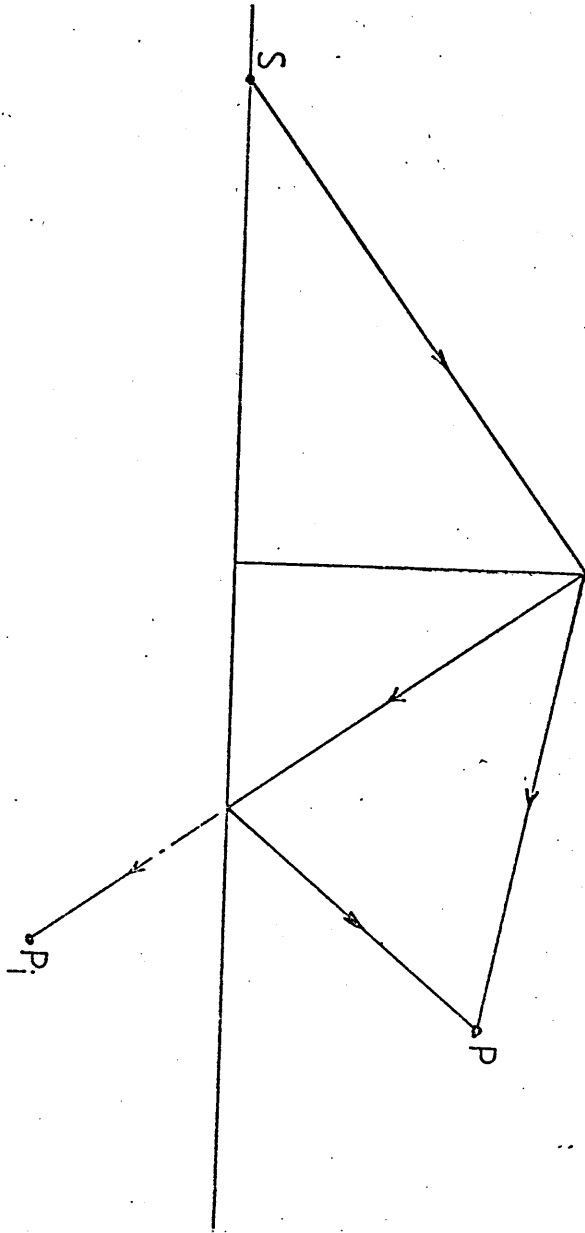


Figure 3.13. Ray Paths when S is on the Ground

therefore are given by the first and third formulae in equations (3.17). It follows that in this case,  $U(P)$  is given as follows:

$$\frac{U(P)}{A} = I_n(\ell, m) + R_2(\ell, m') + \frac{e^{ikd}}{d} + \frac{ie^{ikd}}{2d} \cdot G(w) + (-|)^E \frac{R_2 ie^{ik\bar{d}}}{\bar{d}} + \frac{1}{2} (1+(-1)^E) \frac{e^{ik\bar{d}}}{\bar{d}} \quad (3.41)$$

[Compare with equation(3.39)].

### Formulation of $SPL_B(P)$

$SPL_B(P)$  is expressed in terms of  $\frac{U(P)}{A}$  by combining equations (2.4) and (2.6) to give:

$$SPL_B(P) = SPL_1 + |0| \log_{10} \left| \frac{U(P)}{A} \right|^2 \quad (3.42)$$

From this, the Sound Pressure Level  $SPL_B(P)$  in the presence of the barrier is given by substituting either equation (3.39) or (3.41) into equation (3.42) according as the source S is respectively above or at ground level.

### 3.2.3 Formulation of $IL(P)$

The Insertion Loss  $IL(P)$  at P due to interposing the barrier follows from equation (3.1) and has two possible solutions.

Firstly, if the source is above ground level then  $IL(P)$  is given by substituting equations (3.8) and (3.42) into equation (3.1), where  $\frac{U(P)}{A}$  is given by equation (3.39).

Secondly, if the source is on the ground, then  $IL(P)$  is given by substituting equations (3.10) and (3.42) into equation (3.1), where  $\frac{U(P)}{A}$  is given by equation (3.41).

Note now that the above equations, in a similar way to that described in 2.2.4 for the free field case, can be solved if the parameters relating to the configuration are known. These parameters are those listed in 2.2.4 with the addition of the coefficients of ground reflections  $R_1$  and  $R_2$ . Hence, as was the case in Chapter 2, a computer program can again be written which performs the calculations in a given configuration. This program was developed by the author and is described in Chapter 4.

### 3.3. Summary

It was the aim of this chapter to obtain information about the sound pressure distribution when a plane finite barrier is placed in position on a reflecting ground. The theory makes use of the results obtained in Chapter 1 and in addition the 'Method of Images' of ground reflection is incorporated. The sound field between the source S and the monitoring position P is considered as the summation of separate sound fields, which follow different reflected paths between S and P. Formulae are obtained separately for the disturbances at P due to the separate component sound paths, and each formula is obtained by combining the theory of Chapter 2 with the theory of diffraction by a semi-infinite half-plane screen. The physical configuration of a finite barrier and reflecting ground is simulated by an equivalent theoretical combination of finite barrier and half-plane screen in order to obtain these formulae.

The ground reflection is considered to be a constant in the range 0 to 1. This constant may take different values on either side of the screen, but each value must remain constant over the ground's surface on the side of the screen for which it applies. All other parameters concerning the configuration remain the same as those described in 2.1.

The principle of determining formulae for the Sound Pressure Levels at P first in the absence of the barrier and then with the barrier in position, is used in the same way as in Chapter 2. The Insertion Loss at P is then taken to be the difference between these two results.

It should also be noted that the two situations where the sound source is above ground level and where the source is on the ground, need to be considered separately. This was covered in 3.2 and the two resulting formulae for the Insertion Loss were duly noted in 3.2.3.

As in Chapter 2, the results are applicable in a wide variety of configurations due to the flexibility of the formulae used and are also applicable for a finite screen of any shape, which may have holes in it. A computer program for this part of the work has been developed by the author and is described in Chapter 4. The formulae here were derived in such a way that the calculations by computer could be made, given the parameters listed in 2.2.4 and in addition the two ground reflection coefficients  $R_1$  and  $R_2$ . Results obtained by using the computer for particular configurations are also presented in Chapter 4.

Finally a discussion of how this technique can be further extended so that it applies to surroundings which include reflecting walls, ceiling and other modifications, is given in Chapter 5.

## 4. Predicted and Measured Results

### 4.1 Introduction

In this Chapter, predicted and measured results of Insertion Loss are presented and compared. Various test configurations were used both in the free field and with the addition of a reflecting ground. Three different barriers were used and various positions of source and receiver were considered, representing different aspects of diffraction effects and barrier performance.

The predicted results in the free field were obtained using the theory of Chapter 2. The theory was converted into a computer program, which in a given configuration performs the necessary calculations and gives the resulting Sound Pressure Level predictions. Similarly, the results in the reflecting ground environments were obtained using the theory of Chapter 3 and again a computer program was written to perform the required calculations. A description of these programs is given in 4.2 with details of how they are executed.

The experimental results were obtained by constructing the test configuration in an anechoic chamber for both the free field and reflecting ground cases. The experimental procedure is described in 4.3.

Both predicted and experimental results for all of the configurations tested are tabulated together in 4.4 for easy comparison.

Finally the results are analysed and compared in 4.5.

## 4.2 The Use of the Computer Programs in the Prediction of Barrier Performance

### 4.2.1 Description of the Program for Free Field Predictions

Based on the theory of Chapter 2, a computer program was written to enable calculation of the Sound Pressure Levels in the free field. It is necessary for the purpose of executing this program to include the parameters relating to the particular free field configuration. These parameters may be listed as follows:

the co-ordinates  $x_0, y_0, z_0$  of the source position;

the co-ordinates  $x_1, y_1, z_1$  of the receiver position;

the Sound Pressure Level  $SPL_1$  in the free field at a position 1 m from the source;

the absorption coefficient of the barrier;

parameters relating to the subdivision of the barrier;

parameters relating to the sketch of the barrier which is produced on the print-out.

As an illustration, it will be demonstrated which values were input in order to achieve three of the sets of results given later. First the results listed in table 2 were obtained as follows. It was assumed that the Sound Pressure Level  $SPL_1$  at 1 m from the source was 90 dB at all frequencies and that the subdivision of the barrier was into 25 x 25 equal elements each having dimension 0.04 m. It was also assumed that the transmission through the barrier was zero. The parameters input were

90, 0.5, 0, -1, 0.5, 0, 1.5, 0, 0	}	(A)
0.02, 0.02, 25, 25 0, 0		
0		

The first parameter is  $SPL_1$ , the next six are the co-ordinates  $x_0, y_0, z_0, x_1, y_1, z_1$ , followed by the transmission coefficient  $\alpha$  and finally a value of 0 to indicate that the barrier is square (if the barrier had been rectangular, this value would be 1 - see below). This parameter will be denoted by SR in this section.

The second line contains  $\xi$  and  $\eta$ , the half-dimensions of each rectangular element (values  $\xi = 0.02$  and  $\eta = 0.02$ ) and the number of elements in the x- and y- directions (both = 25). The next parameter indicates the number of areas missing from the square barrier and the final parameter of the second line is a similar parameter for the purpose of the printed diagram. These 2 parameters will be denoted BSA and DSA here and are both set to zero in this example because the barrier is square with no parts 'cut out'. The third example describes a case where these values are non-zero.

Finally, the third line has a single value 0 to indicate that the program has finished. This value could be set to 1 to indicate that another set of parameters of the type of the second line could be input giving an alternative subdivision of the barrier. For example

90, 0.5, 0, -1, 0.5, 0, 1.5, 0, 0

0.02, 0.02, 25, 25, 0, 0

1

0.05, 0.05, 10, 10, 0, 0

0

would also give results for the same configuration but calculated on the basis of a subdivision of 10 x 10 elements, rather than 25 x 25.

The print-out for example A is shown in figure 4.1.

The general case may be written as follows, using the already defined symbols:

SPL<sub>1</sub>, x<sub>0</sub>, y<sub>0</sub>, z<sub>0</sub>, x<sub>1</sub>, y<sub>1</sub>, z<sub>1</sub>, α, SR

ξ, η, NX, NY, BSA, DSA

REP

The second example corresponds to the configuration described in table 12. In this case the parameters input were

90, 0.38, 0, -1, 0.38, 0, 3, 0, 1

0.025, 0.025, 15, 30, 0, 0

0

} (B)

Note that SR = 1 in this case, which results in a rectangularly-shaped sketch on the print-out, rather than a square one. For the purpose of the subdivision, it was decided that the barrier should be mapped as 15 x 30 equal elements each of dimension 0.05 x 0.05 m. The print-out is shown in figure 4.2.





The third example shows the output when predicting the results for a barrier which is not a perfect square or rectangle. In this case the parameters input were

90, 0.5, 0, -1, 0.5, 0, 3, 0, 0

0.02, 0.02, 25, 25, 1, 1

13, 25, 7, 19

XXXXXXXXX

7, 12, 6, 15

0

} (C)

Here it may be noted that  $SR = 0$ , to indicate that the general shape is square, but that  $BSA$  is non-zero, to indicate that there are areas which have been cut out. Since  $BSA = 1$ , this indicates that one area has been cut away. It is then necessary to describe which area this is. The information is given in line 3, which shows that in the  $25 \times 25$  element representation of the barrier, the area cut away is that defined by the 13th to the 25th rows of elements and by the 7th to the 19th columns (see figure 4.3). The 4th row of parameters, although shown in this case as 7 asterisks can, if required, be a brief description of the barrier, which will then be shown on the print-out. Up to 50 characters are allowed for this description. The 5th row is similar to the 3rd row except that it is for the purpose of the sketch in the print-out. This can be seen by comparing the values with the produced sketch in figure 4.4. Also note that this line is allowed because the parameter  $DSA$  in the 2nd row is set to 1.

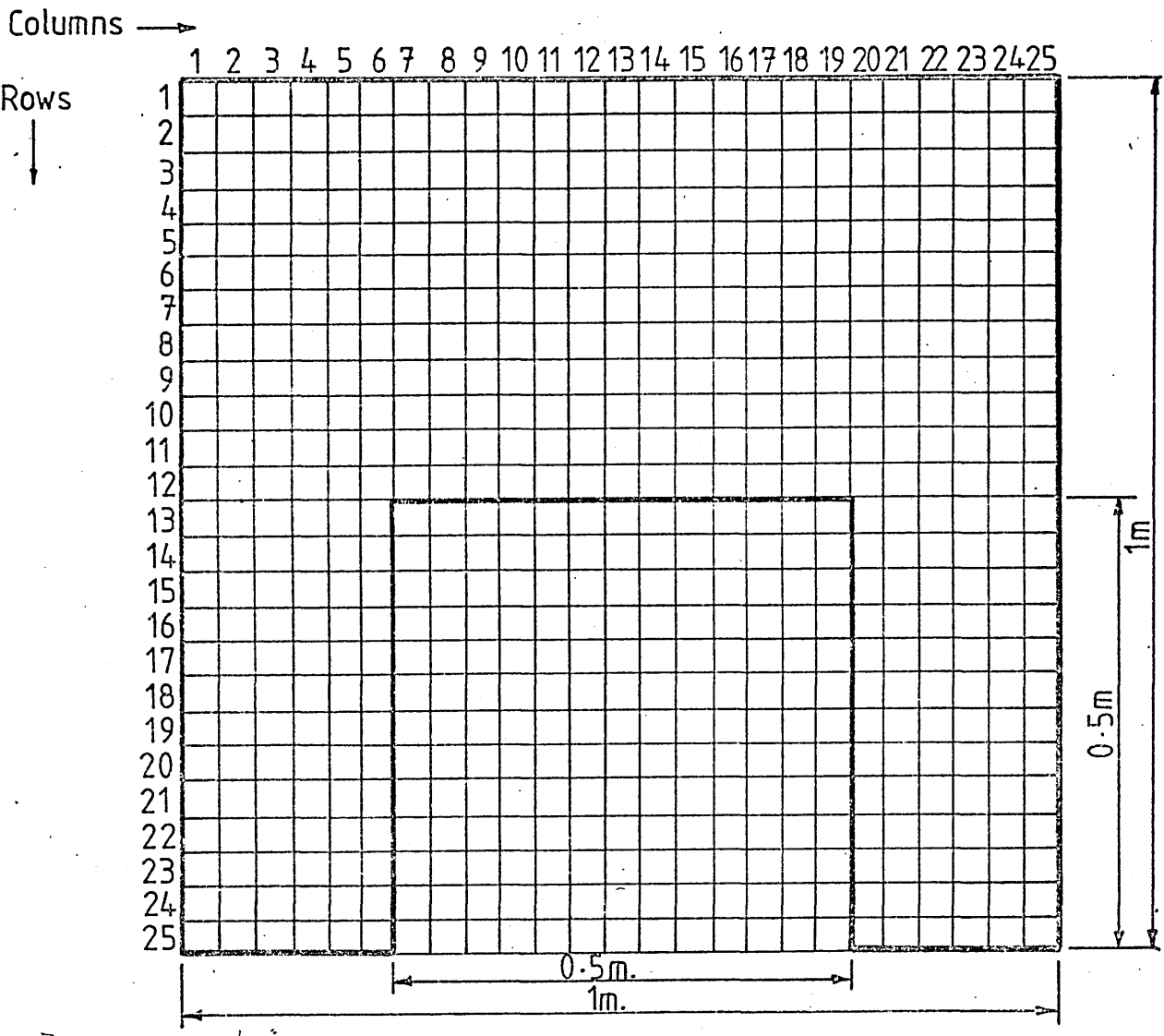


Figure 4.3. Representation of the Missing Portion of the 1m x 1m Barrier by Elements in a 25 x 25 Element sub division



The predicted free field results for the configurations investigated in this thesis are tabulated in full in 4.4.

#### 4.2.2 Description of the Program for Reflecting Ground Predictions

A computer program was written, based on the theory of Chapter 3, to enable calculation of Sound Pressure Levels in the presence of a reflecting ground. As in the case of the corresponding program for free field predictions, it is necessary to include the parameters relating to the particular configuration. The parameters are the same as those for the free field program with the addition of the ground reflection coefficients  $R_1$ ,  $R_2$ , where  $R_1$  is the reflection coefficient of the ground on the source side of the barrier and  $R_2$  that on the receiver's side.

In order to obtain the results which appear in the following tables, the procedure is similar to that by which the free field predictions were obtained. The principal difference is that the coefficients of ground reflection,  $R_1$  and  $R_2$  must be included. For example, the results listed in table 15 were obtained by inputting the parameters as follows:

90, 0.5, 0, -1, 0.5, 0, 2, 1, 1, 0, 0

0.02, 0.02, 25, 25, 0, 0

125

2

250

2  
500  
2  
1000  
2  
2000  
2  
4000  
2  
8000  
0

Note that the frequencies are input separately. This enables the programmer to select individual frequencies if required, rather than the full frequency range being automatically assumed. In this case the ground reflections,  $R_1$  and  $R_2$  are both equal to 1 and this is indicated by the 8th and 9th parameter on the first input line. The single entry of '2' between each frequency input indicates that another frequency is to be entered on the next time. If this parameter was '0', it would indicate that it is required to end the program execution (see last parameter) and if it was '1' it would indicate that a new subdivision was required, that is an entry of the type indicated by the second input line.

The configuration representing table 23 is the same as table 15 with the exception that  $R_1$  and  $R_2$  were both assumed equal to 0.5. The parameters input in this case were thus

90, 0.5, 0, -1, 0.5, 0, 2, 0.5, 0.5, 0, 0  
0.02, 0.02, 25, 25, 0, 0

125

2

250

2

500

2

1000

2

2000

2

4000

2

8000

0

The general case may be written as follows, using the symbols defined earlier in this Chapter (compare the free field case).

$SPL_1, x_0, y_0, z_0, x_1, y_1, z_1, R_1, R_1, \alpha, SR$

$\xi, \eta, NX, NY, BSA, DSA$

$f_1$

2

$f_2$

2

...

2

$f_n$

0,

where  $f_1, f_2, \dots, f_n$  are frequencies.

The predicted reflecting ground results for all of the configurations investigated in this thesis are tabulated in full in 4.4.

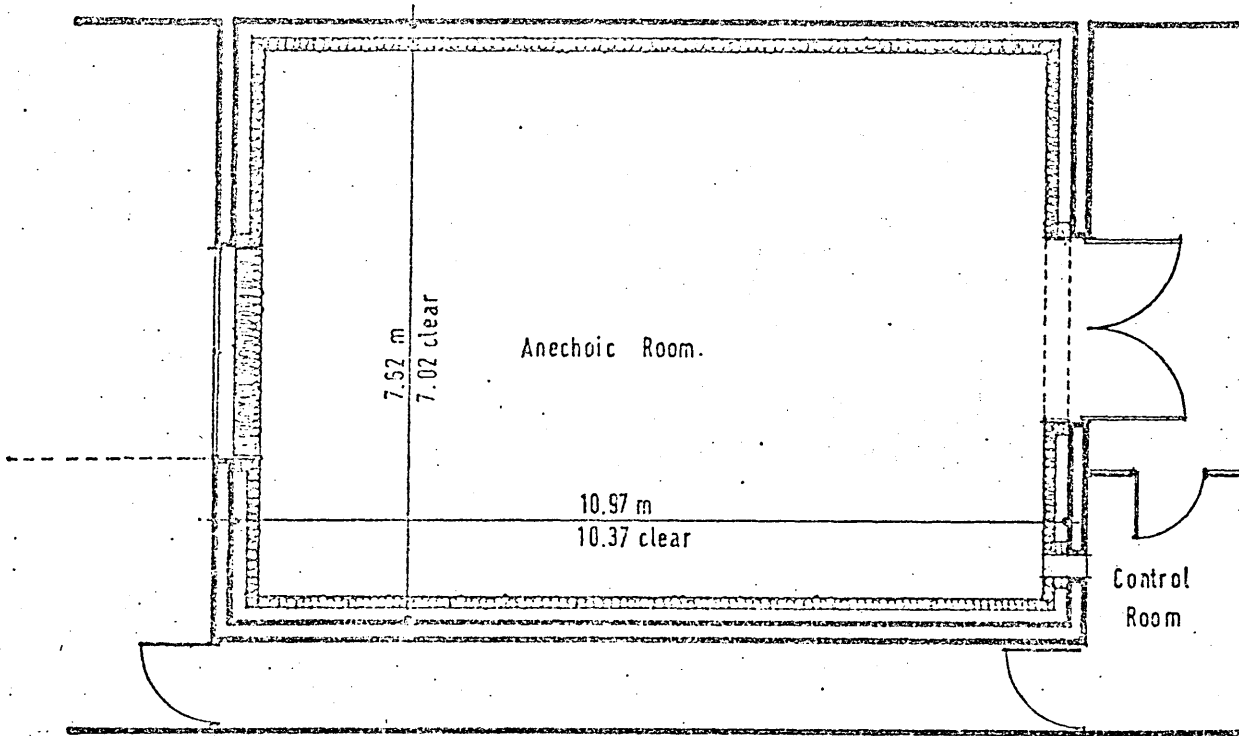
### 4.3 The Experimental Procedure

#### 4.3.1 General Description

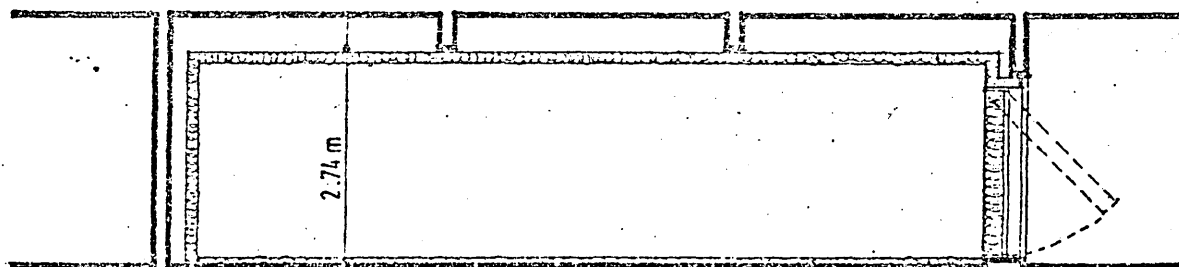
The experiments for sound attenuation by finite barriers were conducted in the anechoic chamber belonging to the Building Science and Mechanical Engineering Departments of the University of Sheffield and which is situated at Harpur Hill near Buxton, in Derbyshire.

The internal dimensions of the anechoic chamber are 10.97 m long by 7.62 m wide and 2.74 m high. The walls and ceiling are lined with four layers of absorbent material having a total thickness of 0.15 m with an air gap of 0.15 m between the walls and the material and of 0.3 m between the ceiling and the material (see figure 4.5).

The three barriers used were made of blockboard of 0.02 m thickness. The dimensions of the two principle barriers used were 1 m width by 1 m height and 1.5 m width by 0.75 m height. The third barrier used was the same as the 1 m x 1 m barrier with the exception that a 0.5 m x 0.5 m section was removed. This was done in order to demonstrate that the shape of the barrier may be arbitrary for the theory developed in this work to apply. The barrier has



PLAN.



LONGITUDINAL SECTION.

FIG. 4.5 THE ANECHOIC CHAMBER

already been discussed in 4.2 in the description of the computer programs, and is illustrated in figure 4.3.

The simulated point sound source was a small speaker emitting single frequencies determined by a Bruel and Kjaer Sine Random Generator. The intensity of the emitted sound was kept constant by using a compressor circuit including a microphone set at a constant distance from the centre of the speaker. The receiver microphone was connected to a Level Recorder which traced the Sound Pressure Levels over a full range of audio frequencies. The Level Recorder was mechanically driven by the Sine Random Generator.

Only the essential parts of the apparatus, that is the speaker, barrier and receiver microphone were placed within the chamber. The remainder of the equipment was kept outside the chamber in a control room (see figure 4.6 and plates 1-2).

#### 4.3.2 Free Field Experiments

The free field environment was simulated by ensuring that the ceiling, walls and floor of the chamber were all covered in absorbent materials. In order that diffraction could take place around all of its perimeter, the barrier was suspended by thin wires from the ceiling of the chamber. The experiments for sound attenuation by the barrier were performed by monitoring the sound pressure levels at the receiver's point first with no barrier and then with the

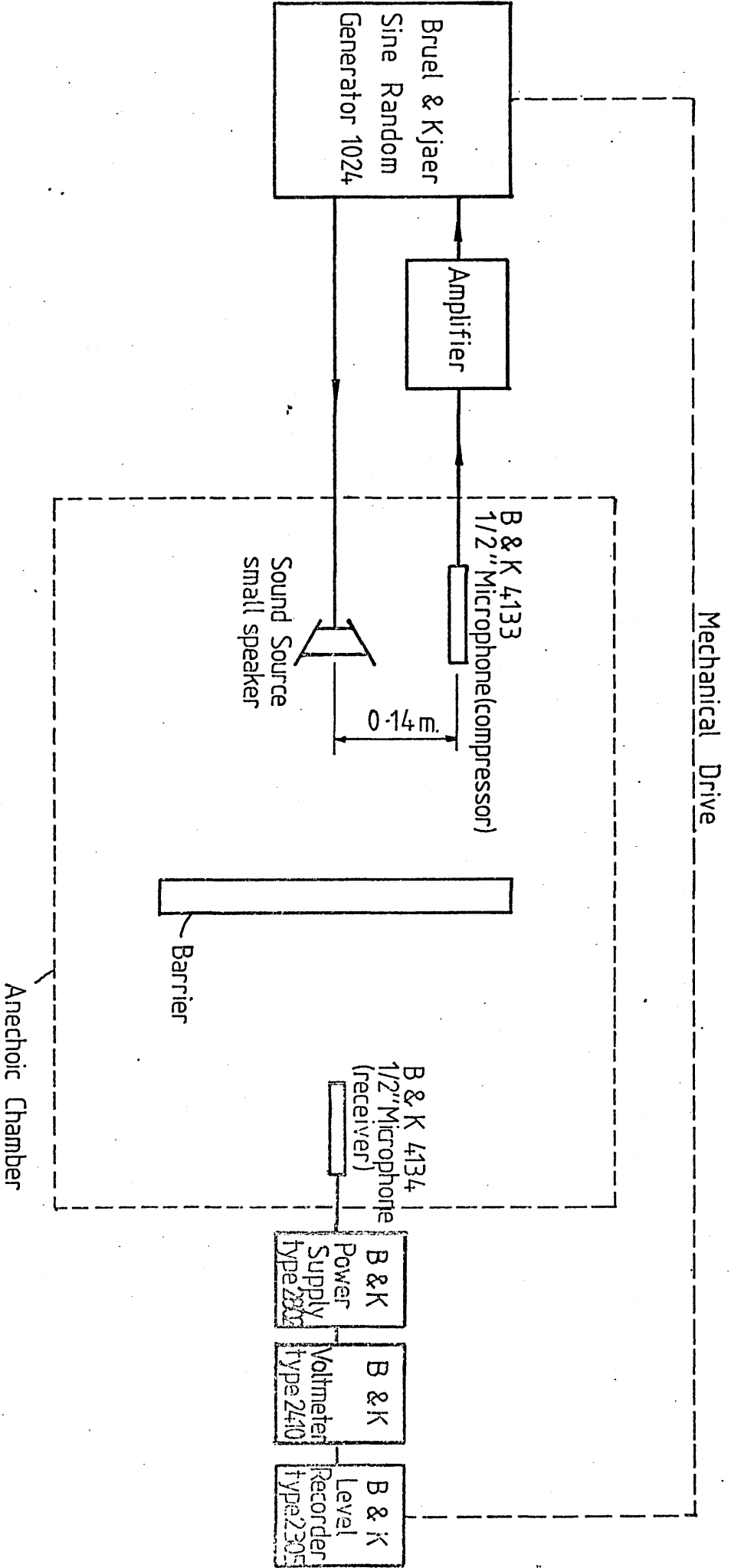


Figure 4.6 Schematic Representation of the Apparatus for Determination of Attenuation by Barriers

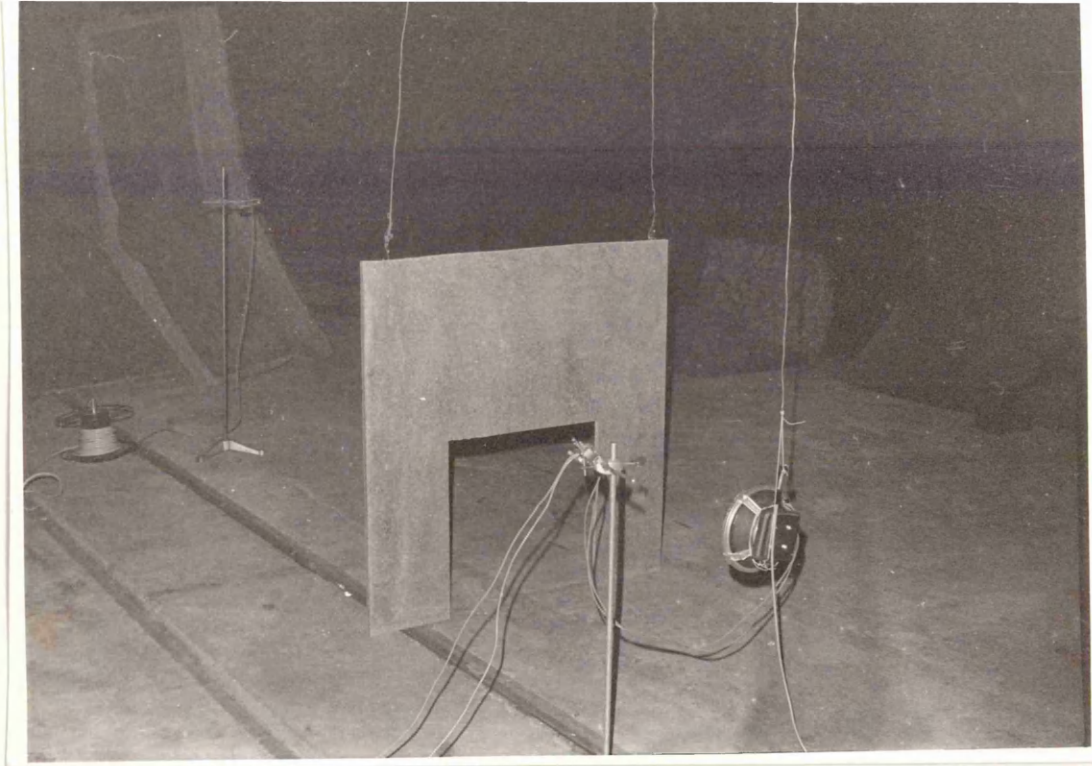


PLATE 1. SOUND SOURCE, BARRIER & MONITORING MICROPHONE ON THE CONCRETE FLOOR OF THE ANECHOIC CHAMBER

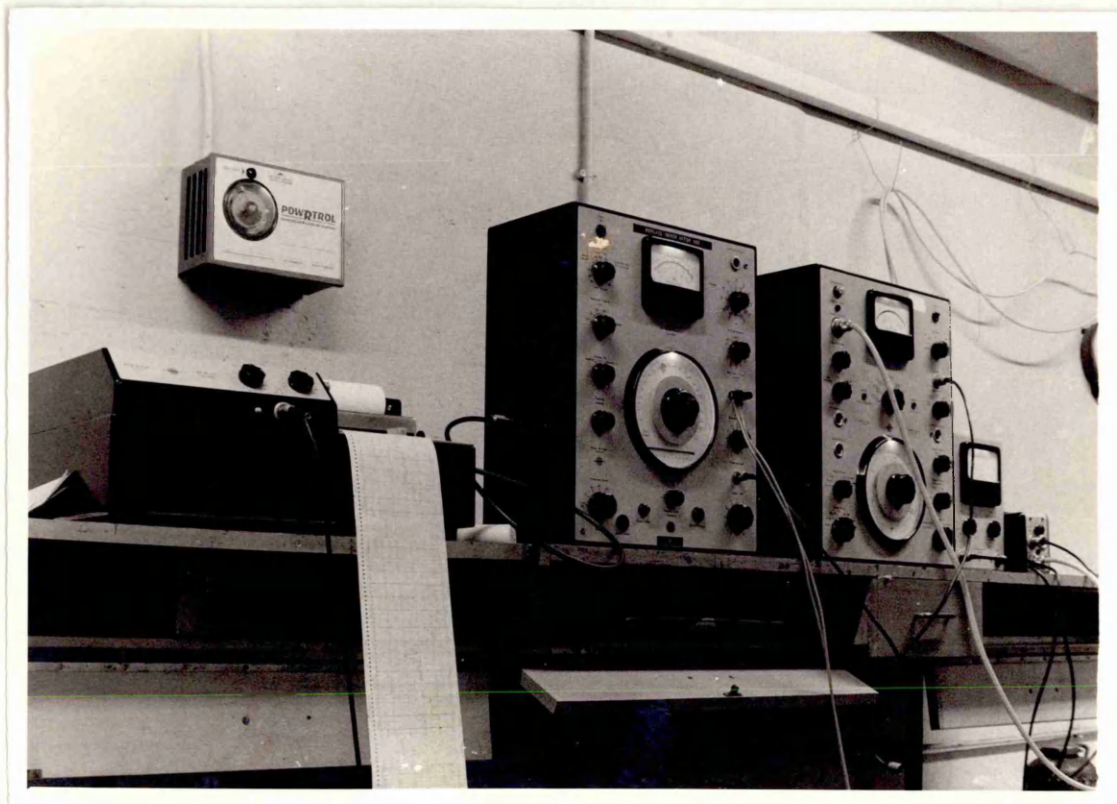


PLATE 2. THE APPARATUS IN THE CONTROL ROOM EXTERNAL TO THE ANECHOIC CHAMBER.

barrier in position. The insertion losses afforded by the barrier could then be determined by comparing the two sets of results. The results are tabulated in 4.4.

In all experiments, the barrier is assumed to be in the xy-plane of a Cartesian co-ordinate system, with the y-axis corresponding to the bottom edge of the barrier and the origin 0 on the centre of this edge. The direction of the z-axis is chosen so that the receiver's position has positive z-co-ordinate and the source has negative z-co-ordinate. Two of the configurations for the 1 m x 1 m barrier and two for the 1.5 m x 0.75 m barrier are illustrated in figure 4.7.

The results for the 1 m x 1 m barrier are tabulated in 4.4 in tables 1-10. The results for 1.5 m x 0.75 m barrier appear in tables 11-14.

#### 4.3.3 Experiments with a Reflecting Ground

The reflecting ground environment was simulated in the anechoic chamber in a similar way to that of the free field, except that only the walls and ceiling were kept fully absorbent, while the floor was designed to allow for ground reflections. In all cases the barrier was positioned on the ground, as this represents the most typical position. Note that in the free field situation, the barrier was suspended to allow a truly representative free field configuration. The diffraction therefore is allowed to take place around the three edges of the barrier not in

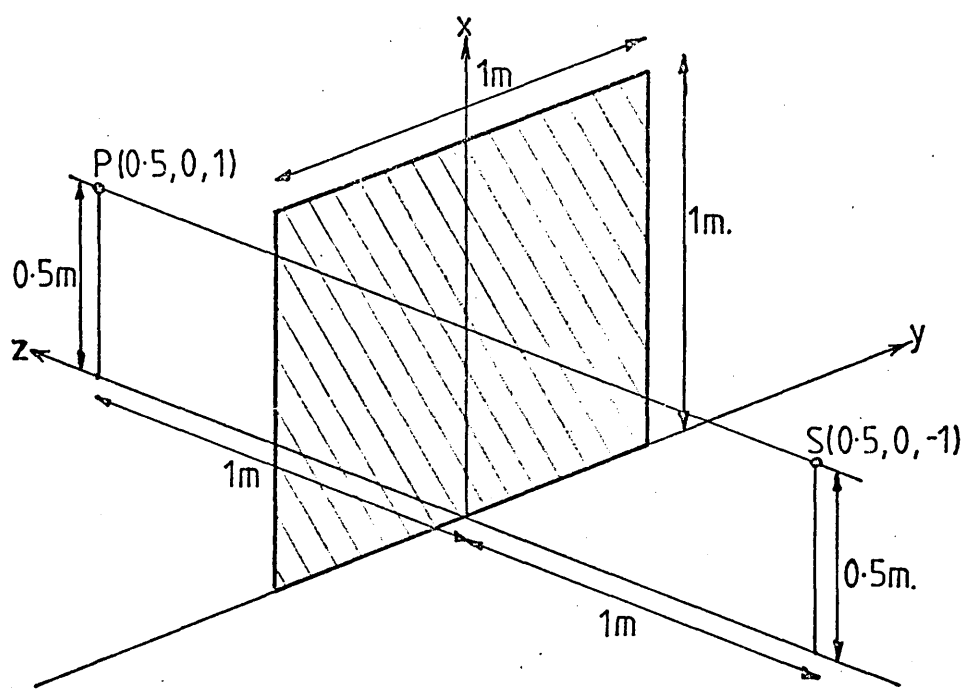


Figure 4.7.a.

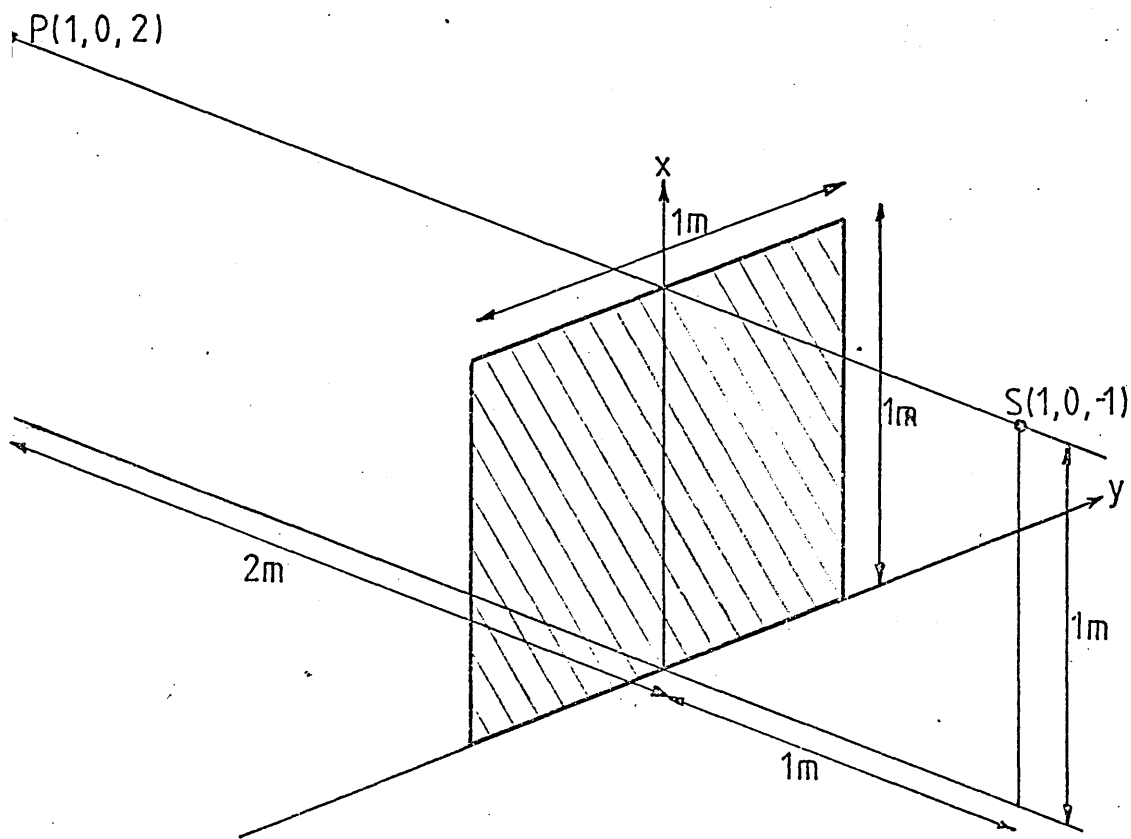


Figure 4.7.b.

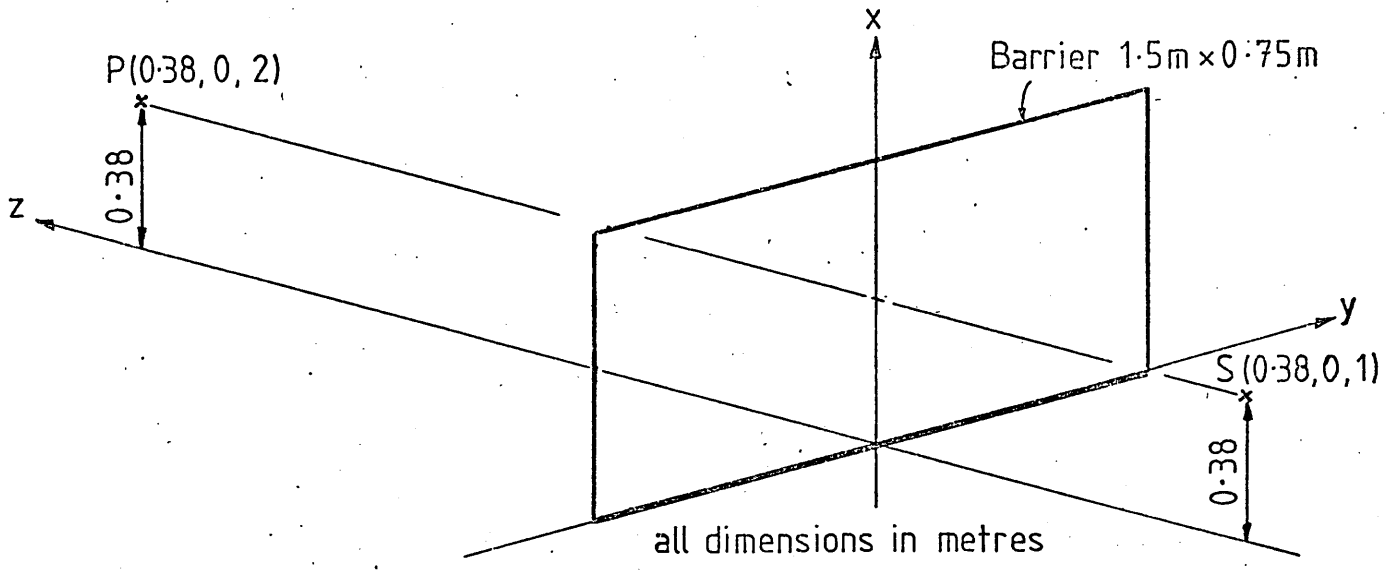


Figure 4.7c.

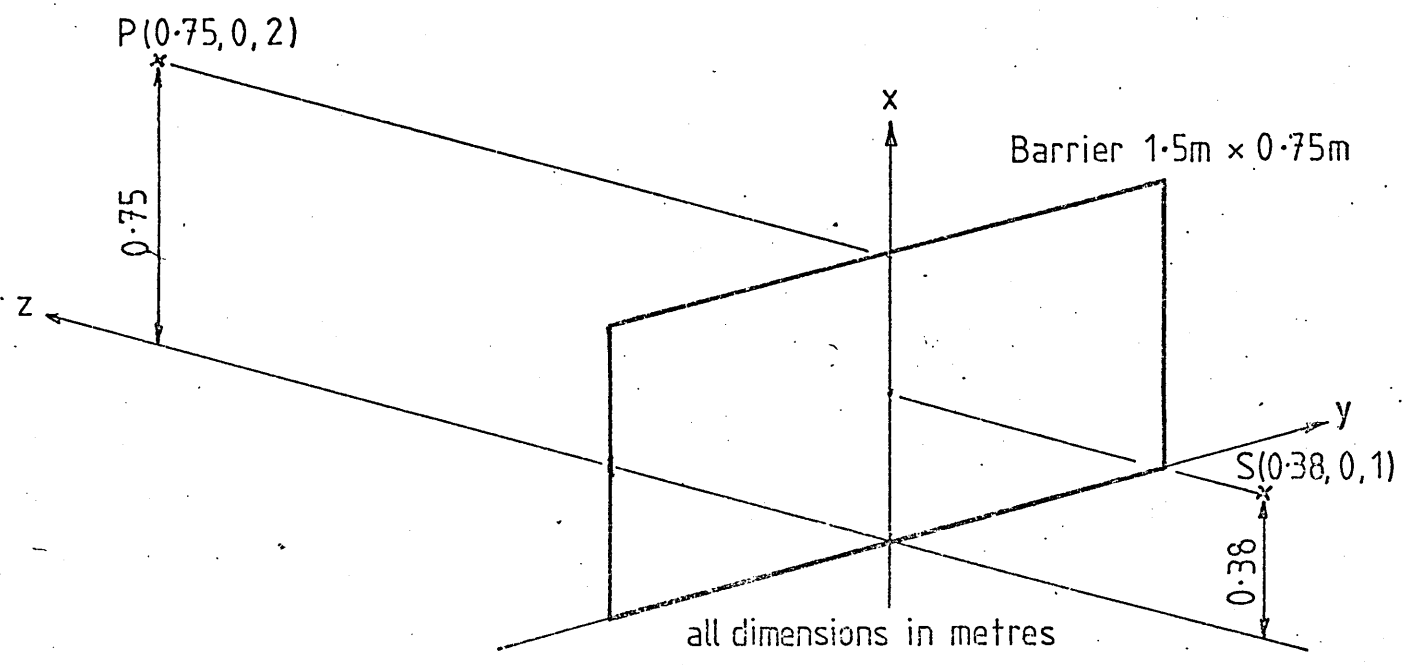


Figure 4.7d.

Rectangular Barrier Showing Source Position 'S' and Monitoring Position 'P'

contact with the ground. The method of ascertaining the sound pressure levels at the monitoring position P both with and without the barrier at monotonic frequencies were the same as in the free field case.

The two barriers used were the 1 m x 1 m square barrier and the 1 m x 1 m barrier with a 0.5 m x 0.5 m section removed (see figure 4.3). The Cartesian co-ordinate reference system was also chosen in the same way in relation to the barrier, so that in this case, the origin O was the point of contact between the barrier and the ground in the centre of the bottom edge of the barrier.

The following tables represent the experimental results obtained for the two barriers. It should also be noted that two different ground surfaces were assumed. The first of these was the base concrete floor of the chamber and the second was where the floor was covered with a partially absorbent material. The results for the base concrete ground are given first. In the results for the absorbent ground, the 'Insertion Loss' is taken to be the sound level difference obtained by the combined effect of inserting the barrier and covering the ground with the absorbent material, so that the 'sound pressure level without the barrier' may be interpreted as the sound pressure level with no barrier and no absorbent covering of the ground, whilst the 'sound pressure level with the barrier' is taken to be the sound pressure level when the floor is covered with absorbent material and the barrier is placed in position.

The results for the square barrier on the concrete floor of the chamber are tabulated in 4.4 in tables 15-18 and the results for the barrier with the cut away section on the same surface appear in tables 19-22. The results for the square barrier on the partially-absorbent ground are tabulated in tables 23-30.

#### 4.4 Tables of Predicted and Measured Results

Both measured and predicted results are presented in this section. Free field results appear in 4.4.1 and reflecting ground results appear in 4.4.2.

##### 4.4.1 Tables of Insertion Losses in the Free Field

The predicted results were obtained using the computer program described in 4.2.1 based on the free field theory developed in Chapter 2. Two different barriers were used, the 1 m x 1 m square barrier (tables 1-10) and the 1.5 m x 0.75 m barrier (tables 11-14). The source and monitoring positions were raised to represent differing diffraction aspects and distances from the barrier. Four of the configurations represented, those corresponding to tables 1, 6, 11 and 13, are sketched in figure 4.7.

TABLES 1-10 Free Field, Barrier 1 m x 1 m

TABLE 1 Source Position (x, y, z) = (0.5, 0, -1)

Monitoring Position (x, y, z) = (0.5, 0, 1)

Free Field Barrier 1 m x 1 m (see figure 4.7a)

Insertion Losses (dB)

Frequency of Source (Hz)	Measured	Predicted
125	0	0
250	3	1
500	0	3
1k	7	8
2k	20	10
4k	27	14
8k	30	18

TABLE 2 Source Position (x, y, z) = (0.5, 0, -1)

Monitoring Position (x, y, z) = (0.5, 0, 1.5)

Free Field Barrier 1 m x 1 m

Insertion Losses (dB)

Frequency of Source (Hz)	Measured	Predicted
125	0	0
250	0	1
500	0	2
1k	5	6
2k	16	9
4k	19	11
8k	27	16

TABLE 3 Source Position (x, y, z) = (0.5, 0, -1)

Monitoring Position (x, y, z) = (0.5, 0, 2)

Free Field Barrier 1 m x 1 m

Insertion Losses (dB)

Frequency of Source (Hz)	Measured	Predicted
125	0	0
250	2	0
500	-3	1
1k	6	5
2k	16	9
4k	20	11
8k	16	13

TABLE 4 Source Position (x, y, z) = (0.5, 0, -1)

Monitoring Position (x, y, z) = (0.5, 0, 3)

Free Field Barrier 1 m x 1 m

Insertion Losses (dB)

Frequency of Source (Hz)	Measured	Predicted
125	-1	0
250	0	0
500	0	1
1k	2	4
2k	11	8
4k	20	11
8k	15	14

TABLE 5 Source Position (x, y, z) = (1, 0, -1)  
Monitoring Position (x, y, z) = (1, 0, 1.5)

Free Field Barrier 1 m x 1 m  
Insertion Losses (dB)

Frequency of Source (Hz)	Measured	Predicted
125	5	1
250	7	5
500	7	6
1k	6	7
2k	6	6
4k	6	8
8k	7	6

TABLE 6 Source Position (x, y, z) = (1, 0, -1)  
Monitoring Position (x, y, z) = (1, 0, 2)

Free Field Barrier 1 m x 1 m (see figure 4.7b)  
Insertion Losses (dB)

Frequency of Source (Hz)	Measured	Predicted
125	-2	1
250	4	5
500	5	5
1k	6	6
2k	3	5
4k	4	6
8k	7	6

TABLE 7 Source Position (x, y, z) = (1, 0, -1)

Monitoring Position (x, y, z) = (1, 0, 3)

Free Field Barrier 1 m x 1 m

Insertion Losses (dB)

Frequency of Source (Hz)	Measured	Predicted
125	1	1
250	4	4
500	3	6
1k	6	8
2k	6	5
4k	10	5
8k	4	6

TABLE 8 Source Position (x, y, z) = (1, 0, -1)

Monitoring Position (x, y, z) = (0.5, 0, 3)

Free Field Barrier 1 m x 1 m

Insertion Losses (dB)

Frequency of Source (Hz)	Measured	Predicted
125	1	1
250	4	2
500	6	8
1k	12	12
2k	7	8
4k	9	9
8k	15	20

TABLE 9 Source Position (x, y, z) = (0.5, 0, -1)

Monitoring Position (x, y, z) = (1, 0, 2)

Free Field Barrier 1 m x 1 m  
Insertion Losses (dB)

Frequency of Source (Hz)	Measured	Predicted
125	0	0
250	1	1
500	1	4
1k	11	13
2k	12	17
4k	20	15
8k	23	19

TABLE 10 Source Position (x, y, z) = (0.5, 0, -1)

Monitoring Position (x, y, z) = (1, 0, 3)

Free Field Barrier 1 m x 1 m  
Insertion Losses (dB)

Frequency of Source (Hz)	Measured	Predicted
125	2	0
250	1	1
500	3	2
1k	9	9
2k	17	22
4k	13	11
8k	25	18

TABLES 11-14 Free Field, Barrier 1.5 m x 0.75 m

TABLE 11 Source Position (x, y, z) = (0.38, 0, -1)  
Monitoring Position (x, y, z) = (0.38, 0, 2)

Free Field Barrier 1.5 m x 0.75 m (see figure 4.7c)  
Insertion Losses (dB)

Frequency of Source (Hz)	Measured	Predicted
125	-8	2
250	-3	5
500	6	7
1k	5	6
2k	16	7
4k	18	7
8k	23	6

TABLE 12 Source Position (x, y, z) = (0.38, 0, -1)  
Monitoring Position (x, y, z) = (0.38, 0, 3)

Free Field Barrier 1.5 m x 0.75 m  
Insertion Losses (dB)

Frequency of Source (Hz)	Measured	Predicted
125	-2	1
250	-5	4
500	5	6
1k	7	5
2k	17	6
4k	16	5
8k	38	5

TABLE 13 Source Position (x, y, z) = (0.38, 0, -1)

Monitoring Position (x, y, z) = (0.75, 0, 2)

Free Field Barrier 1.5 m x 0.75 m (see figure 4.7d)

Insertion Losses (dB)

Frequency of Source (Hz)	Measured	Predicted
125	-10	2
250	-5	4
500	2	6
1k	9	4
2k	20	7
4k	16	8
8k	27	5

TABLE 14 Source Position (x, y, z) = (0.38, 0, -1)

Monitoring Position (x, y, z) = (0.75, 0, 3)

Free Field Barrier 1.5 m x 0.75 m

Insertion Losses (dB)

Frequency of Source (Hz)	Measured	Predicted
125	-4	2
250	-8	4
500	4	6
1k	4	4
2k	18	6
4k	14	6
8k	33	5

#### 4.4.2 Tables of Insertion Losses in the Reflecting Ground Environment

The predicted results were obtained using the computer program described in 4.2.2 based on the free field theory developed in Chapter 3. Two different ground surfaces were employed in the anechoic chamber for the experimental results. First, the uncovered concrete floor of the chamber and secondly, the same floor covered with partially-absorbent material. These surfaces were represented in the theoretical case by assuming ground reflection coefficients of 1 in the case of the concrete floor and of 0.5 in the case of the partially-absorbent ground.

Two different barriers were used, the 1 m x 1 m square barrier and the 1 m x 1 m barrier with the 0.5 m x 0.5 m section cut away (see figure 4.3). The results for the concrete ground configurations are tabulated in tables 15-18 for the 1 m x 1 m barrier and in tables 19-22 for the barrier with a cut away section. The results for the partially-absorbent ground configurations in the presence of the 1 m x 1 m barrier are presented in tables 23-30.

TABLES 15-22 Ground Surface - Concrete

TABLES 15-18 Ground Surface - Concrete, Barrier 1 m x 1 m

TABLE 15 Source Position (x, y, z) = (0.5, 0, -1)

Monitoring Position (x, y, z) = (0.5, 0, 2)

Ground Surface - Concrete Barrier 1 m x 1 m

Insertion Losses (dB)

Frequency of Source (Hz)	Measured	Predicted
125	0	-2
250	3	-1
500	6	6
1k	0	13
2k	22	10
4k	21	12
8k	28	22

TABLE 16 Source Position (x, y, z) = (0.5, 0, -1)

Monitoring Position (x, y, z) = (0.5, 0, 3)

Ground Surface - Concrete Barrier 1 m x 1 m

Insertion Losses (dB)

Frequency of Source (Hz)	Measured	Predicted
125	0	-2
250	1	1
500	7	4
1k	3	8
2k	5	11
4k	19	22
8k	20	19

TABLE 17 Source Position (x, y, z) = (0.5, 0, -1)  
 Monitoring Position (x, y, z) = (1, 0, 2)

Ground Surface - Concrete Barrier 1 m x 1 m  
 Insertion Losses (dB)

Frequency of Source (Hz)	Measured	Predicted
125	0	-1
250	5	5
500	3	11
1k	16	7
2k	13	24
4k	23	23
8k	23	16

TABLE 18 Source Position (x, y, z) = (0.5, 0, -1)  
 Monitoring Position (x, y, z) = (1, 0, 3)

Ground Surface - Concrete Barrier 1 m x 1 m  
 Insertion Losses (dB)

Frequency of Source (Hz)	Measured	Predicted
125	2	-1
250	1	3
500	2	10
1k	6	7
2k	17	20
4k	17	17
8k	27	17

TABLE 19-22 Ground Surface - Concrete, Barrier 1 m x 1 m with 0.5 m x 0.5 m Section Cut Away (see figure 4.3)

TABLE 19 Source Position (x, y, z) = (0.5, 0, -1)

Monitoring Position (x, y, z) = (0.5, 0, 2)

Ground Surface - Concrete Barrier 1 m x 1 m with  
0.5 m x 0.5 m section cut away

Insertion Losses (dB)

Frequency of Source (Hz)	Measured	Predicted
125	0	-1
250	1	1
500	8	8
1k	3	5
2k	2	2
4k	0	2
8k	10	5

TABLE 20 Source Position (x, y, z) = (0.5, 0, -1)

Monitoring Position (x, y, z) = (0.5, 0, 3)

Ground Surface - Concrete Barrier 1 m x 1 m with  
0.5 m x 0.5 m section cut away

Insertion Losses (dB)

Frequency of Source (Hz)	Measured	Predicted
125	1	-2
250	1	1
500	1	8
1k	12	12
2k	0	3
4k	1	7
8k	0	4

TABLE 21 Source Position (x, y, z) = (0.5, 0, -1)  
 Monitoring Position (x, y, z) = (1, 0, 2)  
 Ground Surface - Concrete Barrier 1 m x 1 m with  
 0.5 m x 0.5 m section cut away  
 Insertion Losses (dB)

Frequency of Source (Hz)	Measured	Predicted
125	0	-1
250	0	4
500	1	17
1k	9	13
2k	0	8
4k	7	6
8k	10	5

TABLE 22 Source Position (x, y, z) = (0.5, 0, -1)  
 Monitoring Position (x, y, z) = (1, 0, 3)  
 Ground Surface - Concrete Barrier 1 m x 1 m with  
 0.5 m x 0.5 m section cut away  
 Insertion Losses (dB)

Frequency of Source (Hz)	Measured	Predicted
125	-1	-1
250	1	2
500	1	9
1k	3	10
2k	3	14
4k	2	5
8k	10	4

TABLES 23-30 Ground Surface - Partially Absorbent,

Barrier 1 m x 1 m

TABLE 23 Source Position (x, y, z) = (0.5, 0, -1)

Monitoring Position (x, y, z) = (0.5, 0, 2)

Ground Surface - Partially Absorbent Barrier 1 m x 1 m

Insertion Losses (dB)

Frequency of Source (Hz)	Measured	Predicted
125	4	2
250	10	4
500	7	6
1k	-10	12
2k	26	12
4k	17	14
8k	35	20

TABLE 24 Source Position (x, y, z) = (0.5, 0, -1)

Monitoring Position (x, y, z) = (0.5, 0, 3)

Ground Surface - Partially Absorbent Barrier 1 m x 1 m

Insertion Losses (dB)

Frequency of Source (Hz)	Measured	Predicted
125	7	2
250	11	3
500	13	6
1k	4	9
2k	4	13
4k	18	19
8k	22	19

TABLE 25 Source Position (x, y, z) = (0.5, 0, -1)  
Monitoring Position (x, y, z) = (1, 0, 2)  
Ground Surface - Partially Absorbent Barrier 1 m x 1 m  
Insertion Losses (dB)

Frequency of Source (Hz)	Measured	Predicted
125	5	3
250	6	5
500	4	8
1k	18	9
2k	14	23
4k	26	19
8k	27	19

TABLE 26 Source Position (x, y, z) = (0.5, 0, -1)  
Monitoring Position (x, y, z) = (1, 0, 3)  
Ground Surface - Partially Absorbent Barrier 1 m x 1 m  
Insertion Losses (dB)

Frequency of Source (Hz)	Measured	Predicted
125	4	2
250	7	5
500	6	7
1k	9	9
2k	16	24
4k	24	17
8k	31	20

TABLE 27 Source Position  $(x, y, z) = (1, 0, -1)$   
Monitoring Position  $(x, y, z) = (0.5, 0, 2)$   
Ground Surface - Partially Absorbent Barrier 1 m x 1 m  
Insertion Losses (dB)

Frequency of Source (Hz)	Measured	Predicted
125	5	2
250	7	5
500	0	15
1k	18	15
2k	8	10
4k	17	14
8k	18	18

TABLE 28 Source Position  $(x, y, z) = (1, 0, -1)$   
Monitoring Position  $(x, y, z) = (0.5, 0, 3)$   
Ground Surface - Partially Absorbent Barrier 1 m x 1 m  
Insertion Losses (dB)

Frequency of Source (Hz)	Measured	Predicted
125	5	2
250	8	3
500	2	14
1k	15	11
2k	4	9
4k	14	16
8k	12	20

TABLE 29 Source Position (x, y, z) = (1, 0, -1)  
 Monitoring Position (x, y, z) = (1, 0, 2)  
 Ground Surface - Partially Absorbent Barrier 1 m x 1 m  
 Insertion Losses (dB)

Frequency of Source (Hz)	Measured	Predicted
125	9	4
250	5	10
500	11	7
1k	-7	13
2k	16	9
4k	19	8
8k	10	9

TABLE 30 Source Position (x, y, z) = (1, 0, -1)  
 Monitoring Position (x, y, z) = (1, 0, 3)  
 Ground Surface - Partially Absorbent Barrier 1 m x 1 m  
 Insertion Losses (dB)

Frequency of Source (Hz)	Measured	Predicted
125	10	3
250	6	9
500	12	6
1k	8	8
2k	-5	8
4k	8	8
8k	0	9

## 4.5 Analysis of Results

### 4.5.1 Free Field Environment

#### 1. Barrier 1 m x 1 m

##### (a) Both S and P in Line with the Centre of the Barrier

(Tables 1-4)

The experimental results show a decrease in Insertion Loss with distance from 30 dB with P at 1 m from the screen to 20 dB with P at 3 m. The theoretical results show a similar statistic except that the values are smaller at 18 dB and 14 dB respectively. In all of the tables 1-4, the values of Insertion Loss over the frequency range show a similar trend in that the values are relatively low for frequencies of up to 1k and larger for the higher frequencies.

##### (b) Both S and P in Line with the Top Edge of the Barrier

(Tables 5-7)

This situation represents the limiting diffraction case. The results here show no decrease in the Insertion Loss with increase of distance of P from the screen. The Insertion Loss appears to be fairly constant at distinct frequency bands from 250 Hz to 8k Hz. In these cases, there is an extremely good correspondence between the predicted and measured results.

##### (c) One of S or P in Line with the Centre of the Barrier, whilst the other is in Line with an Edge (Tables 8-10)

The experimental results show that there is an increase in Insertion Loss with distance of P from the screen.

It is of interest to note that the Insertion Loss is greater when the source S is in line with the centre of the barrier and P in line with the edge than when S is in line with the edge and P in line with the centre. This can be seen by comparing tables 8 and 10. Comparison between tables 8a and 10a show that the theory upholds this observation. This is to be expected because the source is nearer to the barrier in both cases and the barrier would tend therefore to move effective in its sound reducing capacity when the source is in line with the centre. Again there is a very good correspondence between predicted and measured results.

2. Barrier 1.5 m x 0.75 m

(a) Both S and P in Line with the Centre of the Barrier  
(Tables 11, 12)

Both the experimental and theoretical results show that Insertion Loss does not decrease with increase in distance of P from the screen. However, the theoretical results show generally lower levels of Insertion Loss throughout and indicate that the Insertion Loss is more constant with changes of frequency than the measured results.

(b) S in Line with the Centre of the Barrier and P in Line with the Edge (Tables 13, 14)

The comments in (a) above are also applicable here, the correspondence between predicted and measured results again being rather poor.

#### 4.5.2 Barrier in the Presence of a Reflecting Ground

##### 1. Barrier 1 m x 1 m on the Fully Reflecting Concrete Ground

###### (a) Both S and P in Line with the Centre of the Barrier

(Tables 15, 16)

In this case there is a good correspondence between the predicted and measured results. There were generally low values of Insertion Loss at frequencies below 1k Hz and higher value at the higher frequencies.

###### (b) S in Line with the Centre of the Barrier and P in Line with the Top Edge (Tables 17, 18)

Here there is a fairly good correspondence between the predicted and measured results. Again the Insertion Losses are higher at the upper end of the frequency range. An interesting observation is that the predicted Insertion Losses at the frequencies 500 Hz and 1k Hz are of a rather unexpected nature in both cases (i.e. P at 2 m and 3 m from the barrier).

##### 2. Barrier 1 m x 1 m with a 0.5 m x 0.5 m Cut Away Section

###### (a) Both S and P in Line with the Centre of the Barrier

(Tables 19, 20)

Here there is a fairly good correspondence between the predicted and measured results. It is interesting to note that there is a tendency for higher Insertion Losses at the middle range of frequencies rather than at the upper end, and indeed that in the case where P

is 3 m from the screen, the measured Insertion Losses were practically zero at 2k Hz, 4k Hz and 8k Hz.

(b) S in Line with the Centre of the Barrier and P in Line with the Top Edge (Tables 21, 22)

Here there is a poor correspondence between the predicted and experimental results. Although these are higher predictions of Insertion Losses at the middle range of frequencies (as was observed in 2(a) above), this was not borne out in practice.

3. Barrier 1 m x 1 m on the Partially Absorbent Ground Surface

(a) Both S and P in Line with the Centre of the Barrier  
(Tables 23, 24)

The experiment yielded erratic results for the Insertion Loss. The theoretical results appear to be more steady. Again there is a tendency for higher Insertion Losses at the upper end of the frequency range.

(b) S in Line with the Centre of the Barrier and P in Line with the Top Edge (Tables 25, 26)

Again the experimental measurements are somewhat erratic, although more stable than in (a). There is a fairly good correspondence between the predicted and measured results, although the measured Insertion Losses are consistently higher than predicted.

(c) S in Line with the Top Edge of the Barrier and P  
in Line with the Centre (Tables 27, 28)

The measured Insertion Losses are higher with P at a distance of 2 m from the screen than at 3 m, although this does not seem to be borne out by the computed values. Otherwise there is a fairly good correspondence between the predicted and measured results.

(d) Both S and P in Line with the Edge of the Barrier  
(Tables 29, 30)

The measured results are somewhat erratic especially with P at a distance of 3 m from the screen. It appears that the higher values of Insertion Loss are not necessarily at the higher frequencies.

#### 4.5.3 Summary of Results

The free field predictions of Insertion Loss due to interposing the 1 m x 1 m barrier were usually well supported by the site tests in the anechoic chamber. It was noted that the correspondence when the source and monitoring position were both in line with the edge of the barrier (the limiting diffraction case). The results were poor in the case of the rectangular 1.5 m x 0.75 m. It is not yet clear why this has happened, but a possibility is that there may be a flaw in the computer program for this particular dimension.

In the fully reflecting ground situation, the predicted results were generally quite good. With the 1 m x 1 m barrier with a missing section of 0.5 m x 0.5 m the results were better where the source was in line with the centre of the barrier and the monitoring position in line with the top edge than when both positions were in line with the source. Where the 1 m x 1 m barrier was used, the correlation between predicted and measured results were reasonably acceptable.

In the partially-reflecting ground situation, the predicted results were better when the monitoring position was in line with the top edge of the barrier and especially accurate when the source was also in line with the barrier's edge.

In most cases, the Insertion Losses tended to increase with increasing frequencies. Exceptions to this were in those cases where both the source and monitoring position were simultaneously in line with the same edge of the barrier.

In some cases it was noted that Insertion Loss decreased with increase in distance of monitoring position from the barrier, whereas in other cases, the Insertion Loss tended to remain constant.

## 5. Conclusions and Recommendations for Further Research.

### 5.1 Conclusions

As explained in Chapter 1, the aim of this thesis was to formulate a method of predicting the Insertion Loss due to finite barrier of arbitrary shape based on the theory of diffraction around the edges of the barrier. This aim has been achieved in the cases of a free field environment and in the presence of a reflecting ground - The theory is based on Fresnel-Kirchhoff diffraction theory and is applicable to any shape and size of barrier. The source and monitoring positions are both supposed to be single points in space and they can assumed to be anywhere in relation to the barrier.

Transmission of sound through the barrier may be assumed a constant in the range 0 to 1. The theory applies only for single monotonic source frequencies. Suggestions for extending this to multiple frequencies and frequency ranges appear in 5.2. In the case of a reflecting ground environment, the amount of reflection from the ground is simplified to two constant parameters in the range 0 to 1, the separate parameters representing reflection for the ground on the two sides of the barrier. The theory incorporated a technique of mathematically subdividing the region of the barrier's surface into finite elements for the purpose of providing a solution to the Fresnel-Kirchhoff diffraction formula.

In the reflecting ground case, the theory also employed the 'Method of Images' of ground reflection in order to solve the diffraction problem for the separate component ray paths which occur when reflections take place.

The theory was converted into computer programs in order to effect the calculations for particular configurations of source, barrier and monitoring position. These programs were executed for test configurations and the results compared with corresponding experimental site tests conducted in an anechoic chamber. The results were compared and discussed.

In all, the aims of this work were achieved to a satisfactory extent in view of the above discussion.

## 5.2 Recommendations for Further Research

### 5.2.1 Extension of the sound source properties.

It was assumed that the sound emanated from a single point source of monotonic frequency. The theory could be extended to allow for multiple sources of multiple frequencies (using summation techniques) or of frequency ranges (using integration over the frequency range).

### 5.2.2 Extension of the environment to allow for further reflections

The reflecting ground environment could be extended to a totally enclosed environment by considering reflections from walls and ceiling, too. The 'Method of Images' would also be used on the additional surfaces in extending the theory. Also the possible presence within the environment of other objects which would influence the sound field could be considered, for example 'furniture' or large machinery.

### 5.2.3 In-situ representation.

If the above recommendation were to be implemented, then the resulting theory would act as a very flexible method of predicting performance of a noise-reducing finite barrier in a typical in-situ environment, such as an office or factory.

### 5.3 Optimization of the elements forming the subdivision of the barrier's surface.

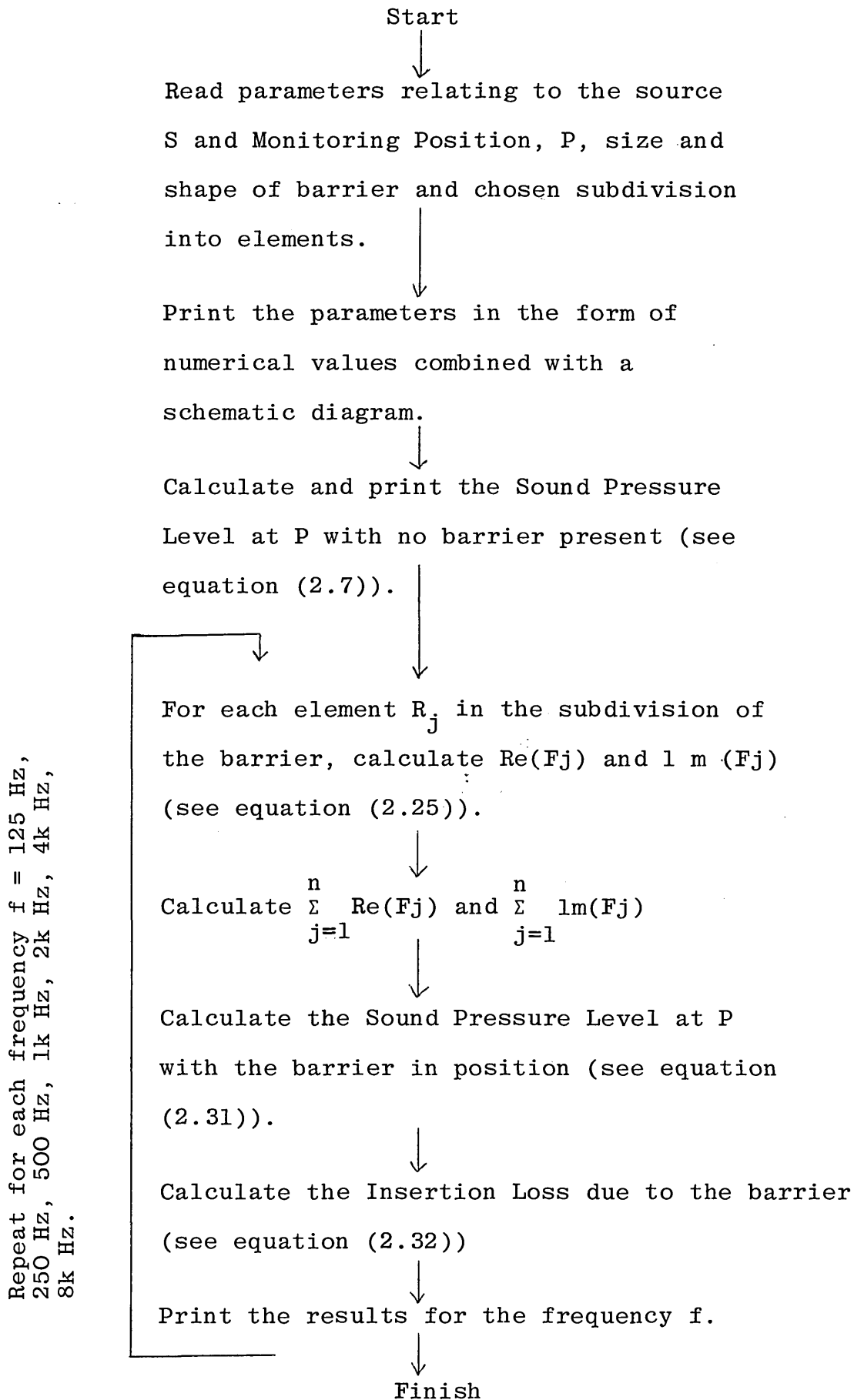
It was stated earlier in this work that a discussion would be given on optimizing the choice of the finite elements  $R_j, j=1,2,\dots,n$  forming the mathematical subdivision of the barrier's surface. It may be noted that in Chapter 4 where the computer predictions were made, the subdivision of the barrier was always into the same number of elements, given the size of the barrier. Some work was done during the development of this thesis in choosing these optimum numbers

of elements. This was done by running the programs in given configurations of source, barrier and monitoring positions a number of times, varying only the number of elements comprising the theoretical subdivision. It was found, as would be expected, that the Sound Pressure predictions obtained were poor when the subdivision consisted of few elements and then converged to steady values upon reaching an optimum number of elements. By frequent test-running of this kind, it became obvious which numbers of elements was a most satisfactory optimum for most barrier configurations. If more elements than the optimum are chosen, the results will be just as accurate, of course, but the computer programs would in these circumstances perform more calculations making them more costly to run. For this reason, the optimum should be decided upon in given configuration for most economical use of the computer.

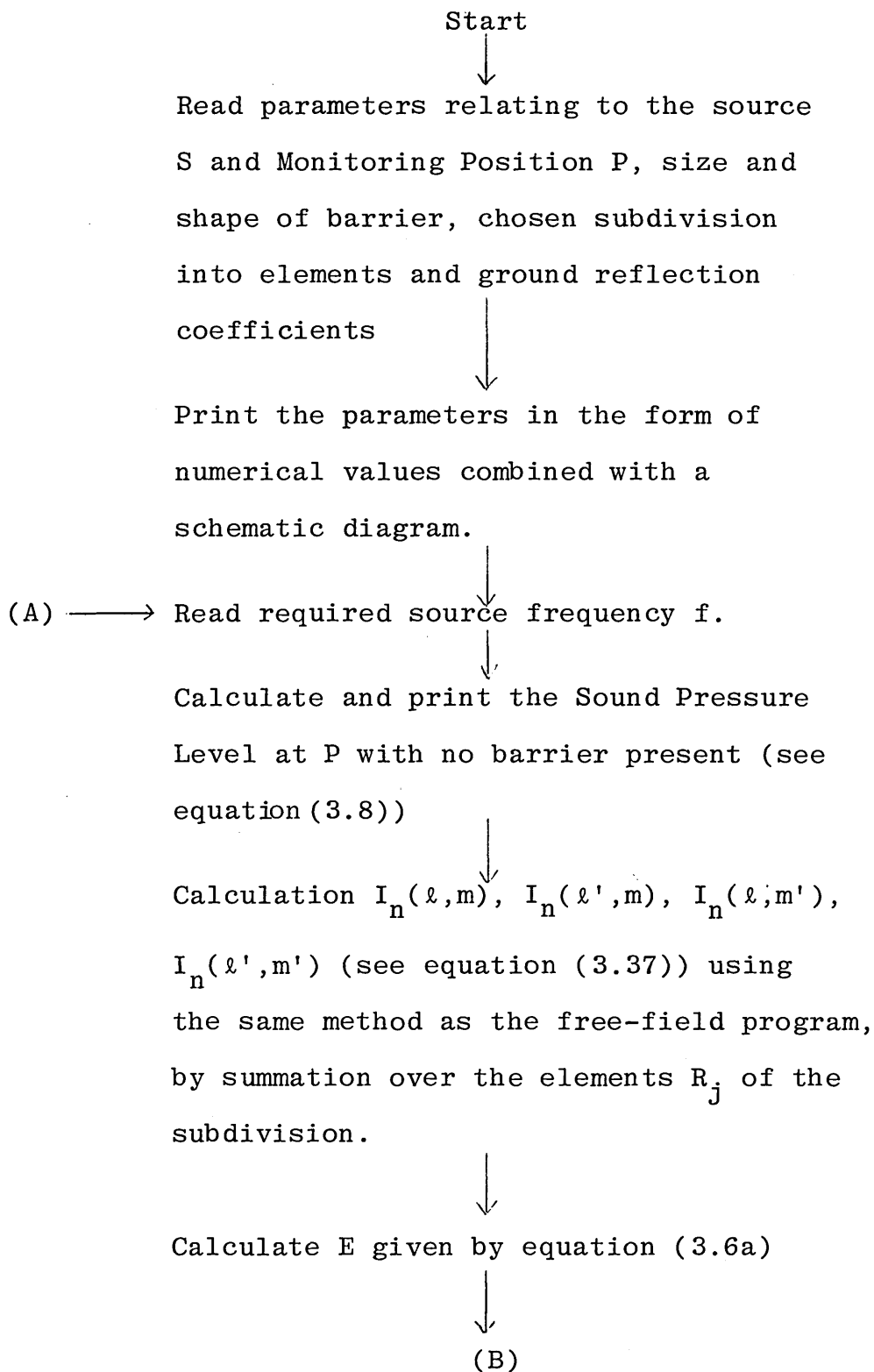
## APPENDIX 1 Computer Flow Diagrams

This appendix comprises flow diagrams of the two computer diagrams which were used in the calculation of predicted results. The first diagram represents the program used for predictions of Insertion Losses in the free field and which is described in 4.2.1. The second diagram represents the program used for predictions in reflecting ground environments and which is described in 4.2.2.

Flow Diagram 1 - Calculation of predicted Insertion Loss due to an arbitrarily-shaped barrier in the free field.



Flow Diagram 2 - Calculation of predicted Insertion Loss due to an arbitrarily-shaped barrier in a reflecting ground environment.



(B)



Calculate  $w$  and  $\bar{w}$  (equations (3.29) & (3.36))



Calculate  $G(w)$  and  $G(\bar{w})$ , using a Fresnel  
Integral subroutine and equation (3.38)



Calculate the disturbance  $U(P)$  at  $P$  in the  
presence of the barrier from equation (3.39)  
[or equation (3.41) if the source is on the  
ground].



Calculate the Sound Pressure Level at  $P$   
with the barrier in position, using equation  
(3.42).



Calculate the Insertion Loss due to the  
barrier from equation (3.1) for the  
frequency  $f$ .



(A) ← Yes Are predictions required for another  
frequency?



No

Finish

Reference List.

1. H.G.Jonasson, "Sound Reduction by Barriers on the Ground", J.Sound Vib. (1972) 22 (1), 113-126.
2. A.D.Pierce, "Diffraction of Sound Around Corners and Over Wide Barriers", J.Acoust. Soc.Am.(1974)55(5),941-955.
3. W.E.Scholes, A.C.Salvidge, J.W.Sargent, "Field Performance of a Noise Barrier", J.Sound Vib. (1971)16(4), 627-642.
4. U.J. Kurze, "Noise Reduction by Barriers", J.Acoust.Soc.Am. (1974) 55 (3), 504-518.
5. Z.Maekawa, "Noise Reduction by Screen of Finite Size", Mem.Fac.Eng., Robe Univ. (1966) 12, 1-12.
6. Z.Maekawa, "Noise Reduction by Screens", App Acoust. (1968) 1, 157-173.
7. U.J.Kurze, G.S.Anderson, "Sound Attenuation by Barriers", App. Acoust. (1971) 4, 35-53.
8. J.B.Moreland, R.F.Minto, "An Example of In-Plant Noise Reduction With an Acoustical Barrier", App.Acoust (1976) 9, 205-214.
9. L.H.Royster, J.E.Stephenson, "Characteristics of Several Industrial Noise Environments", J.Sound Vib.(1976) 43 (3), 313-322.
10. S.Phillips, G.J. McNulty, "Sound Reduction by a Finite Barrier of Arbitrary Shape", Proc. Institute of Acoustics (4) No.15 G3.1, 1978.

11. G.J.McNulty, S.Phillips, "A Theoretical Analysis of the Subdivision of Finite Plane Barriers", Proc. Institute of Acoustics (4) No.15 G2.1, 1978
12. M.Born,E.Wolf, "Principles of Optics", 4th Ed., Pergamon Press, Oxford (1970), 374-387.
13. E.M.Kerwin, Jr., "Decibels and Levels", "Noise Reduction", ed.L.L. Beranek, McGraw - Hill, New York (1960), pp 49-53.
14. G.Rosenhouse, G.J. McNulty, F.Ollendorf, "Integration of the Far Field Diffraction of Plane Noise Barriers by Mapping Their Surface", Israel J. of Tech.(1976) 14, 124-132.
15. Z.Maekawa, "Noise Reduction by Screens", 5th International Congress of Acoustics, 7-14 Sep, 1965.
16. A.J.W. Sommerfeld, "Optics", Academic Press, Inc., New York, 1954.